

FIRST ROW TRANSITION METAL CARBENES: FROM SUPPORTING LIGANDS TO ORGANIC REACTIVE FRAGMENTS

Mònica Rodríguez Serrat

Per citar o enllaçar aquest document:

Para citar o enlazar este documento:

Use this url to cite or link to this publication:

<http://hdl.handle.net/10803/668829>

ADVERTIMENT. L'accés als continguts d'aquesta tesi doctoral i la seva utilització ha de respectar els drets de la persona autora. Pot ser utilitzada per a consulta o estudi personal, així com en activitats o materials d'investigació i docència en els termes establerts a l'art. 32 del Text Refós de la Llei de Propietat Intel·lectual (RDL 1/1996). Per altres utilitzacions es requereix l'autorització prèvia i expressa de la persona autora. En qualsevol cas, en la utilització dels seus continguts caldrà indicar de forma clara el nom i cognoms de la persona autora i el títol de la tesi doctoral. No s'autoritza la seva reproducció o altres formes d'explotació efectuades amb finalitats de lucre ni la seva comunicació pública des d'un lloc aliè al servei TDX. Tampoc s'autoritza la presentació del seu contingut en una finestra o marc aliè a TDX (framing). Aquesta reserva de drets afecta tant als continguts de la tesi com als seus resums i índexs.

ADVERTENCIA. El acceso a los contenidos de esta tesis doctoral y su utilización debe respetar los derechos de la persona autora. Puede ser utilizada para consulta o estudio personal, así como en actividades o materiales de investigación y docencia en los términos establecidos en el art. 32 del Texto Refundido de la Ley de Propiedad Intelectual (RDL 1/1996). Para otros usos se requiere la autorización previa y expresa de la persona autora. En cualquier caso, en la utilización de sus contenidos se deberá indicar de forma clara el nombre y apellidos de la persona autora y el título de la tesis doctoral. No se autoriza su reproducción u otras formas de explotación efectuadas con fines lucrativos ni su comunicación pública desde un sitio ajeno al servicio TDR. Tampoco se autoriza la presentación de su contenido en una ventana o marco ajeno a TDR (framing). Esta reserva de derechos afecta tanto al contenido de la tesis como a sus resúmenes e índices.

WARNING. Access to the contents of this doctoral thesis and its use must respect the rights of the author. It can be used for reference or private study, as well as research and learning activities or materials in the terms established by the 32nd article of the Spanish Consolidated Copyright Act (RDL 1/1996). Express and previous authorization of the author is required for any other uses. In any case, when using its content, full name of the author and title of the thesis must be clearly indicated. Reproduction or other forms of for profit use or public communication from outside TDX service is not allowed. Presentation of its content in a window or frame external to TDX (framing) is not authorized either. These rights affect both the content of the thesis and its abstracts and indexes.



Doctoral Thesis

**First row transition metal carbenes: from
supporting ligands to organic reactive
fragments**

Mònica Rodríguez Serrat

2019

Doctoral programme in Chemistry

Supervised by: Dr. Miquel Costas Salgueiro and Dr. Alberto
Hernán-Gómez Robledo

Tutor: Miquel Costas Salgueiro

Presented in partial fulfilment of the requirements for a doctoral
degree from the University of Girona



Dr. Miquel Costas Salgueiro and Dr. Alberto Hernán-Gómez Robledo of
Universitat de Girona,

WE DECLARE:

That the thesis “First row transition metal carbenes: from supporting ligands to organic reactive fragments”, presented by Mònica Rodríguez Serrat to obtain a doctoral degree, has been completed under our supervision.

For all intents and purposes, we hereby sign this document.

Dr. Miquel Costas Salgueiro

Dr. Alberto Hernán-Gómez Robledo

Girona, 2 de Maig de 2019

List of publications

Publications derived from this thesis:

From Chapter IV:

Iron and Manganese Catalysts for the Selective Functionalization of Arene C(sp²)-H Bonds by Carbene Insertion. A. Conde[‡], G. Sabenya[‡], M. Rodríguez[‡], V. Postils, J.M. Luis, M. M. Díaz-Requejo, M. Costas, P. J. Pérez. *Angew. Chem. Int. Ed.* **2016**, 55, 6530-6534.

Mechanism of the Selective Fe-Catalyzed Arene Carbon-Hydrogen Bond Functionalization. V. Postils[‡], M. Rodríguez[‡], G. Sabenya, A. Conde, M. M. Díaz-Requejo, P. J. Pérez, M. Costas, M. Solà, J. M. Luis. *ACS Catal.* **2018**, 8, 4313-4322.

Work from chapters III and V is ongoing and will be published in the future.

List of abbreviations

AcOEt	ethyl acetate
Ad	Adamantyl (tricyclo-[3.3.1.1 ^{3,7}] decane)
aNHC	<i>abnormal</i> N-heterocyclic carbene
Approx.	approximately
av	average
BDE	bond dissociation energy
Bn	benzyl
cAAC	cyclic alkyl amino carbene
cat	catalyst
Cp	cyclopentadienyl
Cy	cyclohexyl
DCM	dichloromethane
Dipp	2,6-Diisopropylphenyl
DMF	<i>N,N</i> -Dimethylformamide
DMSO	dimethyl sulfoxide
EDA	ethyl diazoacetate
equiv.	equivalent
Et	ethyl
Et ₂ O	diethyl ether
h	hour
HAT	hydrogen atom transfer
HMDS	hexamethyldisilazane or bis(trimethylsilyl)amide
ⁱ Bu	isobutyl
ⁱ Pr	isopropyl
KIE	kinetic isotope effect
M	metal
Me	methyl
MeCN	acetonitrile
MeNC	methyl isocyanate
MeOH	methanol
Mes	mesityl (1,3,5-trimethylbenzene)
MIC	mesoionic compound
<i>n</i> -BuLi	<i>n</i> -butyllithium
n.d.	not-detected

NHC	N-heterocyclic carbene
NMR	nuclear magnetic resonance
<i>n</i> NHC	<i>normal</i> N-heterocyclic carbene
n.r.	no reaction
OTf	trifluoromethanesulfonate
Ph	phenyl
PhI=NTs	[N-(<i>p</i> -Toluenesulfonyl)imino]phenyliodinane
PhIO	iodosylbenzene
Py	pyridine
<i>r</i> NHC	<i>remote</i> N-heterocyclic carbene
r.t.	room temperature
s.	second
<i>tacn</i>	1,4,7-triazacyclononane
TBABr	Tetrabutylammonium bromide
^t Bu	<i>tert</i> -butyl
TEMPO	2,2,6,6-Tetramethylpiperidine 1-oxyl
TEP	Tolman electronic parameter
THF	tetrahydrofuran
tmtaa	tetramethyldibenzotetraazaannulene
TPP	5,10,15,20-tetraphenylporphyrin
Tz	1,2,3-triazolylidene
UV-Vis	Ultraviolet-Visible

List of Figures

Figure I.1. Electronic spin states of a carbene.....	9
Figure I.2. Number of publication of N-heterocyclic carbenes per year. Values obtained from ISI WoS (Search criteria used: N-heterocyclic carbene).....	12
Figure I.3. Steric impact of N-heterocyclic carbenes and tertiary phosphines to the metal center.	13
Figure I.4. Collection of different NHCs and its assignation to the different classes of these ligands.	14
Figure I.5. NHC chelating structure of Glorius (left) and Meyer (right).	15
Figure I.6. Different NHC ligands and its δ_p value.....	16
Figure I.7. Isolated free 1,2,3-triazolylidene carbenes.	19
Figure I.8. Number of 1,2,3-triazolylidene metal complexes reported since 2003.	22
Figure I.9. Resume of all structures reported for first row transition metals.	23
Figure I.10. Resume of the BDE of some organic compounds.	25
Figure I.11. Iron complexes structures used for iron carbene isolation.	28
Figure III.1. X-Ray structures of 4-Fe , 4-Zn , 4-Mn , 4-Cu and 4-Ag . 50% ellipsoid probability. Hydrogen atoms, non-coordinating anions and solvents are omitted for clarity.	42
Figure III.2. View of 4-Fe as trigonal bipyramidal (left) and square pyramidal geometries (right).	44
Figure III.3. View of 4-Zn as trigonal bipyramidal (left) and square pyramidal geometries (right).	45
Figure III.4. ORTEP diagram of the single crystal X-Ray structure for 1-Fe (left) and 1-Zn (right). 50% ellipsoid probability. H atoms have been omitted and only O-bound atoms of the triflate anions are shown for clarity. 1-Fe selected distances (Å): Fe-N1: 2.231, Fe-N2: 2.251, Fe-N3: 2.205, Fe-N4: 2.165, Fe-O1: 2.055, Fe-O2: 2.165. 1-Zn selected distances (Å): Zn-N1: 2.136, Zn-N2: 2.159, Zn-N3: 2.184, Zn-N4: 2.087, Zn-O1: 2.183, Zn-O2: 2.073.	46
Figure III.5. X-Ray structure for 2-Cu . 50% ellipsoid probability. H atoms and non-coordinating anions are omitted for clarity. 2-Cu selected distances (Å): Cu-N1: 2.167, Cu-N2: 2.108, Cu-N3: 2.134, Cu-N4: 1.940.	47
Figure III.6. ¹ H-NMR spectrum of 4-Fe in CD ₂ Cl ₂ at 300K with the assignment of the tert-butyl and N-CH ₃ signals (top) and ¹ H-NMR spectrum of 4-Fe in CD ₃ CN at 300K with the assignment of the tert-butyl signal (bottom).	49
Figure III.7. ¹ H-NMR spectrum of 4-Zn in acetone-d ⁶ at 300K with partial assignment.	50

Figure III.8. $^1\text{H-NMR}$ spectrum of 4-Cu in acetone- d^6 at 300K with partial assignment.	50
Figure III.9. $^1\text{H-NMR}$ spectrum of 4-Ag in CD_2Cl_2 at 300K with partial assignment. Inset: $^7\text{Li-NMR}$ of 4-Ag	51
Figure III.10. Cyclic voltammetry of 4-Fe from 0 to 1.5V (top), 4-Fe from -1 to 1.5V (middle) and 1-FeX₂ (bottom) in MeCN (versus 0.01M Ag/AgNO ₃ electrode). Scans were run at 50 mV/s. The arrows show scan direction.	52
Figure III.11. Cyclic voltammetry of 4-Cu in MeCN (versus 0.01M Ag/AgNO ₃ electrode). Scan was run at 50 mV/s. The arrow shows scan direction.	53
Figure III.12. UV-Vis absorption spectrum of 1mM solution of 4-Fe in DCM at -40°C (yellow), the specie formed after the addition of tetrabutylammonium periodate (orange) and the self-decay of the new specie (dark orange).	55
Figure III.13. UV-Vis absorption spectrum of the formation of the Cu-O ₂ adduct in a solution at 0.9mM in acetone. Dark grey: initial 4-Cu complex. Green: 4-Cu-O₂ adduct.	57
Figure III.14. UV-Vis absorption spectrum of the formation (right) and disappearance (left) of the 4-Cu-O₂ adduct in a solution at 0.9mM in acetone at different temperatures.	58
Figure III.15. UV-Vis absorption spectrum of the initial 4-Cu-O₂ adduct (green) and the proposed copper-hydroperoxide specie (yellow) in a solution at 0.9mM in acetone at -90°C.	58
Figure III.16. UV-Vis absorption spectrum of the initial 4Cu-O₂ adduct (green) and the final spectrum after the addition of 2,6-di-tert-butyl-4-methoxyphenol (grey) in a solution at 0.9mM in acetone at -90°C.	59
Figure IV.1. Different iron complexes used in the functionalization of benzene in carbene transfer reactions.	68
Figure IV.2. Substrate scope in the functionalization of arenes in the decomposition of EDA. Isolated yields. Isomer ratios determined by $^1\text{H-NMR}$. ^a Work performed by Gerard Sabenya.	70
Figure IV.3. ORTEP diagram of the single crystal X-Ray structure for 1-Fe ¹³⁸ (left) and $[\text{Fe}_2(\mu\text{-OTf})_2(\text{Me}_2\text{Pytacn})_2](\text{BAR}_4\text{F})_2$, 20-Fe (right). 50% ellipsoid probability, H atoms have been omitted for clarity. 1-Fe selected distances (Å): Fe-N1: 2.231, Fe-N2: 2.251, Fe-N3: 2.205, Fe-N4: 2.165, Fe-O1: 2.055, Fe-O2: 2.165. 20-Fe selected distances (Å): Fe-N1: 2.200, Fe-N2: 2.210, Fe-N3: 2.187, Fe-N4: 2.142, Fe-O1: 2.060, Fe-O2: 2.189... 73	73
Figure V.1. Bidentate iron complexes tested for the activation of diazo compounds... 84	84
Figure V.2. Substrate scope with the yield determined by $^1\text{H-NMR}$ and the isolated yield in parenthesis. Diastereomeric ratio of isolated samples determined by GC-MS in	

brackets. Reactions carried out at 25°C with 0.025 mmol of 22-Fe , 0.25 mmol of [LiAl(OC(CF ₃) ₃) ₄] and 1 mmol of SX in 12.5 mL of dichloromethane, during 24h.....	90
Figure V.3. IR spectra of different mmolar mixtures of S20 :[LiAl(OC(CF ₃) ₃) ₄]. a) 1:0.05; b) 1:0.15; c) 1:0.25.....	92
Figure V.4. Plot of Ln[S20] vs time (h) for C-H functionalization of S20 under optimized reaction conditions.....	93
Figure VII.1. IR spectrum of 22-Fe	145
Figure VII.2. IR spectrum of S20	145
Figure VII.3. IR spectrum of S20 : 22-Fe (1:1).....	146
Figure VII.4. IR spectrum of [LiAl(OC(CF ₃) ₃) ₄]	146
Figure VII.5. IR spectrum of S20 :[LiAl(OC(CF ₃) ₃) ₄] (1:0.05).....	147
Figure VII.6. IR spectrum of S20 :[LiAl(OC(CF ₃) ₃) ₄] (1:0.1).....	147
Figure VII.7. IR spectrum of S20 :[LiAl(OC(CF ₃) ₃) ₄] (1:0.15).....	148
Figure VII.8. IR spectrum of S20 :[LiAl(OC(CF ₃) ₃) ₄] (1:0.2).....	148
Figure VII.9. IR spectrum of S20 :[LiAl(OC(CF ₃) ₃) ₄] (1:0.25).....	149
Figure VII.10. IR spectrum of S20 :[LiAl(OC(CF ₃) ₃) ₄] (1:0.5).....	149
Figure VII.11. IR spectrum of S20 :[LiAl(OC(CF ₃) ₃) ₄] (1:0.75).....	150
Figure VII.12. IR spectrum of S20 :[LiAl(OC(CF ₃) ₃) ₄] (1:1).....	150
Figure VII.13. ¹ H-NMR spectrum of C-H alkylation of [D ₁]- S20 catalyzed by 22-Fe (2.5mol%) and [LiAl(OC(CF ₃) ₃) ₄] (25 mol%)	151
Figure VII.14. ¹ H-NMR spectrum of C-H alkylation of [D ₁]- S20 catalyzed by Rh ₂ (OAc) ₄ (2.5 mol%)	151

List of Schemes

Scheme I.1. Work of Doering and coworkers in the synthesis of tropolones (left) and in the cyclopropanation of olefins (right).	7
Scheme I.2. Chugaev salt, first example of a metal carbene complex.....	7
Scheme I.3. Synthesis of the first Fischer carbene complex (top) and Schrock carbene complex (bottom).	8
Scheme I.4. Synthesis of the first NHC metal complexes reported by Öfele (left) and Wanzlick (right) in 1968.	8
Scheme I.5. First isolated stable NHC by Arduengo in 1991.	8
Scheme I.6. Orbital interaction and M-C bond polarization in Fischer type carbenes.	10
Scheme I.7. Orbital interaction and M-C bond polarization in Schrock type carbenes.	10
Scheme I.8. Differences between first- and second-generation Grubbs catalyst.	12
Scheme I.9. Resonance structure of C2 and C4 carbenes.	14
Scheme I.10. Pd catalyzed Heck Reaction with C2 and C4 bound NHC complexes. Reactions performed 1 mmolar of bromobenzene, 1.6 equiv. of butyl acrylate and 2 equiv. of Cs ₂ CO ₃ , at 120°C for 7 hours.	17
Scheme I.11. Rh catalyzed transfer hydrogenation with aNHC and nNHC as ligands. Reaction performed at 1mmol of benzophenone, 5 mL of iPrOH, 100 µmol of base, in DCM at reflux temperature for 2h.	17
Scheme I.12. Different procedures for the synthesis of 1,2,3-triazoles.....	18
Scheme I.13. Schematic representation of the different transformations that diazo compounds can perform.	24
Scheme I.14. Different performance in the functionalization of mesitylene with (TPP)FeCl with different diazo acetates.	29
Scheme I.15. Derivatization of benzene using (TPP)FeCl and diazoacetates.....	30
Scheme II.1. Schematic representation of the objective of Chapter III.	33
Scheme II.2. Summary of the organic reactions performed in Chapter IV and V.	34
Scheme III.1. Schematic representation of the modification on previously reported tacn-based ligand.	37
Scheme III.2. Simplified retrosynthesis for the synthesis of the targeted NHC ligand.	38
Scheme III.3. Synthetic scheme for the construction of 3	38
Scheme III.4. Two products were obtained from the last reaction step in the synthesis of the NHC ligand.	39
Scheme III.5. Simplified retrosynthesis for the synthesis of the new NHC ligand.	39
Scheme III.6. Synthetic scheme for the construction of 4	40
Scheme III.7. Reaction protocol for the synthesis of the different metal NHC complexes.	41
Scheme III.8. Catalytic N-transfer reactions tested with 4-Fe	55
Scheme III.9. Catalytic carbene transfer reaction tested with 4-Zn complex. Yields determined by GC.	56

Scheme III.10. Formation of trans-1,2-peroxodicopper(II) complex with ligand 2	57
Scheme III.11. Proposed simplified mechanism for the formation of 2,6-di-tert-butyl-1,4-benzoquinone from copper-superoxide species.	59
Scheme IV.1. Different products in metal catalyzed (alkyl)-benzene functionalization by carbene transfer.	63
Scheme IV.2. Decomposition of EDA with iron complexes in the functionalization of benzene.	64
Scheme IV.3. Standard conditions for the functionalization of benzene using different diazoacetates.	71
Scheme IV.4. Role of NaBAR ₄ ^F in the generation of a dicationic specie.	73
Scheme IV.5. Functionalization of aniline using ethyl diazoacetate.	74
Scheme IV.6. Functionalization of mesitylene and 1,3,5-triethylbenzene under standard reaction conditions, giving a mixture of two regioisomers.....	76
Scheme IV.7. Different isomers achieved in the functionalization of 1,2,4-trimethylbenzene under standard conditions.	77
Scheme IV.8. Functionalization of radical clocks under standard conditions for the determination of radical intermediates.	78
Scheme IV.9. Isotopic labelling experiments.	79
Scheme IV.10. Proposed reaction mechanism for the functionalization of benzene. Energy values were calculated by Verònica Postils (Level of theory: UB3LYP-D3BJ/cc-pVTZ/SMD(50%Bz,50%CH ₂ Cl ₂)).	80
Scheme V.1. Resume of different 5-membered ring synthesized molecules through carbene intermediates using rhodium ¹⁸²⁻¹⁸⁵ and iron ^{120,135} complexes.....	83
Scheme V.2. Coordination of Lewis acids into the O atom of the diazo substrate.....	91
Scheme V.3. Functionalization of a radical clock substrate. Isolated yield in parenthesis. Diastereomeric ratio of isolated samples determined by GC-MS in brackets.....	93
Scheme V.4. Functionalization of [D ₁]- 20 for the determination of the KIE using iron and rhodium complexes.	94
Scheme V.5. Proposed reaction mechanism for the catalytic functionalization of C _{sp} ³ -H bonds.	94
Scheme VII.1. NOE of the different isomers for its assignment.	125

List of Tables

Table I.1. $\nu(\text{CO})$ values of different Ir(NHC) complexes.	16
Table I.2. Comparison of CO stretching frequencies between different Ir(CO)(NHC) complexes.	20
Table III.1. Selected bond lengths (Å) and angles ($^{\circ}$) for 4-Fe , 4-Zn , 4-Mn , 4-Cu and 4-Ag and trigonality parameters ^a for 4-Fe and 4-Zn	37
Table III.2. Comparison of the Fe ^{II} /Fe ^{III} redox potential of 1-Fe and 4-Fe complexes in acetonitrile vs 0.01M Ag/AgNO ₃ electrode.	53
Table III.3. Comparison of the oxidation potentials for different reported Cu ^I complexes in acetonitrile vs 0.01M Ag/AgNO ₃ electrode. Conversion of redox potentials from different reference electrodes has been carried out. ¹⁶⁸	54
Table IV.1. Described examples of metal-catalyzed carbene functionalization of benzene with their corresponding product ratio.	64
Table IV.2. Catalytic results of 1-FeX₂ complexes under different reaction conditions.	65
Table IV.3. Catalytic behavior of the different iron complexes tested in the functionalization of benzene.	69
Table IV.4. Functionalization of benzene using different diazoacetates.	71
Table IV.5. Catalytic behavior of different metal complexes with Me ₂ Pytacn ligand.	72
Table IV.6. Decomposition of EDA under iron complexes in the functionalization of aniline at different reaction temperatures.	75
Table V.1. Reaction optimization for intramolecular cyclization via carbene intermediates using iron complexes.	87
Table V.2. Substrate scope in the intramolecular cyclization with products yields and diastereomeric ratios of the cyclized products.	88
Table VII.1. Crystal data for 4-Fe	109
Table VII.2. Crystal data for 4-Zn	109
Table VII.3. Crystal data for 4-Mn	110
Table VII.4. Crystal data for 4-Cu	111
Table VII.5. Crystal data for 4-Ag	112
Table VII.6. Crystal data for 1-Zn	128
Table VII.7. Crystal data for 20-Fe	129

Acknowledgments

This work would have not been possible without the following collaborations:

- Serveis Tècnics de Recerca (STR) from University of Girona for technical support, with especial remark to Dr. Laura Gómez and Xavier Fontrodona.
- Verònica Postils, Dr. Miquel Solà i Dr. Josep M. Luis from the Institut de Química Computacional i Catàlisis (IQCC) of the University of Girona for the theoretical studies.
- Dr. Jordi Benet from the Institut Català d'Investigació Química (ICIQ) for their support and diffraction of the first NHC complex synthesized.
- Prof. Pedro J. Pérez and Dr. M. Mar Díaz-Requejo from the University of Huelva for hosting a scientific visit and the collaborative research in arene functionalization in the carbene transfer project.
- Prof. Martin Albrecht from the University of Bern for hosting a scientific visit and the collaborative research in the synthesis of new NHC complexes.
- Generalitat de Catalunya for the PhD grant "Ajuts per a la contractació de personal investigador novell (FI-2015)".
- Financial support from COST Action CM1305 (ECOSTBio) for STSM grants STSM-CM1305-34058.

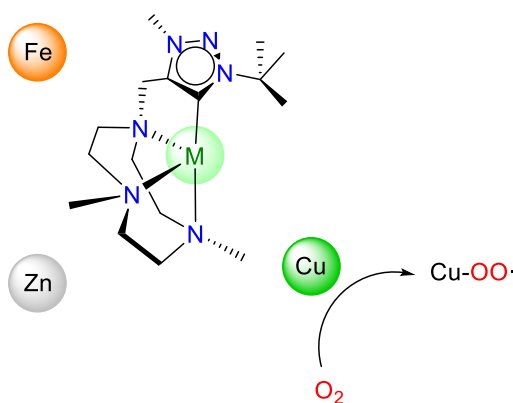
Graphical Abstract

Summary. (p. 1)

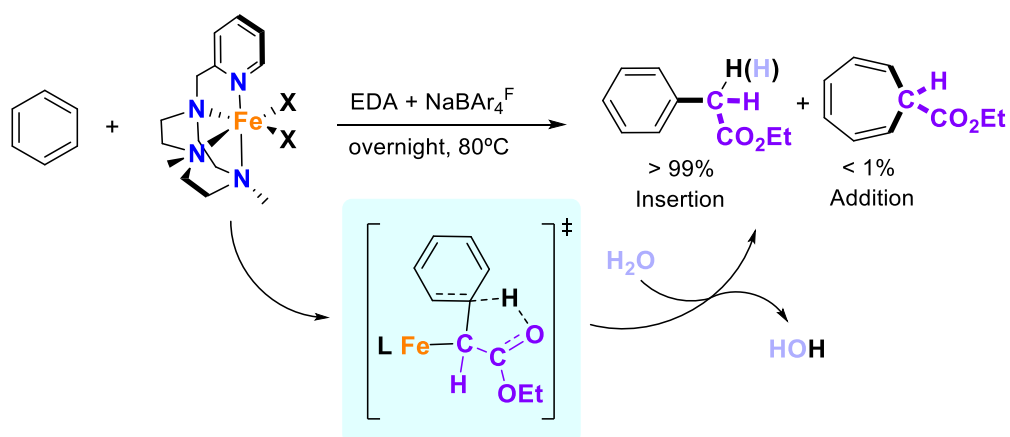
Chapter I. General Introduction (p. 5)

Chapter II. Objectives (p. 31)

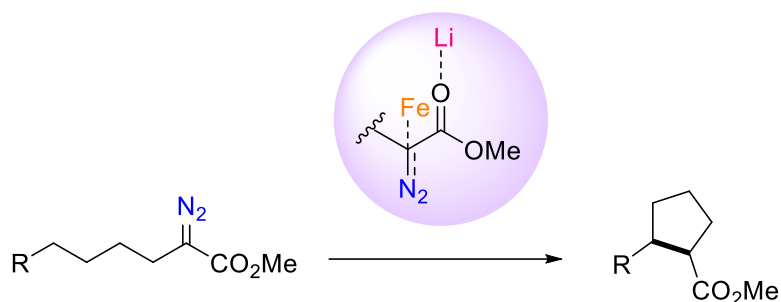
Chapter III. Synthesis of a hybrid tacn-NHC ligand and its related first row transition metal complexes (p. 35)



Chapter IV. Carbene insertion into C_{sp}²-H bonds catalyzed by non-heme iron complexes: catalytic and mechanistic insights (p. 61)



Chapter V. Intramolecular $C_{sp^3}\text{-H}$ alkylation using low-coordinate iron complexes via carbene intermediates (p. 81)



mild reaction conditions
benzylic and alkylic substrates

Chapter VI. General Conclusions (p. 97)

Chapter VII. Experimental Section (p. 101)

References (p. 153)

Table of Contents

Summary	1
Chapter I. General Introduction	5
I.1 History of carbenes	7
I.2 Carbenes in organometallic chemistry	9
I.2.1 Metal-Carbon bond structure	9
I.2.1.1 Fischer type carbenes	9
I.2.1.2 Schrock type carbenes	10
I.2.1.3 N-heterocyclic carbenes	10
I.2.2 N-heterocyclic carbenes as platform for new ligand scaffolds	11
I.2.2.1 Analogies and differences with phosphine ligands.....	12
I.2.2.2 Different classes of N-heterocyclic carbene ligands.....	13
I.2.2.3 Comparison between <i>n</i> NHC and <i>a</i> NHC.....	15
I.2.2.4 1,2,3-triazolylidene ligands	17
I.3 Carbenes as powerful intermediates in organic synthesis	23
I.3.1 C-H bond functionalization by carbene insertion	25
I.3.2 Iron complexes in carbene insertion.....	26
Chapter II. Objectives	31
Chapter III. Synthesis of a hybrid tacn-NHC ligand and its related first row transition metal complexes	35
III.1 Results and discussion	37
III.1.1 Synthesis of the ligands and its metal complexes	37
III.1.2 X-Ray analysis of the metal complexes.....	42
III.1.3 Spectroscopic and electrochemical characterization of the metal complexes	48
III.1.3.1 ¹ H-NMR spectroscopy	48
III.1.3.2 Electrochemical properties	51
III.1.4 Reactivity studies of the metal complexes.....	54
III.2 Summary.....	60

Chapter IV. Carbene insertion into C_{sp}²-H bonds catalyzed by non-heme iron complexes: catalytic and mechanistic insights	61
IV.1 Results and discussion	63
IV.1.1 Catalytic studies	64
IV.1.2 Mechanistic studies	73
IV.2 Summary	80
Chapter V. Intramolecular C_{sp}³-H bond alkylation using low-coordinate iron complexes via carbene intermediates	81
V.1 Results and discussion	83
V.1.1 Catalytic studies	84
V.1.2 Mechanistic studies	91
V.2 Summary	94
Chapter VI. General Conclusions	97
Chapter VII. Experimental Section	101
VII.1 Experimental Section Chapter III	103
VII.1.1 Instrumentation	103
VII.1.2 Materials	103
VII.1.3 Synthesis of ligands	103
VII.1.4 Synthesis of complexes	106
VII.1.5 Crystal data	109
VII.1.6 Copper-superoxide experiments	113
VII. 2 Experimental Section Chapter IV	114
VII.2.1 Instrumentation	114
VII.2.2 Materials	114
VII.2.3 Synthesis of ligands	114
VII.2.4 Synthesis of complexes	118
VII.2.5 Synthesis of substrates	122
VII.2.5.1 Synthesis of diazo acetates	122
VII.2.5.2 Synthesis of fast radical clock	123
VII.2.6 Catalytic procedures	124

VII.2.6.1 Reaction protocol for catalysis.....	124
VII.2.6.2 General procedure for product isolation.....	124
VII.2.7 Characterization of isolated products.....	124
VII.3 Experimental Section Chapter V	131
VII.3.1 Instrumentation.....	131
VII.3.2 Materials.....	131
VII.3.3 Synthesis of diazo acetates	131
VII.3.4 Catalytic procedures	140
VII.3.4.1 Reaction protocol for catalysis.....	140
VII.3.4.2 General procedure for product isolation.....	141
VII.3.5 Characterization of isolated products.....	141
VII.3.6 IR studies	145
VII.3.6 KIE studies	150
References	153

Supplementary digital material

The material listed below can be found in the attached CD:

- PDF file of the PhD dissertation.
- PDF files containing spectroscopic and spectrometric characterization. Each file can be found in their corresponding chapter folder.
- CIF files for each crystal structure presented in this thesis. They can be found in the corresponding chapter folder, named as in the PhD dissertation.

Summary

In the last decades, carbenes have shown a huge potential and versatility in organometallic and organic chemistry. In organometallic chemistry, a large library of carbene ligands with high σ -donor properties can be designed and synthesized, allowing the construction of metal complexes with different properties and reactivities. In organic chemistry, carbenes can be used as reactive intermediates for the functionalization of C-H bonds, forming new C-C bonds, a reaction that provides access to the synthesis of very different structures. In each of these fields, first row transition metal chemistry is less developed than noble metal complexes. In the pursuit of more environmentally friendly systems, this thesis will be focused on the development of new organometallic complexes and reactivities using earth abundant metals for organic and organometallic chemistry.

In the organometallic field, the synthesis of a novel ligand bearing a chelating scaffold and a mesoionic carbene moiety has allowed the preparation of a family of first row transition metal complexes. Different metal complexes have been described and characterized and promising reactivities could be envisioned based on their characteristics. In a particular case, the reactivity of the Cu(I) complex in presence of oxygen has been studied, and the system allowed the reversible binding and activation of oxygen, forming a superoxide species, which is the first organometallic copper superoxide described up to date.

Using carbenes as intermediates in organic synthesis, the intermolecular functionalization of aromatic C_{sp^2} -H bonds by the activation of diazoacetates could be developed using iron complexes with aminopyridine ligands. The unique selectivity shown by those complexes allowed the description of a very chemoselective system for non-activated aromatic substrates, even though no regioselectivity could be achieved and the reaction conditions needed are quite harsh.

Finally, the same reactivity could be applied in an intramolecular version. The functionalization of C_{sp^3} -H bonds for the selective formation of cyclopentane rings has been developed using low-coordinate iron complexes. The role of a lithium salt for the assistance in the formation of the metallocarbene intermediate provided a useful methodology to promote carbene transfer reactions using non-toxic iron complexes under mild reactions conditions, which was an important challenge to be overcome in iron carbene chemistry.

Resum

En les últimes dècades, els carbens han mostrat un gran potencial i versatilitat tan en la química organometàl·lica com en la orgànica. En química organometàl·lica, una extensa llibreria de lligands amb unes altes propietats σ -donadores han estat dissenyats i sintetitzats, permetent la formació de complexos metàl·lics amb diferents propietats i reactivitats. En química orgànica, els carbens es poden utilitzar com a intermedis reactius per a la funcionalització d'enllaços C-H, formant nous enllaços C-C que permeten la construcció d'una llarga varietat de molècules. En qualsevol d'aquest camps, els metalls de la primera sèrie de transició han estat menys utilitzats que els metalls nobles. Davant la recerca de sistemes que siguin més benignes amb el medi ambient, aquesta tesi està enfocada al desenvolupament de nous complexos organometàl·lics i reactivitats utilitzant metalls abundants a la natura tan per la química organometàl·lica com per la orgànica.

En el camp de la organometàl·lica, la síntesi d'un lligand nou el qual combina una estructura quelatant i un carbè mesoiònic va permetre la síntesi de complexos amb metalls de la primera sèrie de transició. Diferents complexos han estat descrits i caracteritzats i una reactivitat prometedora es pot preveure gràcies a les seves característiques. En un cas particular, la reactivitat del complex de Cu(I) en presència d'oxigen ha estat estudiada. El sistema és capaç d'activar oxigen a través de la formació d'un superòxid, el qual és el primer sistema organometàl·lic descrit fins l'actualitat.

Utilitzant carbens com a intermedis en síntesi orgànica, s'ha descrit la funcionalització intermolecular d'enllaços aromàtics a través de l'activació de diazoacetats, utilitzant complexos de ferro amb lligands aminopiridínics. La exclusiva selectivitat mostrada per aquests complexos va permetre la descripció d'un sistema quimioselectiu per a la funcionalització de substrats aromàtics no activats, tot i que la regioselectivitat de la reacció no era bona i les condicions de reacció necessàries són agressives.

Finalment, la mateixa reactivitat va ser aplicada en una versió intramolecular. La funcionalització d'enllaços C_{sp^3} -H per a la formació selectiva d'anells ciclopentans s'ha desenvolupat utilitzant complexos de ferro estèricament poc saturats. La participació d'una salt de liti per a l'assistència en la formació de l'intermedi de metal·locarbè ha permès obtenir una metodologia eficient per promoure les reaccions de transferència de carbè utilitzant metalls no tòxics en condicions suaus de reacció; un repte important en la química de carbens de ferro que encara no s'havia superat.

Resumen

En las últimas décadas, los carbenos han mostrado un gran potencial tanto en la química organometálica como en orgánica. En química organometálica, una extensa librería de ligandos con unas altas propiedades σ -dadoras han sido sintetizados, permitiendo la formación de complejos metálicos con distintas propiedades. En química orgánica, los carbenos se han podido utilizar como intermedios reactivos para la funcionalización de enlaces C-H, permitiendo construir una larga variedad de moléculas. En cualquiera de estos campos, los metales de la primera serie de transición han estado menos estudiados que los metales nobles. De cara a la investigación de nuevos sistemas que sean más benignos con el medio ambiente, esta tesis está enfocada al desarrollo de nuevos complejos y reactividades utilizando metales abundantes en la naturaleza, tanto en química organometálica como en química orgánica.

En el campo de la química organometálica, se ha desarrollado un nuevo ligando combinando una estructura quelatante y un carbeno mesoionico, a partir del cual se ha realizado la síntesis de complejos con metales de la primera serie de transición. Distintos complejos han estado descritos y caracterizados y una reactividad prometedora se puede prever gracias a sus características. En un caso particular, la reactividad del complejo de Cu(I) en presencia de oxígeno ha estado estudiada. Este sistema es capaz de enlazar y activar oxígeno de manera reversible a través de la formación de un superóxido, el cual corresponde al primer sistema organometálico descrito actualmente.

Utilizando carbenos como intermedios en síntesis orgánica, se ha descrito un sistema para la funcionalización intermolecular de enlaces C_{sp^2} -H a través de la activación de diazoacetatos, utilizando complejos de hierro con ligandos con aminopiridinas. La exclusiva selectividad mostrada por este sistema permitió la descripción de un sistema quimioselectivo para la funcionalización de sustratos aromáticos no activados, aunque no se consiguió una regioselectividad buena y las condiciones de reacción necesarias son agresivas.

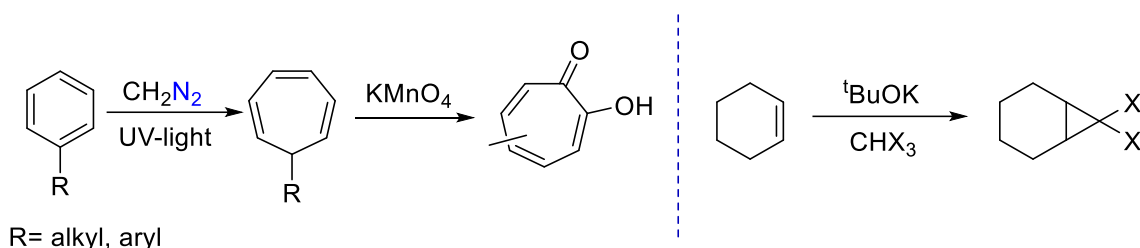
Finalmente, la misma reactividad se aplicó a la funcionalización intramolecular de enlaces C_{sp^3} -H. La formación de ciclopentanos se ha desarrollado utilizando complejos de hierro con bajo número de coordinación. La participación de una sal de litio asistiendo la formación del intermedio del metalocarbeneo ha permitido obtener una metodología eficiente para promover las reacciones de transferencia de carbenos utilizando metales no tóxicos, en condiciones suaves de reacción; un desafío importante en la química de carbenos de hierro que no se había superado hasta el momento.

Chapter I

General Introduction

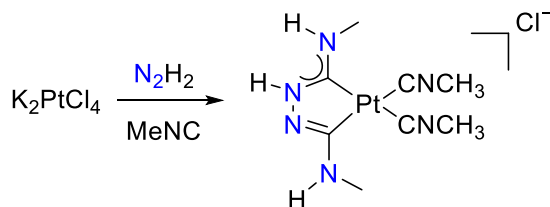
I.1 History of carbenes

The postulation and use of carbenes started more than 150 years ago, in the pursuit of the isolation of a neutral divalent carbon atom; although all the attempts failed due to its high reactivity.¹⁻³ Nevertheless, carbenes were used as transient radical intermediates in many organic reactions. The first example was carried out by Buchner in 1903, describing the thermal decomposition of ethyl diazoacetate for the cyclopropanation of toluene and styrene.^{4,5} Some years later, Doering and coworkers described the synthesis of tropolones by the addition of methylene to arenes (Scheme I.1, left),⁶ and more remarkably, in 1954 the same group report the cyclopropanation reaction of olefins using chloroform or bromoform as carbene transfer reagents (Scheme I.1, right).⁷ Their experiments showed evidences of the formation of a dihalocarbene intermediate.



Scheme I.1. Work of Doering and coworkers in the synthesis of tropolones (left) and in the cyclopropanation of olefins (right).

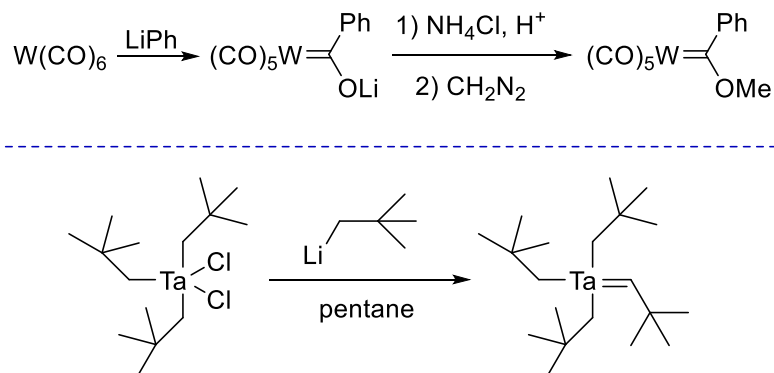
Notwithstanding, free carbenes were still elusive and impossible to be isolated. For this reason, a new approach in carbenes chemistry began with the isolation of metal carbene complexes. Indeed, the first example of a metal carbene complex was achieved back in 1925 by the group of Chugaev, where they reported the reaction of a methyl isocyanate platinum complex with hydrazine.⁸ However, the limited techniques at that time made impossible the elucidation of the structure of the first metal carbene complex. It was not until the 70's when finally, X-Ray and NMR analysis revealed the real structure of the Chugaev salt as a platinum carbene complex (Scheme I.2).⁹⁻¹¹



Scheme I.2. Chugaev salt, first example of a metal carbene complex.

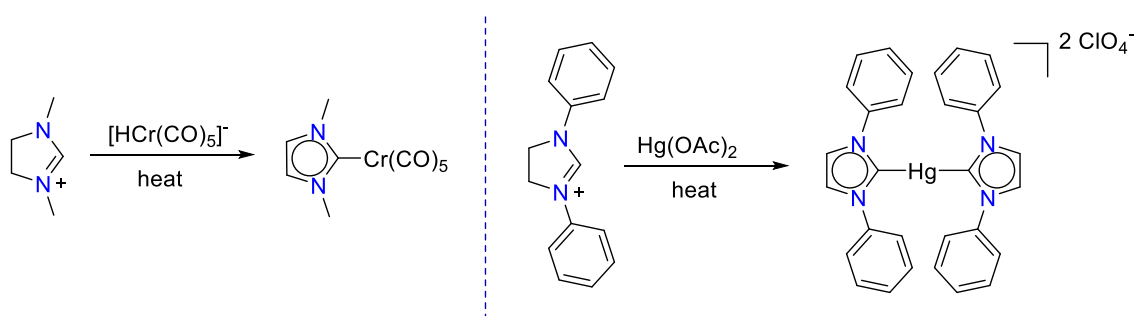
Prior to the resolution of the previous structure, in 1964, Fischer prepared what in that moment was the first unambiguously described carbene metal complex, with tungsten as metal center (Scheme I.3, top).¹² A similar approach was followed by

Schrock years later for the synthesis of a tantalum carbene complex in high oxidation state (Scheme I.3, bottom).¹³



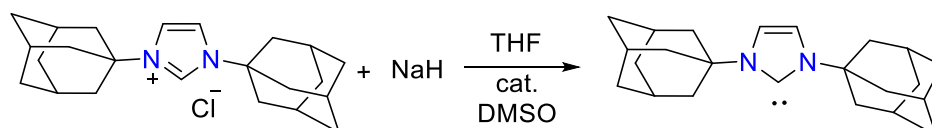
Scheme I.3. Synthesis of the first Fischer carbene complex (top) and Schrock carbene complex (bottom).

At the end of the 60's, Öfele and Wanzlick were independently working in a different type of metal carbenes, in which the carbenic carbon is stabilized by two neighboring heteroatoms. In 1968, both groups reported separately two different N-Heterocyclic Carbene (NHC) metal complexes (Scheme I.4).^{14,15}



Scheme I.4. Synthesis of the first NHC metal complexes reported by Öfele (left) and Wanzlick (right) in 1968.

Some years later, in 1988, Bertrand and coworkers reported the preparation of the first isolable free carbene. However this compound did not show any abilities as ligand for metal complexes.¹⁶ Finally, in 1991, Arduengo was able to isolate and crystallize the first stable and “bottleable” NHC by the deprotonation of an imidazolium salt using a strong base.¹⁷ This was the beginning of the so-called persistent carbenes.



Scheme I.5. First isolated stable NHC by Arduengo in 1991.

A new period in organic and inorganic chemistry started with the discovery and use of carbenes, and nowadays they are widely extended. Along all these years, carbenes

have gone from being very reactive intermediates, difficult to be detected and isolated; to be also stable compounds (either stabilized by electronics and sterics of the molecule or in a coordination sphere of a metal), with many different applications, such as transition metal catalysis and organocatalysis,^{18,19} as well as medicinal²⁰ and material applications.²¹

I.2 Carbenes in organometallic chemistry

I.2.1 Metal-Carbon bond structure

Carbenes are neutral molecules containing a divalent carbon atom. In the ground state, the two nonbonding electrons of the carbon atom can have either antiparallel spins, where the sp^2 orbital is doubly occupied and the p_z orbital is unoccupied (singlet state) or parallel spins, where the sp^2 and p_z orbitals are singly occupied (triplet state) (Figure I.1). The different spin configuration of the carbene (which depends on the relative energy values between sp^2 and p orbitals) and its overlapping with the orbitals of the metal determines the nature of the metal carbene complex.

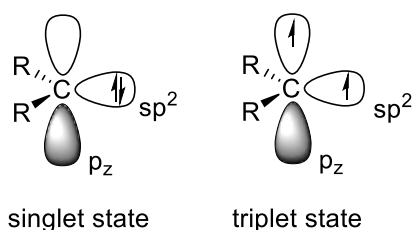


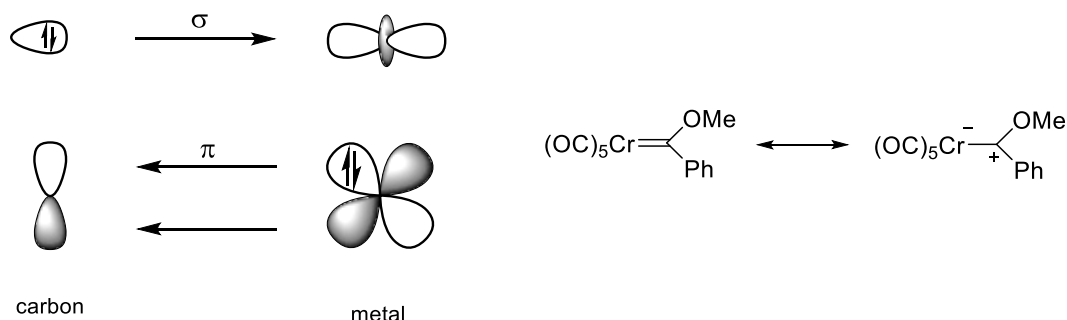
Figure I.1. Electronic spin states of a carbene.

As seen in the previous chapter, there are a large number of different types of carbenes stabilized by a metal, all of them with very different electronic properties of the M-C bond. These organometallic complexes can be classified in three different groups: Fischer type carbenes, Schrock type carbenes and N-Heterocyclic carbenes.

I.2.1.1 Fischer type carbenes

Fischer carbenes^{22,23} are mainly based on metals in low oxidation states in combination with singlet carbenes. The bond is based on a σ -donation from the carbene to the empty d orbital of the metal and π back-donation from the metal to the carbon. The M-C bond is slightly longer than Schrock carbenes (thus, the bond order is less than 2) and the π electrons are polarized towards the metal (Scheme I.6). This polarization generates a carbon that is electrophilic in nature and they have to be stabilized by a

heteroatom directly linked to the electrophilic carbon, such as alkoxides or alkylated amino groups.

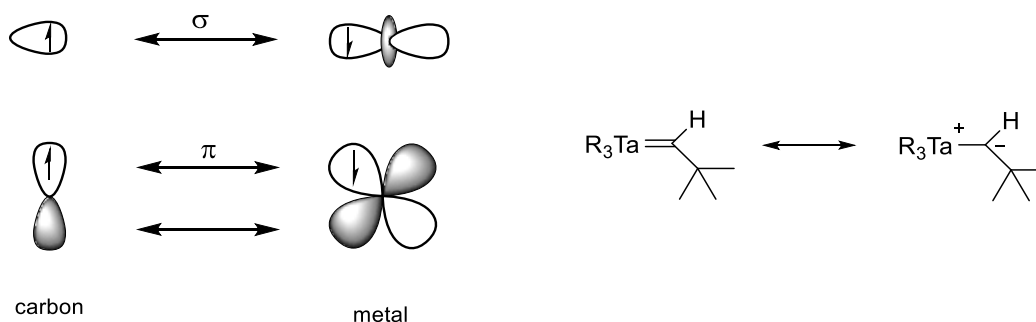


Scheme I.6. Orbital interaction and M-C bond polarization in Fischer type carbenes.

The so-called non-heteroatom-stabilized carbenes²⁴ are a particular type of Fischer carbenes, with some similarities, such as the low oxidation state metals and the electrophilicity of the carbene, but it lacks the stabilization of the neighboring heteroatom, thus generating a less stable metal complex.

I.2.1.2 Schrock type carbenes

Schrock carbenes^{22,23} are based on metals in high oxidation states in combination with triplet carbenes. The π electrons are equally distributed between the metal-carbon bond, generating a real double bond, therefore the M-C bond distance is shorter than Fischer carbenes. Schrock carbenes are nucleophilic at the carbon center (Scheme I.7). These carbene complexes are poorly stabilized with alkylidenes or dialkylcarbenes. However, despite their moisture and air sensitivity, molybdenum alkylidenes are amongst the most powerful olefin metathesis catalyst known to date.



Scheme I.7. Orbital interaction and M-C bond polarization in Schrock type carbenes.

I.2.1.3 N-heterocyclic carbenes

Although NHCs can be considered as a type of Fischer carbenes, its particular properties motivate their study separately from the other carbenes. NHCs are nitrogen

containing heterocycles with a carbene motif with special electronics and steric characteristics that makes them perfect candidates as ligands for metal complexes. NHCs are capable to bind strongly to a metal by σ -bonding interactions. In the beginning, NHCs were described as simple σ -donor ligands due to the electron density donated from the two neighboring nitrogen atoms to the empty π orbital of the carbene. However, over the years, its π -back donation ability has been gaining more importance with different reports suggesting its contribution,²⁵⁻²⁷ although that contribution is much smaller than the σ character.

Nevertheless, the large number of different heterocycles and their coordination ability to bind different metals accounts for very different electronic properties, thus hampering the task to describe their properties with general trends.²⁸

I.2.2 N-heterocyclic carbenes as platform for new ligand scaffolds

N-heterocyclic carbenes were first discovered back in the 1968, by Öfele¹⁴ and Wanzlick,¹⁵ almost simultaneously. However, the exploit of NHCs as possible ligands started more than 20 years later, when Arduengo isolate the first organic NHC that was stable enough to be stored.¹⁷ The isolation of this stable NHC promoted an intense research for the isolation of new NHCs with different heteroatoms and ring sizes and have allowed the coordination of the NHCs to almost all transition metals, increasing exponentially their use (Figure I.2).^{19,29,30} The high performance of NHCs in some catalytic systems, such as the Grubbs second-generation olefin metathesis catalyst³¹ or Pd-NHC catalyst for cross-coupling reactions³² have let a huge increase in the interest of these compounds that even some precursors have been patented and are commercially available.

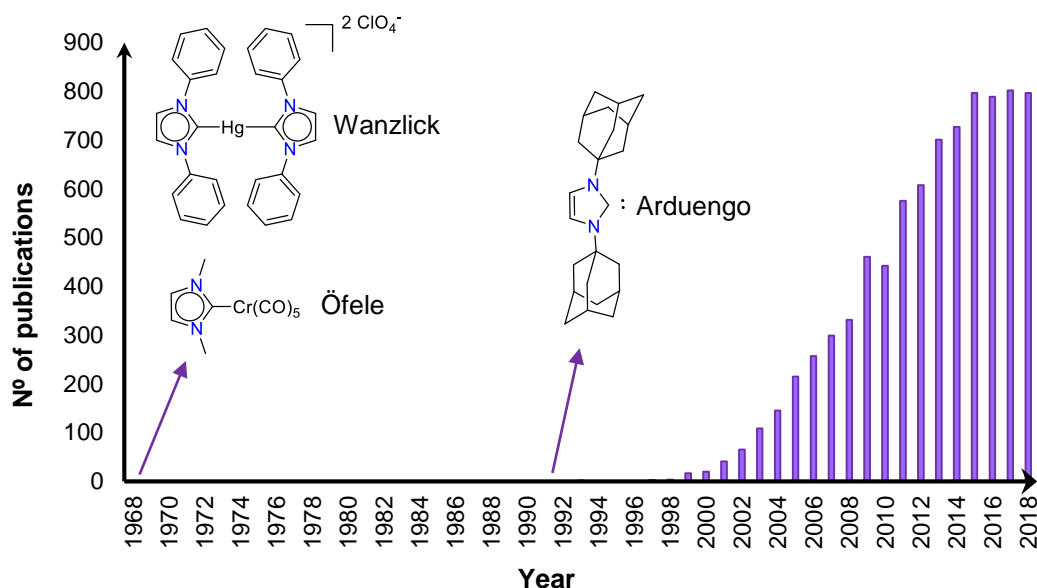
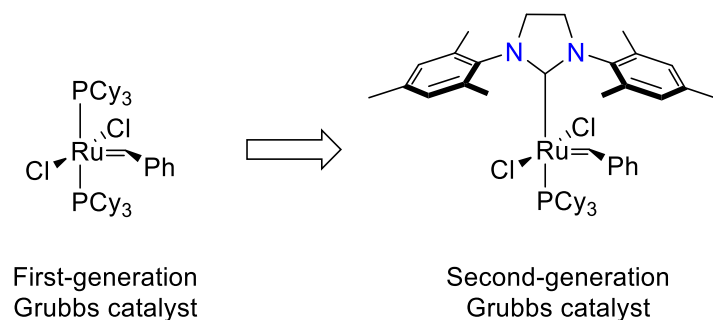


Figure I.2. Number of publication of N-heterocyclic carbenes per year. Values obtained from ISI WoS (Search criteria used: N-heterocyclic carbene).

I.2.2.1 Analogies and differences with phosphine ligands

In the beginning, NHCs were considered as tertiary phosphine mimics, because both are monodentate 2-electron donor ligands. However, over the years, NHCs have gained more attention and have become often a better choice than phosphines.

Although NHCs and tertiary phosphines are both σ -donor ligands, it has been reported by Nolan and coworkers³³ that NHCs are stronger σ -donor ligands, even compared to the most basic phosphine. This stronger donation ability can generate strong M-C bonds, which are less prone to dissociation, thus generating catalyst with high turnover numbers. An example of this behavior is the evolution from first to second generation Grubbs catalyst, in which the substitution of one of the phosphine ligands for a NHC ligand lead to a more robust catalyst with better performance (Scheme I.8).³¹



Scheme I.8. Differences between first- and second-generation Grubbs catalyst.

In terms of steric properties, NHC and phosphine ligands are completely different. Back in 1977, Tolman described a method that allowed the measurement of the volume and the geometry of the phosphine ligands in a metal coordination sphere, based on the assumption that phosphines can be described as cone shape ligands (Figure I.3, right).³⁴ With this shape, the substituents of the phosphine points away of the metal center, decreasing the steric impact in the environment of the metal. In contrast, NHCs adopt a fan or an umbrella shape, in which the nitrogen-substituents adjacent to the carbenic carbon are pointing towards the metal center, generating a more sterically demanding active center (Figure I.3, left). The NHC geometry is more difficult to determine rather than phosphines, since the Tolman method does not fit with NHC shape. For this reason, a different methodology was described in order to compare the sterics between phosphines and NHCs.³⁵

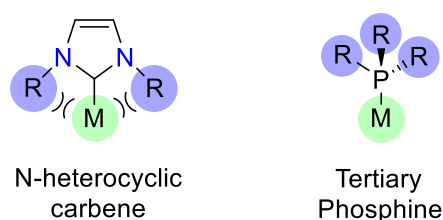


Figure I.3. Steric impact of N-heterocyclic carbenes and tertiary phosphines to the metal center.

Another difference between NHCs and phosphines is their synthesis. While tertiary phosphines are difficult to prepare and difficult to modify its steric and electronic properties, NHCs are easier to modify thanks to the large number of synthetic routes available.³⁶ Moreover, in phosphine ligands, a change in the P-substituents causes a change in the steric and also in the electronics of the ligand, because the substituent is directly attached to the donor atom. On the contrary, in NHCs, since the substituents are attached to the adjacent N-atom from the donor, the electronic and steric parameters can be modified separately.

I.2.2.2 Different classes of N-heterocyclic carbene ligands

As a result of the extensive research in the exploration of new NHCs, very different structures, differing from the original Arduengo's carbene with the imidazol-2-ylidene structure (Figure I.4, **A**), have been prepared. Different α -heteroatom and ring structures have been modified (Figure I.4, **B-E**). Also one or both α -heteroatom of the structure have been substituted for a carbon center, leading to ligands with reduced heteroatom stabilization, thus generating less stable carbene in its free form (Figure I.4, **F-K**).

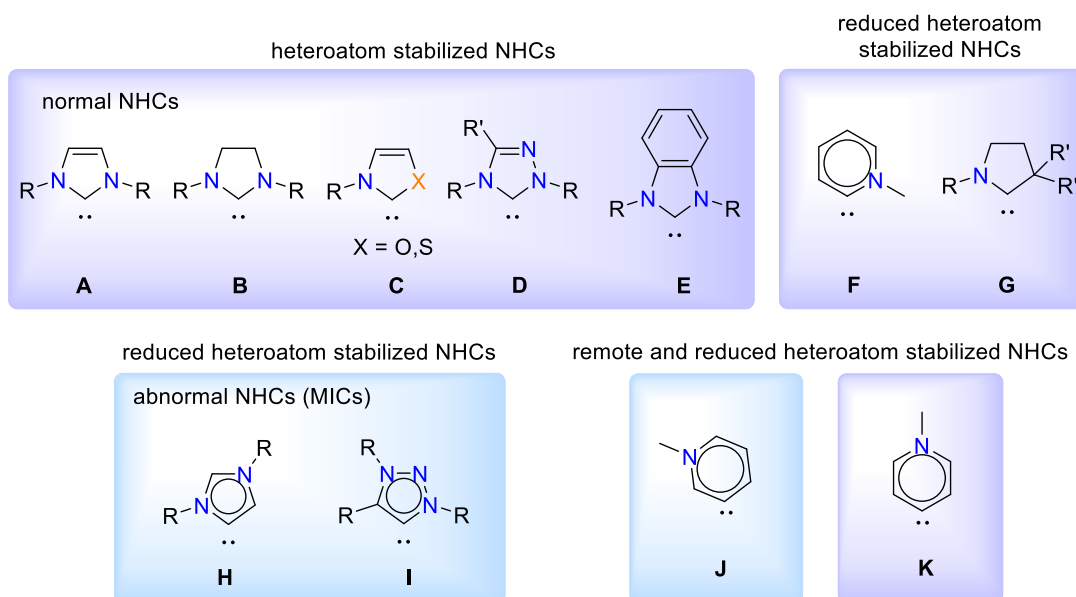
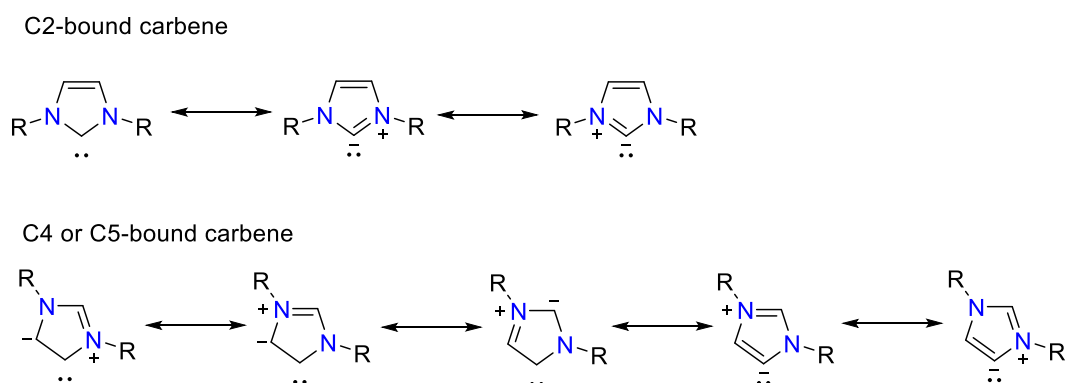


Figure I.4. Collection of different NHCs and its assignment to the different classes of these ligands.

As a consequence of these modifications, structures that do not totally fulfill in the initial description of carbenes required for a new nomenclature. The first disagreements started in the isolation of imidazolidene complexes with different coordination mode in the ring, from the original C2 coordination (Figure I.4, **A**) to C4 (or C5, depending on the N-substituents) coordination (Figure I.4, **H**).³⁷ This type of binding mode provided access to a different type of NHCs in which only one heteroatom is placed in α -position to the carbene center. Consequently, no neutral canonical resonance form of the carbene can be drawn, unlike typical NHC (Scheme I.9).



Scheme I.9. Resonance structure of C2 and C4 carbenes.

This special characteristic required a new naming for those compounds, that were named as *abnormal* NHC (aNHC) while the original ones were called *normal* NHC (nNHC). However, since the description of the aNHCs fit well with the IUPAC description of mesoionic compounds,³⁸ those ligands are also named as mesoionic compounds

(MICs). Nowadays, the name *abnormal* or MIC has been extended to all those carbene compounds that cannot be represented by any neutral resonance form.

Another nomenclature used in these kind of compounds is the *remote* NHC (*r*NHC). This nomenclature refers to those compounds in which no heteroatom is adjacent to the carbene center, for this reason those are the less stable compounds. These *r*NHCs can be either *n*NHCs or *a*NHCs depending on their resonance structure (Figure I.4, J-K).

Apart from different NHC structures, different architectures of chelating ligands have been also nicely described, which includes coordination of bis-, tris- and tetra-NHCs or structures with N or O donor atoms³⁹, such as the diamine-bridged bis-NHC iron complex of Glorius and coworkers, which is capable to perform the hydrosilylation of acetophenone (Figure I.5, left)⁴⁰; or the phenolate/NHC ligand of Meyer and coworkers, coordinated to different metal centers (Figure I.5, right).⁴¹

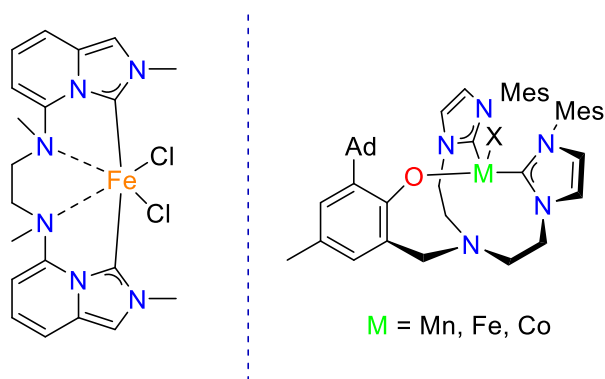


Figure I.5. NHC chelating structure of Glorius (left) and Meyer (right).

I.2.2.3 Comparison between *n*NHC and *a*NHC

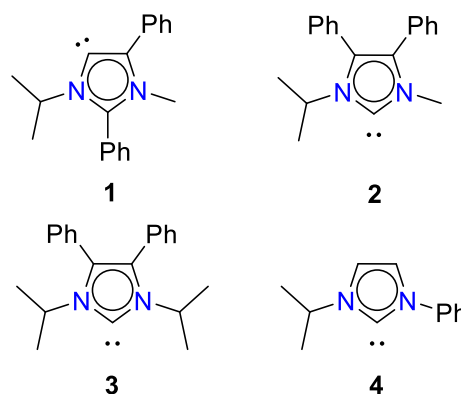
Many studies have been carried out in order to disclose the electronic differences in the M-C bond between *normal* and *abnormal* NHCs. Among all of them, a general conclusion can be extracted: *a*NHCs are stronger σ -donor ligands than its *normal* counterparts. Different techniques have been used to demonstrate their differences in the σ -donor ability. In 2004, Crabtree⁴² synthesized different Ir(I)(CO)₂(NHC) complexes *abnormally* and *normally* bound, and compared their $\nu(\text{CO})$ value to determine the donation properties of the NHC ligands, as it was proposed by Tolman³⁴ back in the seventies. The Tolman electronic parameter (TEP) is based on measuring the IR stretching frequencies of M(CO) complexes. Carbonyl ligands are very good π -acceptors and have a useful IR band between 1800-2200 cm^{-1} , which can be easily identified without the contamination of other vibrations of the molecule. A strongly donating ligand would increase the electron density in the complex and enhance the π -backdonation to

the carbonyl ligand. This enhancement will generate a weaker CO bond, thus lowering the stretching IR value. For this reason, lower values of $\nu(\text{CO})$ are correlated to stronger donating properties of the neighboring ligand.

Crabtree reported $\nu(\text{CO})$ values for a range of different NHC complexes and compared them, showing that C5-bound NHC ligand was a more donating ligand than C2-bound complexes, by the presence of lower $\nu(\text{CO})$ values (Table I.1).

Table I.1. $\nu(\text{CO})$ values of different Ir(NHC) complexes.

Ligand	$\nu(\text{CO})$ (cm^{-1})	$\nu_{\text{av}}(\text{CO})$ (cm^{-1})
1	2045	2003
2	2059	2017
3	2061	2017
4	2061	2019
PCy3	2072	2028



Albrecht proposed in 2010 that ^{31}P -NMR was also able to determine the donor power of different NHCs.⁴³ He claim that the more basic carbene ligands, suffers a shift of the δ_{p} values to lower field. In this regard, he reported different Pd(NHC) complexes with their corresponding δ_{p} , which suggests that *n*NHCs are weaker donor ligands and that pyrazol-4-ylidene was the ligand with more donating ability (Figure I.6). He corroborates their results with previously computed TEP for those ligands.⁴⁴

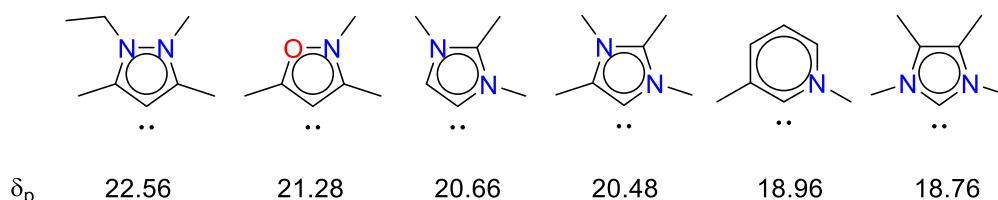
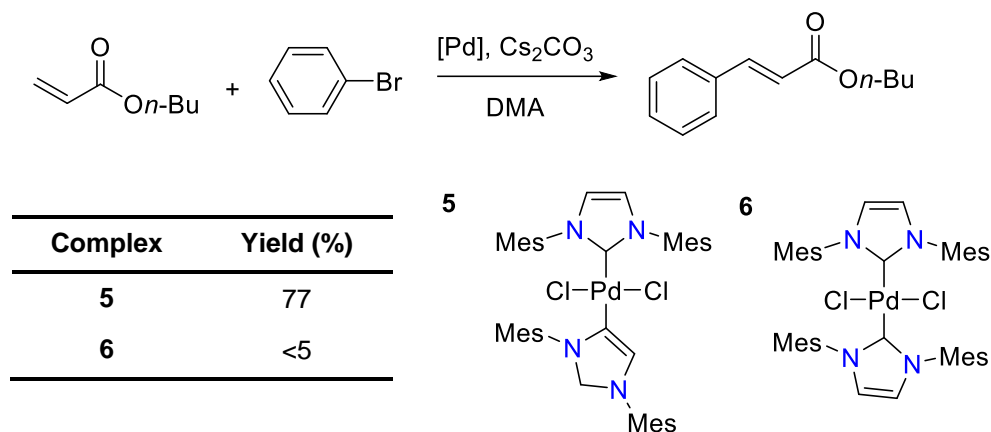


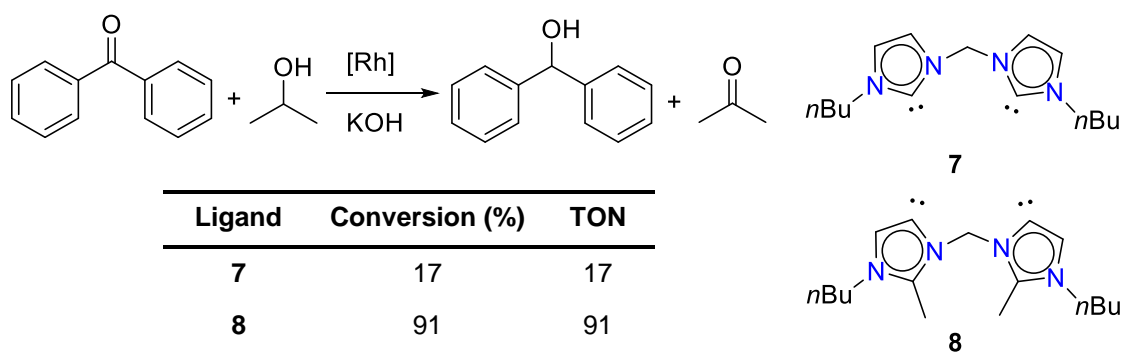
Figure I.6. Different NHC ligands and its δ_{p} value.

These differences in the donor abilities of the ligands can be translated into a better performance in some catalytic reactions. In 2004, Nolan reported the first example of a complex containing two NHC moieties, one C2-bound and the other C4-bound.⁴⁵ This palladium complex proved to be effective in cross-coupling reactions, even more reactive than the analog with the two carbene C2-bounded (Scheme I.10).



Scheme I.10. Pd catalyzed Heck Reaction with C2 and C4 bound NHC complexes. Reactions performed 1 mmolar of bromobenzene, 1.6 equiv. of butyl acrylate and 2 equiv. of Cs_2CO_3 , at 120°C for 7 hours.

In 2008, Albrecht and coworkers reported that C4-bound Rh complexes are better in catalytic transfer hydrogenation of benzophenone rather than C2-bound Rh complexes, attributed to the better donor abilities of the former (Scheme I.11).⁴⁶



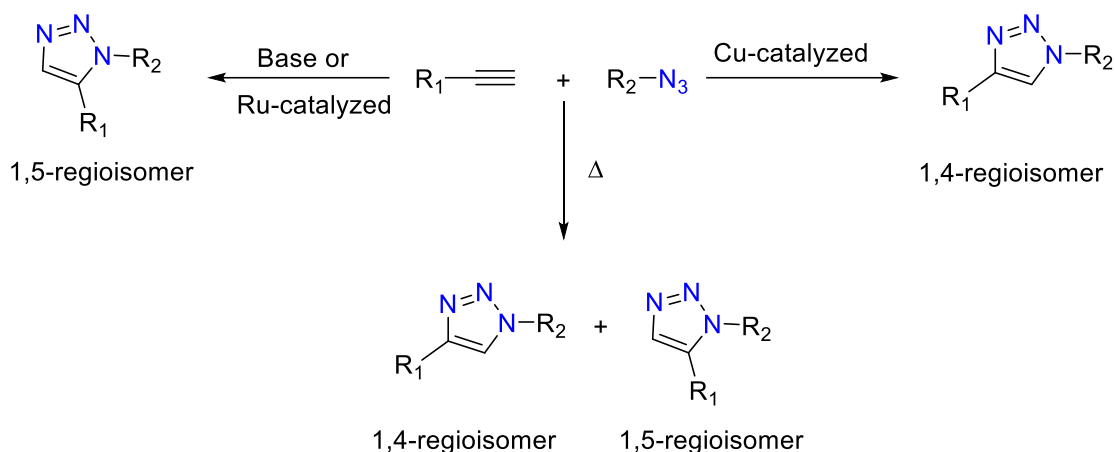
Scheme I.11. Rh catalyzed transfer hydrogenation with aNHC and nNHC as ligands. Reaction performed at 1mmol of benzophenone, 5 mL of $i\text{PrOH}$, 100 μmol of base, in DCM at reflux temperature for 2h.

However, the strong donation properties of the aNHCs does not mean that they are always better catalyst than nNHC. For example, very recently Toste described a nice example of migratory insertion of carbenes in a gold(III) center, using a large library of different NHCs.⁴⁷ Among them, bulky Arduengo's NHC and cAAC ligand were the most efficient catalysts, in detriment of aNHC ligands.

I.2.2.4 1,2,3-triazolylidene ligands

1,2,3-triazolidene containing compounds are a class of molecules that have attracted much interest in the last years. Their easy synthesis and their versatile properties have made them perfect candidates for different applications such as ionic liquids, organocatalysis and carbene ligands among others.⁴⁸

The extended use of those compounds started in 2002, when the catalytic version of a [2+3] cycloaddition of an alkyne and an azide using copper as catalyst (click reaction) allowed the isolation of only one 1,2,3-triazole regioisomer (the 1,4-regioisomer),^{49,50} while the non-catalyzed version gave mixture of two isomers (Scheme I.12). Years later, the isolation of the other isomer was accomplished using either ruthenium or base as catalyst.^{51,52} Those catalytic systems allow the synthesis of different substituted 1,2,3-triazoles with very simple procedures and work-ups, with high yield and selectivity.



Scheme I.12. Different procedures for the synthesis of 1,2,3-triazoles.

Focusing in our context, for their use as carbene ligands, an extra step is needed to synthesize the triazolium salt, where the alkylation of the N3 position takes place using an electrophile as an alkyl halide or alkyl triflate. However, for the introduction of an aryl substituent in that position, a different procedure should be used, which implies the cycloaddition of triazenes with an alkyne.⁵³

1,2,3-triazolylidene carbene ligands are a class of *a*NHC with reduced heteroatom stabilization (I, Figure I.4), thus its isolation as free carbenes is complex. Nevertheless, no dimerization product of 1,2,3-triazolylidene carbenes have been reported, suggesting that one of the most common pathways of carbene decomposition was disfavored for those kind of compounds.⁵⁴ In 2010, Bertrand and coworkers used this advantage to isolate in free form the first 1,2,3-triazolylidene carbene ligands.⁵⁵ Bulky 2,6-diisopropylphenyl (Dipp) substituent in N1 position was used to ensure a better stabilization in free form. The compounds were achieved with a straightforward synthesis including a [2+3] cycloaddition of an alkyne and an azide, followed by an alkylation of the N3 position by methyl or isopropyl trifluoromethanesulfonate and a final deprotonation of the carbonic proton using as base either potassium bis(trimethylsilyl)amide or potassium tert-butoxide (**9**, Figure I.7). The formation of the free carbene ligands was confirmed by

$^1\text{H-NMR}$ spectroscopy and X-Ray analysis. Those compounds were stable at room temperature for few days, ensuring their easy handling.

From that moment on, other free 1,2,3-triazolylidene carbene ligands were isolated. The same group reported a year later the synthesis of bis-carbene ligands with less bulky groups in the N1 position such as phenyl substituents, showing their good stability, although they are sensitive to oxygen and moisture (**10**, Figure I.10). They confirm their formation also by X-Ray diffraction and $^1\text{H-NMR}$ and $^{13}\text{C-NMR}$ spectroscopy.⁵⁶ In 2016, the group of Matsubara isolated the first tridentate bis-aNHC (**11**, Figure I.7).⁵⁷ And a year later, Bezuidenhout and coworkers described the isolation of 1,2,3-triazolylidene carbene ligated to a ferrocene structure (**12**, Figure I.7),⁵⁸ both also characterized by $^{13}\text{C-NMR}$ spectroscopy and X-Ray diffraction.

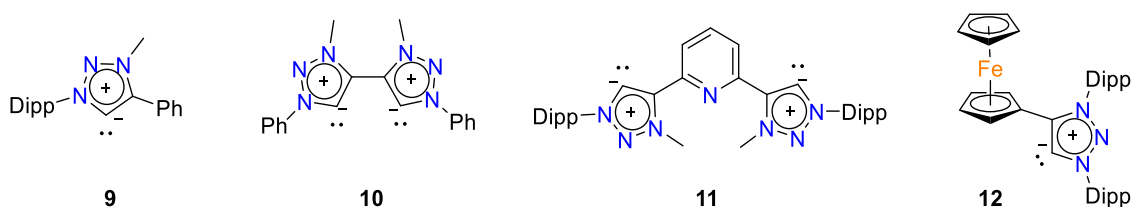


Figure I.7. Isolated free 1,2,3-triazolylidene carbenes.

The synthesis of 1,2,3-triazolidene carbene metal complexes can be achieved through different methodologies. Depending on the metal of choice, different methodologies may be needed.⁵⁹

The isolation of those previously mentioned free aNHCs ligands is a good starting point for the synthesis of metal carbene complexes, just by coordination of the metal precursor to the previously isolated free carbene. This methodology has been widely used either with the isolation of the carbene in its free form or in situ preparation of the compound in presence of the triazolium salt, a strong base (usually KHMDS, $\text{KO}t\text{Bu}$ or $\text{NaO}t\text{Bu}$) and the metal precursor, all in a one pot reaction. This methodology has been applied to first, second and third row transition metals.

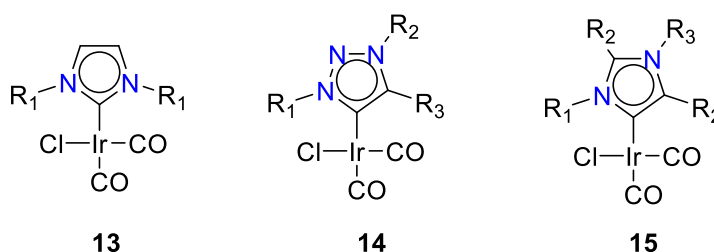
The most used methodology in this field is the transmetalation from a silver complex, usually synthesized by the reaction of the triazolium salt with Ag_2O . The silver complex is most of the times generated in situ and its formation is detected by $^1\text{H-NMR}$ spectroscopy, however, some silver complexes have been structurally characterized before transmetalation.^{60,61} After the formation of the silver complex, the metal precursor is added to induce the carbene transfer. The best metal precursors are dimeric species that can undergo bridge-cleavage or metal complexes with labile ligands, including halides as labile ligands, since the formation of the AgX salt as side product is

thermodynamically favorable. This methodology has been employed for the synthesis of mainly second and third row transition metals complexes.

A less used methodology is the direct metalation of the triazolium salt, using a metal precursor that contains a sufficiently basic ligand, such as $[\text{Pd}(\text{OAc})_2]$ or $[\text{M}(\text{COD})(\text{OR})]$. This procedure has been used for the synthesis of Pd, Rh and Ir complexes. However, this methodology suffers from selectivity problems.^{62,63}

The large number of different complexes reported allows the systematic study of their electronic properties. As mentioned before, 1,2,3-triazolylidene are *a*NHCs, and their donation properties have been compared to *n*NHCs, resulting in a higher donation ability than their normal counterpart. This study can be also done comparing specifically for 1,2,3-triazolylidene complexes with different imidazole-2-ylidenes complexes. The main measurement used to determine the donor properties is by comparison of the CO stretching vibrations of the $\text{M}(\text{CO})(\text{NHC})$ complexes, as mentioned before, using the Tolman's method.³⁴ Different complexes have been synthesized and their CO stretching frequencies have been studied over the years, allowing an easy comparison between them. For example, in the comparison of Ir complexes, C2-bound Arduengo-type carbenes (**13**, Table I.2) show slightly higher values of the CO stretching ($2024\text{-}2020\text{ cm}^{-1}$) than triazolylidene complexes (**14**, Table I.2; $2020\text{-}2018\text{ cm}^{-1}$), suggesting a better donor ability of the latter, although in some particular cases the CO stretching values are the same (**13f**, **13g**, **14a**, Table I.2). However, the lowest value is achieved by the abnormally bound 4-imidazolylidene (**15**, Table I.2). Different substituents in the triazolium structure, either on the adjacent position of the carbene or in the N-groups, does not lead to a dramatic effect in the donation properties, only a moderate effect is observed (**14a-14e**, Table I.2). Although a general tendency can be observed in the donation properties, subtle differences between different examples are observed.

Table I.2. Comparison of CO stretching frequencies between different $\text{Ir}(\text{CO})(\text{NHC})$ complexes.



Complex	R ₁	R ₂	R ₃	$\nu(\text{CO})_{\text{av}}$ (cm ⁻¹)
13a ⁶⁴	Dipp	-	-	2024
13b ⁶⁴	Mes	-	-	2023
13c ⁶⁴	Cy	-	-	2023
13d ⁶⁴	^t Bu	-	-	2022
13e ⁶⁴	Ad	-	-	2022
13f ⁶⁵	4-tolylmethyl	-	-	2020
13g ⁶⁵	<i>n</i> -butyl	-	-	2020
14a ⁵³	Dipp	Dipp	OEt	2020
14b ⁶⁶	Mes	Me	Mes	2019
14c ⁶⁶	Dipp	Me	Dipp	2019
14d ⁵⁵	Dipp	Me	Ph	2019
14e ⁵³	Dipp	Dipp	Dipp	2018
15 ⁴²	ⁱ Pr	Ph	Me	2003

The same trend of donation properties can be obtained comparing the CO stretching values of Rh(CO)(NHC) complexes, where 1,2,3-triazolylidene ligands ($\nu(\text{CO})_{\text{av}} = 2027\text{-}2035 \text{ cm}^{-1}$)⁶⁷⁻⁶⁹ are more donating than normal 2-imidazolylidenes ($\nu(\text{CO})_{\text{av}} = 2035\text{-}2044 \text{ cm}^{-1}$)⁷⁰, yet less donor than abnormally bound 4-imidazolylidene ($\nu(\text{CO})_{\text{av}} = 2026 \text{ cm}^{-1}$).⁷¹

First row transition metal complexes

The synthesis of 1,2,3-triazolylidene metal complexes started in the early 2000s and it has experienced a large increase in the number of complexes that have been described. However, those complexes are mainly based on second and third row transition metals, leaving first row transition metals to account for less than 15% of the complexes described (Figure I.8).

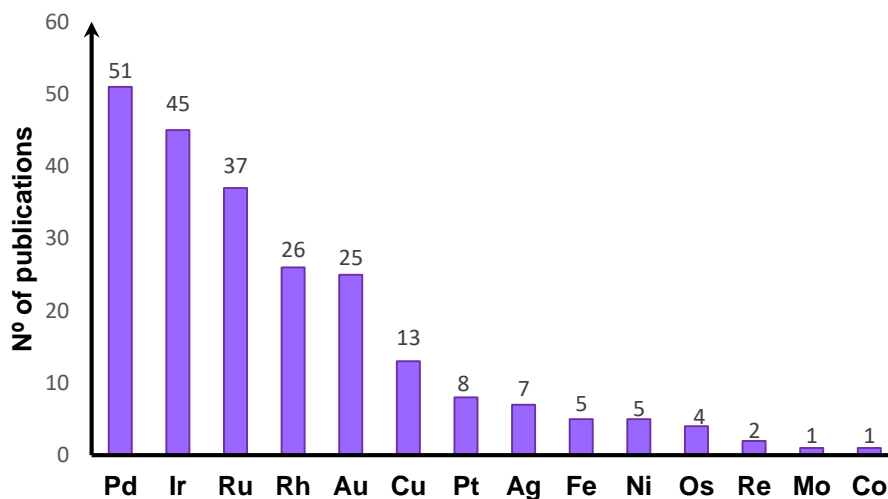


Figure I.8. Number of 1,2,3-triazolylidene metal complexes reported since 2003.

Only Fe, Co, Ni and Cu have been used in the isolation of 1,2,3-triazolylidene complexes, and with very few examples of each of them. Moreover, scarce ligand modification is observed in those complexes, mainly for the difficulty in their isolation. Main ligand modification comes from tuning the steric hindrance of the ligand in position N1 and C4, maintaining in all cases a methyl group in position N3 (Figure I.9, top).⁷²⁻⁸³ Some bimetallic complexes have been also described, using the same 1,2,3-triazolylidene structure, by combining an abnormal and a normal carbene ligand or by combining an abnormal carbene with a phosphine ligand (Figure I.9, middle).⁸⁴⁻⁸⁸ Some triazolylidenes structures have been coupled into a chelating scaffold, most of them based on N-donor ligands, but also an example of bis-carbene has been described using iron as metal center (Figure I.9, bottom).^{57,80,81,89-93}

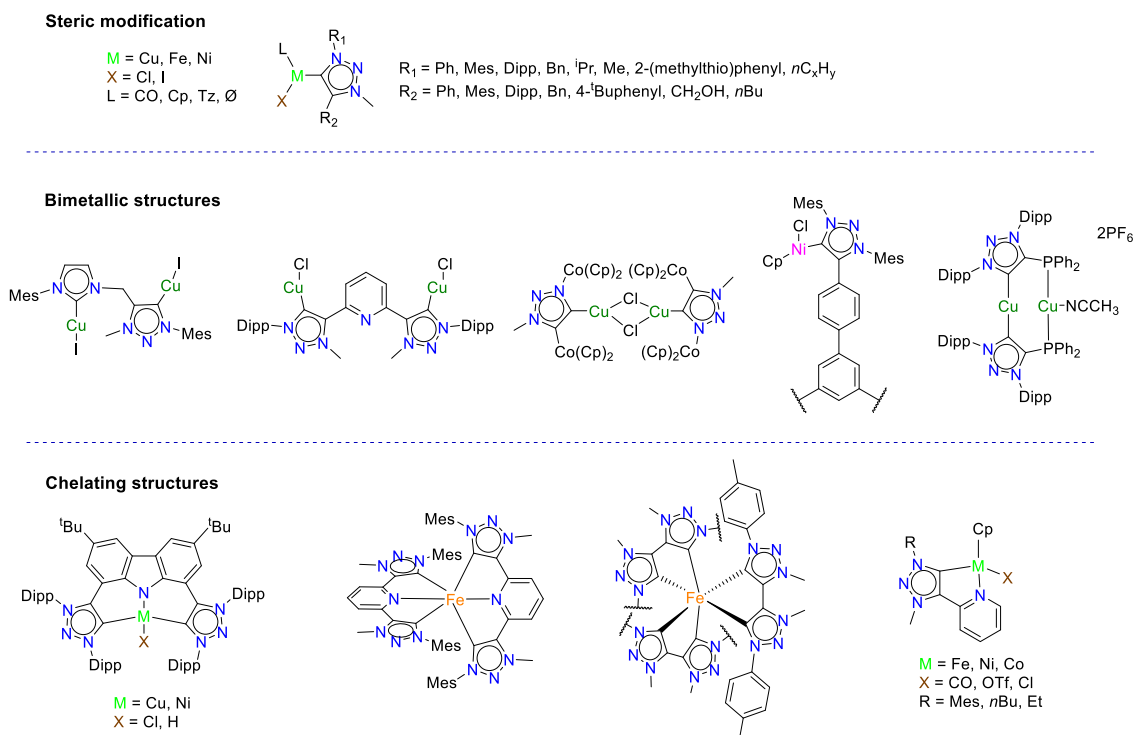


Figure I.9. Resume of all structures reported for first row transition metals.

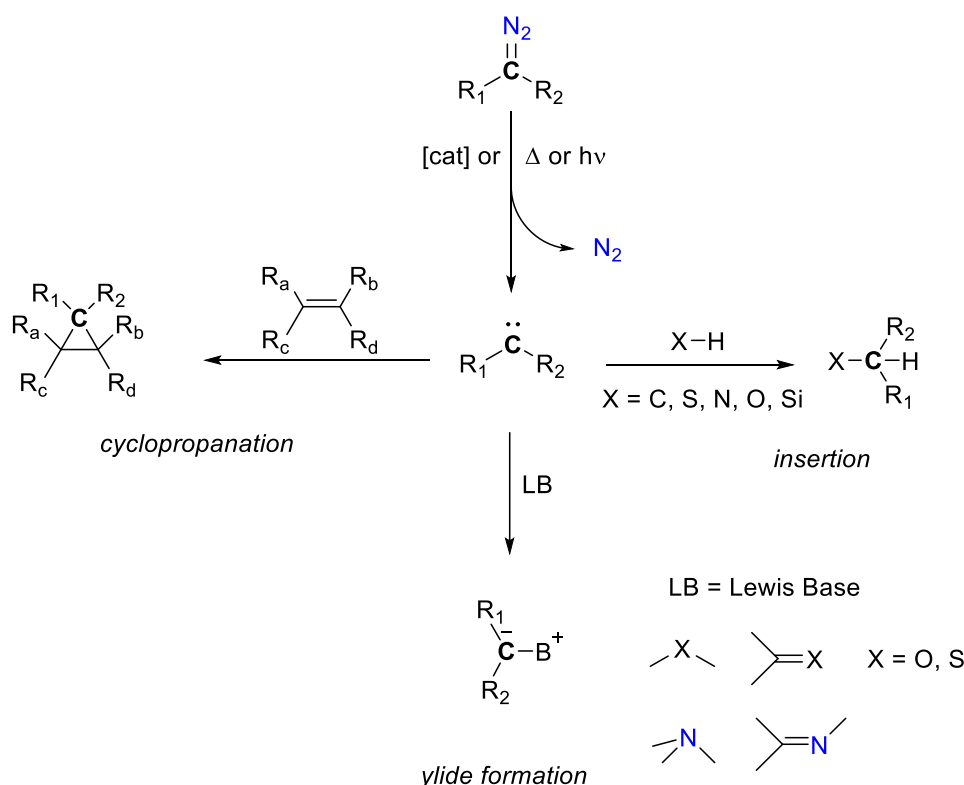
A high number of those complexes have some application. For example, some of the copper complexes are used as catalysts for click reactions,^{72,75,76,78} but also can have other applications such as catalytic hydrosilylation⁷³ and hydroboration⁸⁵ reactions among others. A chelating structure of an iron complex have shown very good performance as long-lived charge-transfer excited states complex in photoluminescence,⁹⁰⁻⁹² but also iron complexes can exhibit activity in hydrosilylation reactions.⁸⁰ Nickel complexes can perform some cross-coupling reactions⁸² as well as hydrosilylations⁸¹ and oxidation of cyclohexane with moderate reactivity.⁸³ And the only example of a cobalt complex showed good performance for electrocatalytic H₂ production.⁹³

I.3 Carbenes as powerful intermediates in organic synthesis

Carbene intermediates have been present in organic synthesis since the beginning of the 20th century. The first example was reported in 1903, when Buchner described the cyclopropanation of toluene and styrene, using ethyl diazoacetate (EDA) as carbene precursor, generated by thermal decomposition.^{4,5} Three years later, Ray and coworkers discovered that EDA can also be decomposed in the presence of a metal.⁹⁴

Since those early results, carbene transformations have been widely used for their potential in forming new bonds in an efficient manner. Along all these years, diazo compounds have been the preferred choice for carbene formation because of their easy preparation and their “green” behavior, as N_2 is the only by-product after the generation of the carbene intermediate. However, some diazo compounds are associated to some safety hazards, because they can be toxic and even explosives. For example, aliphatic diazoalkanes are extremely unstable and should be handled at low temperatures and low concentrations. Nevertheless, they can be used as carbene transfer reagents in a safer way if they are generated in situ, before the formation of the carbene intermediate. On the contrary, diazocarbonyl compounds are highly stable and safer. For this reason, they are commonly used in carbene transformations, even in large scale reactions.⁹⁵

Starting from the diazo compounds, carbenes can be generated photochemically, thermally or in the presence of a transition metal. The carbene intermediate formed can undergo different reactivities, such as cyclopropanation in double and triple bonds, insertion to different X-H bonds, and the formation of ylide compounds that further react to form more stable products (Scheme I.13). A very extensive review of the diazo compounds has been recently published resuming the reactivities of those compounds.⁹⁶



Scheme I.13. Schematic representation of the different transformations that diazo compounds can perform.

Among those reactions, the addition to alkenes to promote cyclopropanation reactions are the first and the most studied reactions of carbenes in terms of mechanistic

elucidation and synthetic applications. Nevertheless, the transformations that attracts also a lot of interest and its development is increasing over the years is the C-H bond insertion reaction.

I.3.1 C-H bond functionalization by carbene insertion

The replacement of a non-activated C-H bond for a more reactive one by an efficient and selective transformation and with minimal waste has become one of the more important challenges in synthetic chemistry. This transformation allows the construction of complex and valuable molecules from available, cheap and simple feedstock. In the beginning, the main problem of this transformation arose from the high bond dissociation energy (BDE) of the C-H bonds of different molecules (Figure I.10).⁹⁷

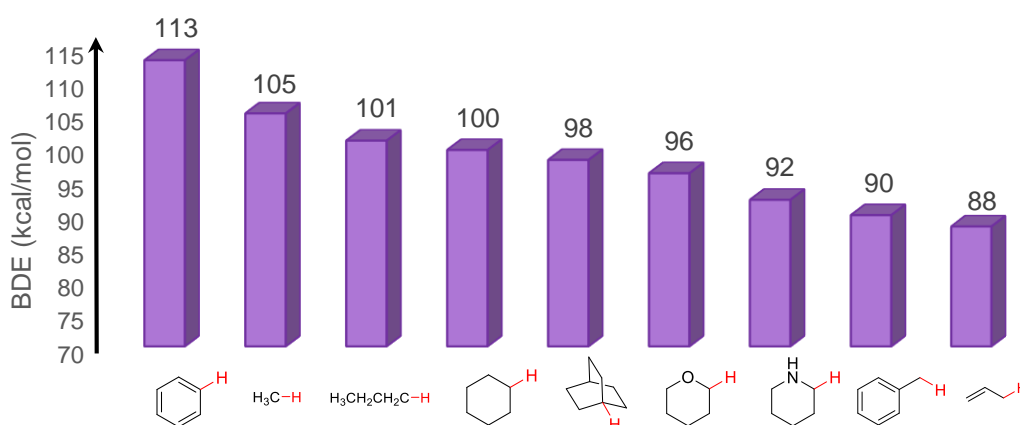


Figure I.10. Resume of the BDE of some organic compounds.

Compounds with the highest BDE values are those with no activating groups adjacent to its position, such as benzene or primary and secondary alkanes, in which a barrier of more than 100kcal/mol has to be overcome to functionalize them. Although C-H bonds have always been considered inert, its functionalization was early achieved and through the years multiple systems have been described and reviewed.^{98,99} Nowadays, the main challenge relies on the selective functionalization of those bonds using simple methodologies and with high atom economy. Those characteristics can be achieved by the use of transition metal complexes. And specifically for this work, we are going to focus on C-H functionalization by carbene insertion reactions.

Although copper salts were firstly reported to promote C-H functionalization, low yields or limitation to very rigid structures diminished the impact of the founding.^{100,101} The major breakthrough on this transformation started in 1981, when Teyssié and coworkers described the functionalization of alkanes using EDA, catalyzed by Rh(II) carboxylate complexes in an intermolecular reaction.¹⁰² A year later, two groups took

advantage of the better performance of intramolecular over intermolecular reactions, to construct favored five-member ring molecules in a regioselective transformation using diazocarbonyl compounds.^{103,104} These works showed up the efficiency of Rh(II) complexes in carbene transfer reaction and started a huge interest on those complexes that have led to a large number of publications describing systems with high regioselectivity and stereoselectivity in either inter- and intramolecular reactions.¹⁰⁵⁻¹⁰⁷

Nevertheless, other metals have proved to be useful. As initiators of C-H bond functionalization by carbene transfer reactions, copper complexes have been very utilized over the years. Nice results using Cu(I) complexes with chiral bis(oxazoline) ligands gave excellent enantioselectivities in cyclization reactions^{108,109} and applications to functionalize alkanes, aromatics and even methane using trispyrazolylborate ligands have also been described by the group of Pérez and coworkers.¹¹⁰⁻¹¹² The same group also have exploited the use of those ligands and NHC ligands for the expansion of the reactivity towards coinage metals (silver and gold).¹¹³

I.3.2 Iron complexes in carbene insertion

Most of the work done in carbene insertion into C-H bonds is based on the use of expensive precious metals complexes as catalysts. For this reason, there is a need to evolve this chemistry towards more environmentally friendly complexes and here is where iron appears to be a good option. Iron is much more abundant and biocompatible compared to precious metals, being involved in a number of biological processes.¹¹⁴ Although seminal work have been described using iron carbenes for C-H bond functionalization, their synthetic applications are limited. However, the promising results shows a huge potential for iron complexes to replace precious metals in these transformations in the long-term.

In 1977, Mansuy and coworkers described the isolation of the first iron-carbene complex upon the reaction of the metalloporphyrin (TPP)Fe^{II} with CCl₄ under reducing conditions.¹¹⁵ In that moment, the complex was characterized by elemental analysis and spectroscopic techniques, but a year later, crystalline material for X-Ray analysis was achieved, describing a carbene complex with an Fe-C bond distances of 1.83 Å.¹¹⁶ However, no C-H functionalization reactivity was reported for that compound. Only cyclopropanation reactions after photolysis was reported years later for those kind of compounds.^{117,118}

The first synthetic application of iron carbene for C-H bond functionalization was described by Helquist and coworkers. The cationic iron carbene complex

([Cp(CO)₂Fe=CH(SPh)]PF₆) previously described¹¹⁹ is competent to be added into an organic enol intermediate, to form a thioalkyliron compound, able to perform C-H bond functionalization for the construction of cyclopentyl rings forming fused systems.¹²⁰ The good performance of this procedure allowed its applications for the synthesis of a natural product.¹²¹ The main drawback of this procedure is the large number of steps needed, generating huge amounts of organic by-products, and the use of stoichiometric amounts of the iron carbene.

Focusing on the use of diazo reagents as carbene source, the isolation of an iron carbene complex from the reaction with a diazo compound (N₂CPh₂) was reported in 1997 using a macrocyclic ligand (tmtaa).¹²² The compound was characterized by NMR spectroscopy and X-Ray diffraction, observing an Fe-C distance of 1.794 Å, similar to previously described iron carbene, and assigning to the complex an Fe(II) center. Although the complex could have served as prove of the intermediacy of iron carbenes in cyclopropanation and C-H functionalization using diazo compounds, no reactivity was observed for that complex. The same authors, three years later reported the isolation of an iron carbene complex using a calixarene as supporting ligand and again diphenyldiazomethane (N₂CPh₂) as carbene source, in which its reactivity for C-H insertion was not described.¹²³

A great breakthrough was achieved by Che and coworkers when the first iron porphyrin carbene complex with no-heteroatom stabilization was achieved, which was the proposed intermediate in cyclopropanation reactions.¹²⁴ The reaction of the (TPFPP)Fe porphyrin with different diazo compounds N₂C(Ph)R (R = Ph, CO₂Et, CO₂CH₂CH=CH₂) allowed the isolation in pure form of the iron carbene complexes, although only crystals suitable for X-ray diffraction were isolated for the (TPFPP)Fe=C(Ph)₂, exhibiting an Fe-C distance of 1.767 Å. Stoichiometric amounts of those complexes promoted the cyclopropanation of styrene and the C-H bond functionalization of different substrates, such as cumene, cyclohexene and THF. The iron carbene complexes were assigned as Fe(II) in low spin state for their diamagnetic ¹H-NMR spectra. However, Mössbauer experiments suggested the presence of an iron center in high oxidation states, as it can be Fe(IV). The elucidation of the electronic nature of the iron porphyrin carbenes is still an ongoing debate that include experimental and computational studies.¹²⁵⁻¹²⁷

A different approach was used by Chirik and coworkers, who used a redox active ligand (^{Me}PDI) for the isolation of an iron carbene complex.¹²⁸ Crystalline material was isolated and its structure was determined by X-Ray analysis, showing an Fe-C bond of

1.936Å. The electronic nature of the iron center was determined by X-Ray diffraction, X-Ray absorption, Mössbauer and computational analysis, concluding the presence of an Fe(II) center. Although the complex was not useful for cyclopropanation reaction or C-H bond functionalization, carbene transfer to CO and aryl azides was quantitatively performed.

The last iron carbene complex isolated was described by Holland and coworkers, who used a Nacnac derivative ligand and (trimethylsilyl)diazomethane as carbene source.¹²⁹ The crystalline material was analyzed by X-Ray diffraction, showing Fe-C bond distance of 1.965Å. Their mössbauer experiments suggest the presence of an Fe(II) center. However, no reactivity was reported for that specie.

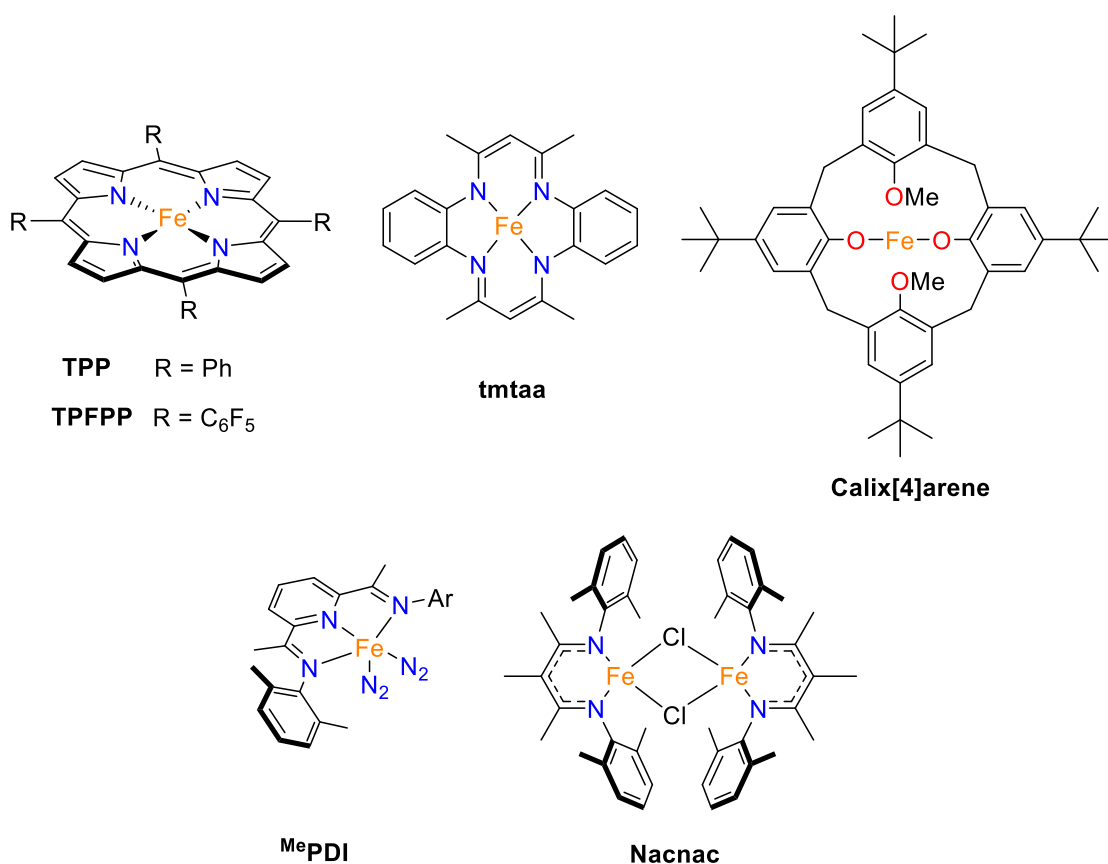
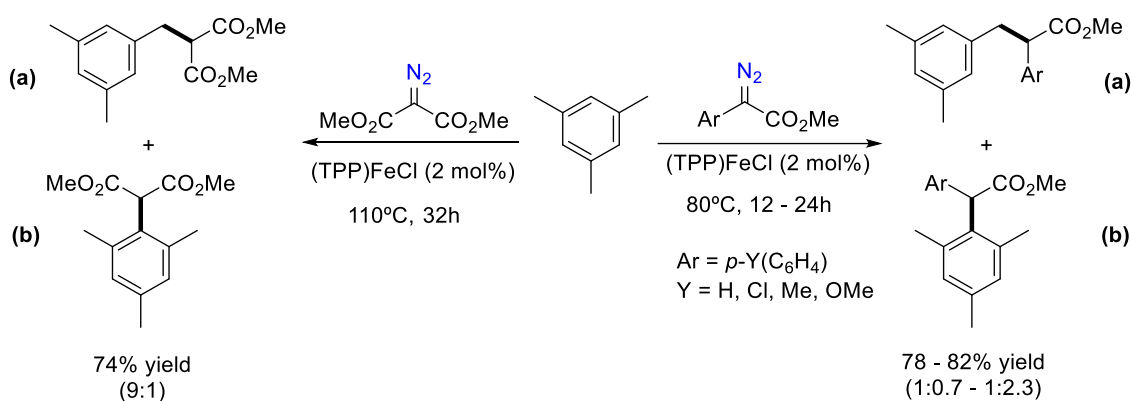


Figure I.11. Iron complexes structures used for iron carbene isolation.

In terms of catalytic performance of iron complexes, just few examples have been described. The first application of this transformation in a catalytic fashion was performed by porphyrinic ligands in 2008, when Woo and coworkers reported the functionalization of different alkane and aromatic substrates with (TPP)FeCl using different types of diazo acetates.¹³⁰ When dimethyl diazomalonate was used in toluene and *p*-substituted toluene, high reaction temperatures (110°C) and long reactions times (32-48h) were needed to promote Csp² and Csp³-H bond functionalization. The change of the diazo

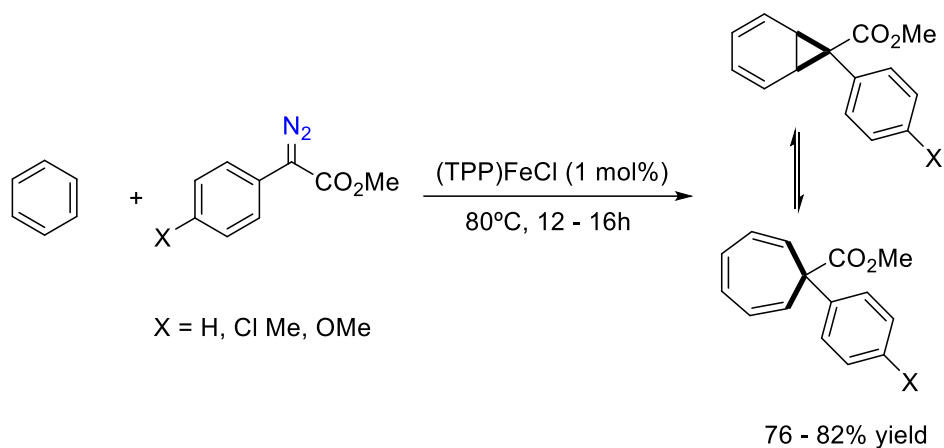
compound for different substituted methyl 2-phenyldiazoacetates, allowed the functionalization of non-activated cyclohexane, with lower reaction temperatures (80°C) and shorter reaction times (16-32h). Direct comparison of the two diazo compounds can be done in mesitylene functionalization, where the use of substituted methyl 2-phenyldiazoacetates allowed the isolation of the final product in higher yields and milder reaction conditions, although the selectivity is compromised since dimethyl diazomalonate showed higher preference for benzylic functionalization rather than methyl 2-phenyldiazoacetates (Scheme I.14).



Scheme I.14. Different performance in the functionalization of mesitylene with (TPP)FeCl with different diazo acetates.

Some mechanistic studies were also performed. First order rates with respect to the substrate were observed, suggesting that the rate determining step of the reaction is the N₂ extrusion and the subsequent carbene formation. The electrophilic nature of the carbene intermediate was measured by Hammett analysis and a KIE value of 1.97 suggest that after carbene formation, there is a H atom abstraction process.

The same authors a year later, reported that the use of the same catalyst and the same substituted methyl 2-phenyldiazoacetates but in presence of benzene did not give the C-H bond functionalization. Instead, the cyclopropanation of the aromatic ring takes place, generating a norcaradiene product, that opens to form a cycloheptatriene, in a fast equilibrium (Scheme I.15).¹³¹ These works show how changes in either the substrate or the diazo compounds can drastically change the reactivity and the selectivity of the carbene reaction.



Scheme I.15. Derivatization of benzene using (TPP)FeCl and diazoacetates.

The use of non-heme iron complexes for this transformation have been recently proved to be plausible and give rise to nice results. In 2011, Zhou reported the functionalization of N-protected indoles using cheap and commercially available $\text{Fe}(\text{ClO}_4)_2$ and TMEDA ligand (*N,N,N',N'*-Tetramethylethylenediamine) in the presence of different substituted methyl 2-phenyldiazoacetates at 60°C, achieving excellent yields. They also described the asymmetric version of this transformation, using chiral spirobisoxazoline ligands, resulting in good to excellent yields and up to 78% *ee*.¹³² Recently, the functionalization of the same N-protected indoles have been also reported using diazoacetone nitrile as carbene source and iron porphyrin as catalyst.¹³³

The use of the same iron salt, $\text{Fe}(\text{ClO}_4)_2$, and similar reaction conditions, but replacing the TMEDA ligand for bpmen ligand (*N,N'*-dimethyl-*N,N'*-bis(pyridin-2-ylmethyl)ethane-1,2-diamine), promoted the functionalization of cyclohexane and other cycloalkanes in good yields.¹³⁴

In the same year, in 2017, White and coworkers also reported the functionalization of $\text{Csp}_3\text{-H}$ bonds.¹³⁵ This specific work described an intramolecular reaction using sulfonate diazoesters. The system was able to functionalize benzylic and allylic positions, without any cyclopropanation product, giving from moderate to good isolated yields in mild reaction conditions.

Although a little bit out of this topic, it is worth mention the incredible goal achieved by Coelho and coworkers in the cyclopropanation of olefins, using an engineered cytochrome P450 in an enantioselective manner.¹³⁶ The possibility of those enzyme to promote cyclopropanation reactions opened the possibility of their engineering to perform C-H bond functionalization. In particular, Arnold and coworkers have recently described the functionalization of activated C-H bonds on benzylic, allylic and alkyl amino substrates using EDA with high yields and high enantiomeric ratios.¹³⁷

Chapter II

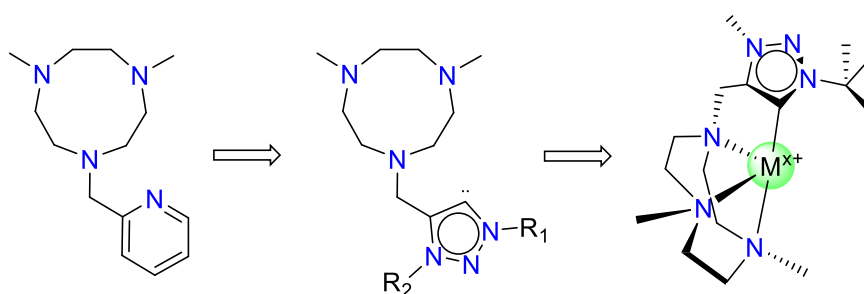
Objectives

The use of carbenes in synthetic organic reactions and in the synthesis of new organometallic complexes has exploded during the last decades. Their high reactivity in C-H bond functionalization reactions and the higher performance of some NHC based complexes compared to phosphine related complexes makes carbenes perfect candidates in the evolution towards more efficient systems in organic and organometallic chemistry.

In this regard, the search for green synthetic systems is one of the current challenges in chemistry. A way to succeed in this demanding task is by the use of abundant and environmentally friendly transition metals, such as iron or copper; two metals present in natural metalloenzymes.

Addressing these challenges, this thesis will be focused on development of new carbene based systems using first row transition metal complexes. Specifically, the synthesis of new organometallic complexes is targeted, as well as the catalytic functionalization of C-H bonds by carbene transfer reactions.

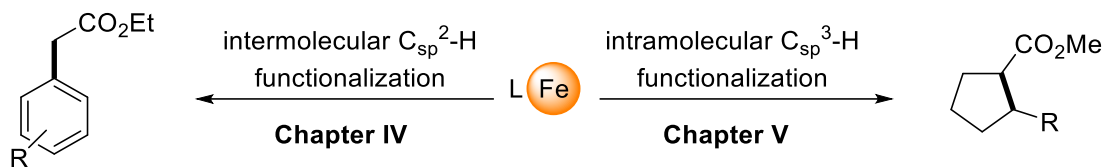
Chapter III will explore the synthesis of new NHC complexes. Our group has previously used aminopyridine based ligands for the development of complexes where metals in high oxidation states are stabilized. For this reason, taking advantage of the higher σ -donation properties of NHC, the objective is to construct a new ligand replacing the pyridine for a NHC moiety. The corresponding first row transition metal complexes will be synthesized and characterized and their electronic properties will be studied (Scheme II.1).



Scheme II.1. Schematic representation of the objective of Chapter III.

Chapter IV and **V** will be focused on the use of non-heme iron systems in carbene based organic transformations. **Chapter IV** will account for the selective intermolecular functionalization of non-activated aromatic substrates with commercially available ethyl diazoacetate. Reaction optimization will be performed and its mechanism will be disclosed. In **Chapter V**, the intramolecular functionalization of C_{sp^3} -H bonds will be

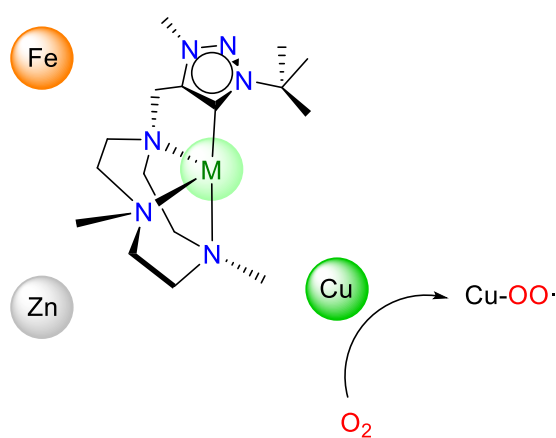
addressed, performing the reaction under mild reaction conditions, envisioning a key role of Lewis acid co-catalysts for the efficient activation of diazoester substrates.



Scheme II.2. Summary of the organic reactions performed in Chapter IV and V.

Chapter III

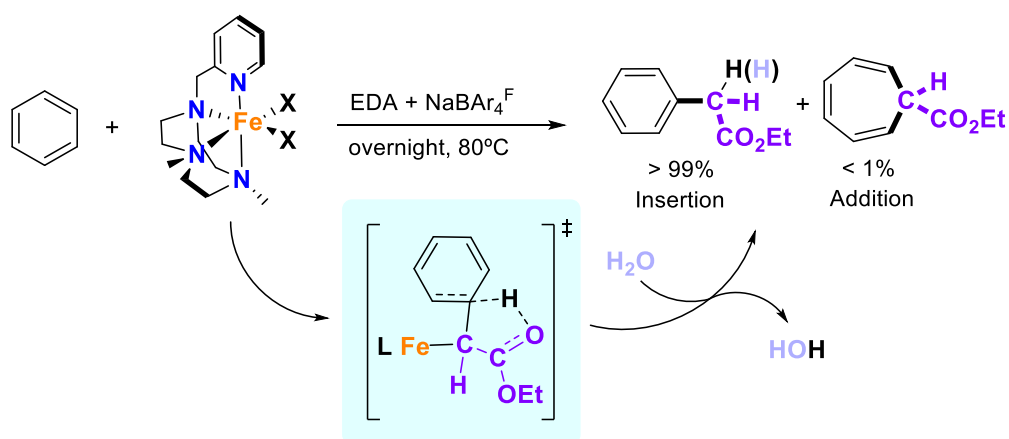
Synthesis of a hybrid tacn-NHC ligand and its related first row transition metal complexes



Article in preparation. Embargo until publication date

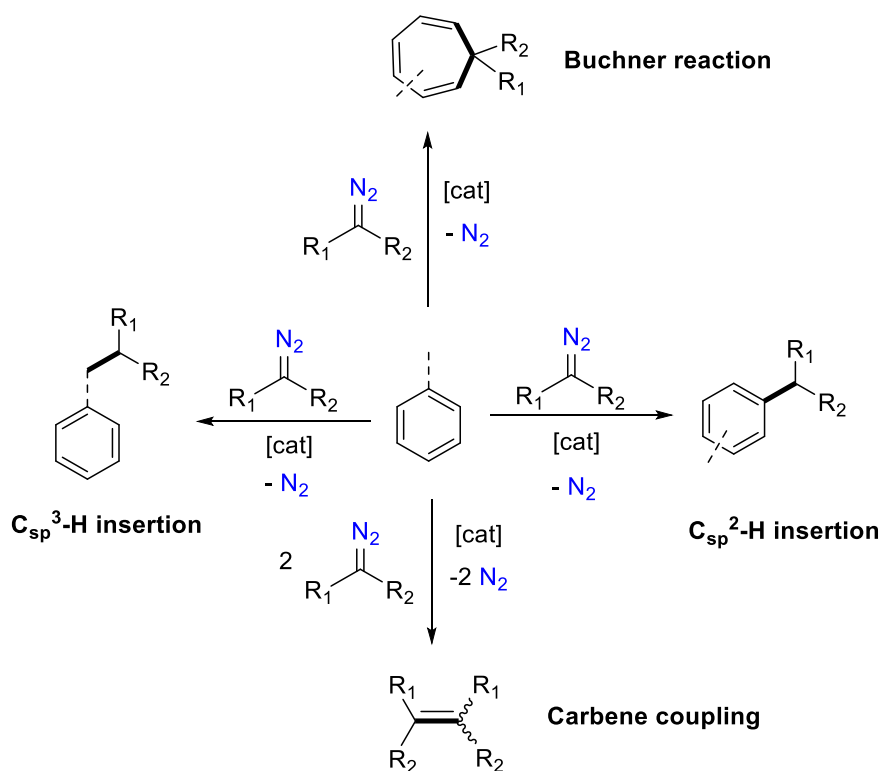
Chapter IV

Carbene insertion into C_{sp}²-H bonds catalyzed by non-heme iron complexes: catalytic and mechanistic insights



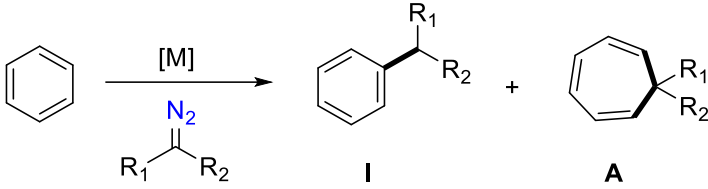
IV.1 Results and discussion

The formation of new C-C bonds through a carbene insertion reaction is an appealing strategy for the construction of complex molecules. In the case of benzene, which is a ubiquitous structure present in added-value compounds, its functionalization by carbene transfer reactions is a challenge due to the diversity of competing reactions that can occur: ring addition to the arene to form a 7 membered-ring (Buchner reaction), carbene dimerization to form olefins, insertion to C_{sp}²-H bonds and, in case of alkyl-substituted arenes, insertion into C_{sp}³-H bonds (Scheme IV.1).



Scheme IV.1. Different products in metal catalyzed (alkyl)-benzene functionalization by carbene transfer.

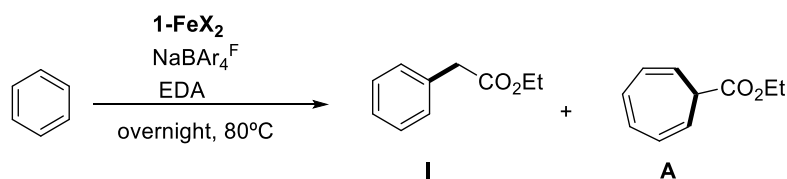
Up to now, since the presence of carbene coupling products can be diminished by different techniques such as slow addition of the diazo compound, the functionalization of non-activated benzene was only achieved as a mixture of insertion (I) and addition (A) products using rhodium, copper, silver and gold as metal catalysts (Table IV.1). The need for the improvement of this reaction encouraged us to study the functionalization of benzene in the decomposition of ethyl diazoacetate (EDA) in presence of iron catalysts, in order to determine their reactivity and selectivity.

Table IV.1. Described examples of metal-catalyzed carbene functionalization of benzene with their corresponding product ratio.


[M]	R ₁	R ₂	I (%)	A (%)
Rh ¹⁷⁶	CO ₂ Me	CO ₂ Me	8	77
Cu ¹⁷⁷	H	CO ₂ Et	30	70
Ag ¹⁷⁷	H	CO ₂ Et	5	95
Au ¹⁷⁷	H	CO ₂ Et	75	25

IV.1.1 Catalytic studies

A group of basic N-based ligands were investigated, since their scaffold have proven to be efficient in the stabilization of iron in high oxidation states and high valent iron carbene species were envisioned as the putative carbene transfer agents. Firstly, **1-FeX₂** (X = Cl or OTf) complexes were taken as starting point for the optimization of the reaction conditions. Previous screening performed by Gerard Sabenya showed that 80°C and NaBAR₄^F as halide scavenger and an overnight reaction were needed to achieve promising reactivity (Scheme IV.2).

**Scheme IV.2.** Decomposition of EDA with iron complexes in the functionalization of benzene.

The use of neat benzene as solvent under previously mentioned reaction conditions, was translated into low yield and low selectivity between insertion (**I**) and addition (**A**) products, either with triflate or chloride complexes (entry 1-2, Table IV.2). On the contrary, a mixture of benzene and dichloromethane 1:1 gave an impressive unprecedented selectivity toward the insertion product (entry 3-4, Table IV.2). The increase in selectivity and reactivity can be attributed to the higher solubility of the iron complexes in dichloromethane rather than benzene. Indeed, the chloride complex, which is less soluble in benzene than the triflate one, gave worst reactivity and selectivity when

neat benzene was used. This problem can be overcome adding dichloromethane in the reaction, which solubilizes completely both complexes giving similar results in the reaction.

Although an excellent selectivity towards the insertion product was achieved, the yield of the reaction remained moderate. To improve the yield, different amounts of NaBAR₄^F, acting as halide scavenger, were tested (entry 5-8, Table IV.2) revealing that 8 equivalents were needed to achieve high yields. The high amounts of NaBAR₄^F needed can be related into an equilibrium between the initial complex and the decoordination of the two halides, generating a dicationic complex, which will act as the active species. The more amount of NaBAR₄^F added, the more active specie accumulated. It can also be observed that the use of either chloride or triflate as counteranion in the initial complex lead to the same yield and same selectivity with the corresponding amount of NaBAR₄^F. This fact suggests that both complexes evolve to the same active species, which will be the complex with two empty positions at the iron center.

Apart from the good selectivity between insertion and addition products, only trace amount of diethyl maleate and diethyl fumarate (sub-products coming from carbene coupling) were detected in the GC, achieving the best system in terms of selectivity for the functionalization of non-activated benzene described up to date.

Table IV.2. Catalytic results of **1-FeX₂** complexes under different reaction conditions.

Entry	X [1-FeX ₂]	Solvent	Equiv. NaBAR ₄ ^F	Yield (%) ^b	Selectivity (I:A) ^b
1	Cl	neat benzene	2	14	57:43
2	OTf	neat benzene	2	31	87:13
3	Cl	dichloromethane:benzene	2	65	>99:1
4	OTf	dichloromethane:benzene	2	69	>99:1
5	Cl	dichloromethane:benzene	4	73	>99:1
6	OTf	dichloromethane:benzene	4	75	>99:1
7	Cl	dichloromethane:benzene	8	86	>99:1
8	OTf	dichloromethane:benzene	8	83	>99:1

^aReactions carried out at 80°C with 0.005 mmol of **1-FeX₂**, *n* equiv. of NaBAR₄^F and 20 equiv. of ethyl diazoacetate in 3 mL of solvent, during 12h. ^bDetermined by ¹H-NMR using trimethoxybenzene as internal standard.

Further study on this reaction was achieved testing different amino and aminopyridine based ligands, with different coordination modes (Figure IV.1). Firstly, different electronic modifications on the Me₂Pytacn (**1**) based ligand were performed to investigate if electronics on the complex can modulate their activity. Electron-donating

groups either on the pyridine and on the N atoms of the triazacyclononane scaffold, showed lower activity (entry 2-4, Table IV.3) than the non-substituted ligand (entry 1, Table IV.3). While introducing electron-withdrawing groups in the pyridine gave different results. A chlorine in the para position of the pyridine gave comparable yields to the non-substituted ligand (entry 5, Table IV.3), whereas a CF₃ in the same position gave very poor yields (entry 6, Table IV.3). The CF₃ complex is very unstable in solution, decomposing along time. This instability can be the responsible for the lowest yield observed for this complex, due to the high reaction temperature.

If we consider that the CF₃ complex gives no representative results for the reaction outcome and we focus on the other results, where electron-donating groups in the ligand decrease the activity of the complex and electron-withdrawing group maintains the high yield in the reaction, we can hypothesize that a very electrophilic specie is needed to functionalize benzene in an efficient manner.

Modification on the sterics and electronic properties of the ligand with the introduction of a methyl group in the sixth position of the pyridine resulted in a decrease of the yield of the reaction (entry 7, Table IV.3).

Different structural modifications in the ligand were also tested. Tetradentate aminopyridine ligands with 1,2-cyclohexanediamine (mcp) and bipyrrolidine (pdp) as backbone exhibited lower activity than the triazacyclononane scaffold (entry 10 and 12, Table IV.3) and its activity was decreased even more introducing bulky substituents on the fifth position of the pyridine, such as triisopropylsilyl group, what makes the active center more sterically impeded (entry 11 and 13, Table IV.3).

Also, different coordination number on the complex was investigated. Tridentate ligands based on the triazacyclononane scaffold gave moderate yields (entry 8-9, Table IV.3), while pentadentate ligand gave no reaction at all (entry 14, Table IV.3). The unexpected inactivity of the pentadentate ligand can be related to the need of having two cis labile positions in the first coordination sphere of the complex to generate the carbene species.

A remarkable result in all these complexes is that all of them have the same selectivity towards the insertion product. In order to know if this is general for non-heme iron complexes or it is related to the basic amino-based ligand properties, two different ligand structures were analyzed. One was a trispyrazolyl amine ligand (**18**) and the other was a tripyrazolyl borate structure (**19**). Both corresponding iron complexes gave moderate activity in the functionalization of benzene (entry 15 and 16, Table IV.3),

however their chemoselectivity dropped significantly affording a 1:1 mixture of the two isomers.

Control experiments were performed, where EDA and NaBAR₄^F in absence of iron catalyst gave no reaction, discarding the possibility of the thermal decomposition of ethyl diazoacetate, as it has been previously reported for other diazoacetates.¹⁷⁸ Also, the precursors iron salts (entry 17-18, Table IV.3) were investigated. Both salts gave reaction product with moderate yields, but no selectivity towards the insertion product was obtained, since a mixture of nearly 1:1 isomers was produced. This results suggest that the combination of pyridines and amines in the ligand structure gave the best performance for the functionalization of benzene with EDA.

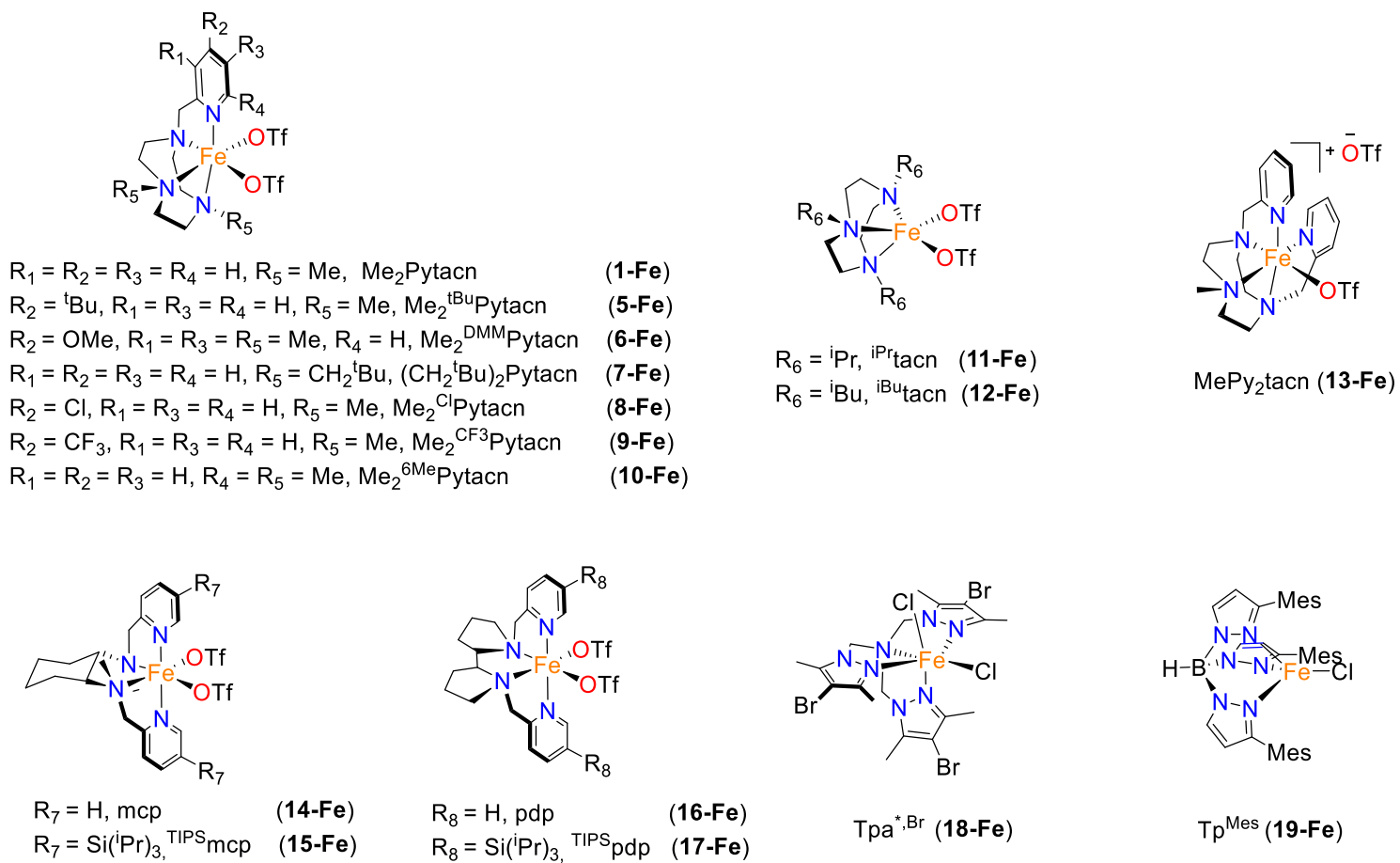


Figure IV.1. Different iron complexes used in the functionalization of benzene in carbene transfer reactions.

Table IV.3. Catalytic behavior of the different iron complexes tested in the functionalization of benzene.

Entry	Complex	Yield (%) ^b	Selectivity (I:A) ^b
1	1-Fe	83	>99:1
2	5-Fe	47	>99:1
3	6-Fe	59	>99:1
4	7-Fe	61	>99:1
5	8-Fe	85	>99:1
6	9-Fe	18	>99:1
7	10-Fe	77	>99:1
8	11-Fe	57	>99:1
9	12-Fe	67	>99:1
10	14-Fe	70	>99:1
11	15-Fe	61	>99:1
12	16-Fe	68	>99:1
13	17-Fe	52	>99:1
14	13-Fe	n.r.	-
15	18-Fe	57	42:58
16	19-Fe	55	53:47
17	Fe(OTf) ₂	55	42:58
18	FeCl ₂	52	69:31

^aReactions carried out at 80°C with 0.005 mmol of the iron complex, 8 equiv. of NaBAR₄^F and 20 equiv. of ethyl diazoacetate in 1.5 mL of benzene and 1.5 mL of dichloromethane, during 12h. ^bDetermined by ¹H-NMR using trimethoxybenzene as internal standard.

With the best reaction conditions in hand, using **1-FeX₂** (5 mol%), 8 equiv. of NaBAR₄^F at 80°C in an overnight reaction, different aromatic substrates were functionalized. Moderate to good yields were obtained for alkyl substituted arenes, but lower yields were observed for electron-poor substrates (**P14** and **P15**, Figure IV.2).

Exclusive selectivity for the aromatic C_{sp}²-H bonds in alkyl substituted substrates was observed, while C_{sp}³-H bonds remains unfunctionalized, which differs from previously reported Woo's system.¹³⁰ Unfortunately, no clear regioselectivity between *ortho*-, *meta*- and *para*- substituted products was observed (regioisomers assigned by 2-dimensional NOESY experiments, see experimental section). The increase of steric effects on alkyl mono-substituted arenes in order to modulate the regioselectivity was only slightly present when using very bulky groups, such as *tert*-butyl, where preferential functionalization towards the less congested positions was observed (**P2-P5**, Figure IV.2). Also, some selectivity can be noticed based on the electron properties of the

arenes. As in an electrophilic aromatic substitution, electron-donating and halide groups are *ortho*- and *para*- directors, exhibiting lower amounts of *meta*- substituted products. Whereas electron-withdrawing groups are *meta*- directing groups. The tendency of this behavior can be appreciated in our substrate scope, where anisole and chlorobenzene (**P6** and **P15**, Figure IV.2) exhibited lower amounts of *meta*-substituted benzene, while trifluoromethylbenzene (**P14**, Figure IV.2) showed high selectivity for the functionalization on the *meta*- position.

Trisubstituted arenes can be also functionalized with our system with moderate yields, including triethylbenzene (**P9**, Figure IV.2), a difficult substrate for its steric encumbrance.

A remarkable result is also the naphthalene functionalization (**P12**, Figure IV.2), since this substrate was known to give preferentially the cyclopropanation product.¹⁷⁹

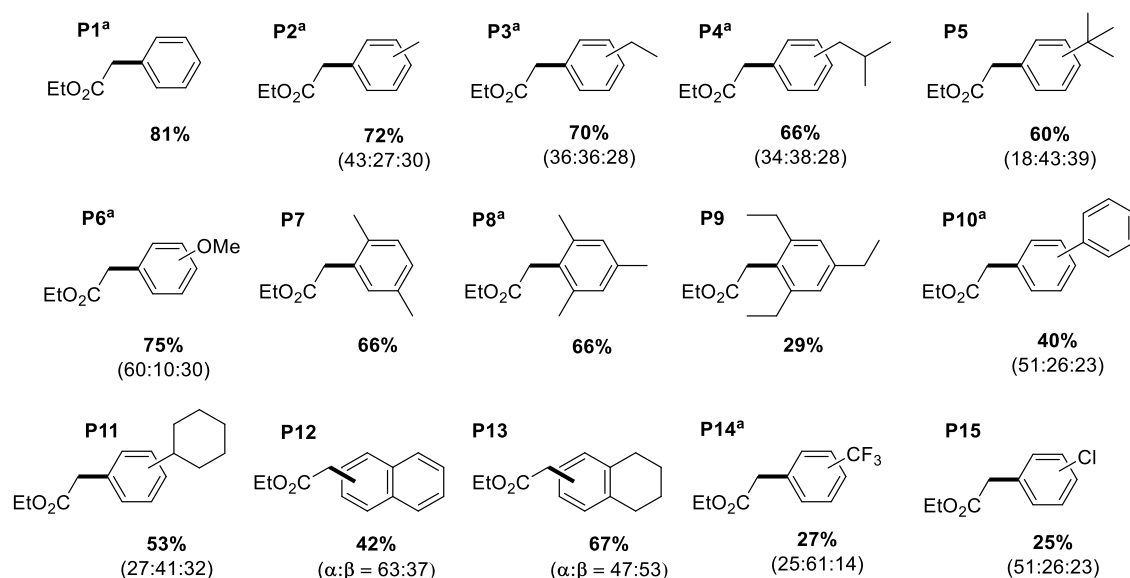
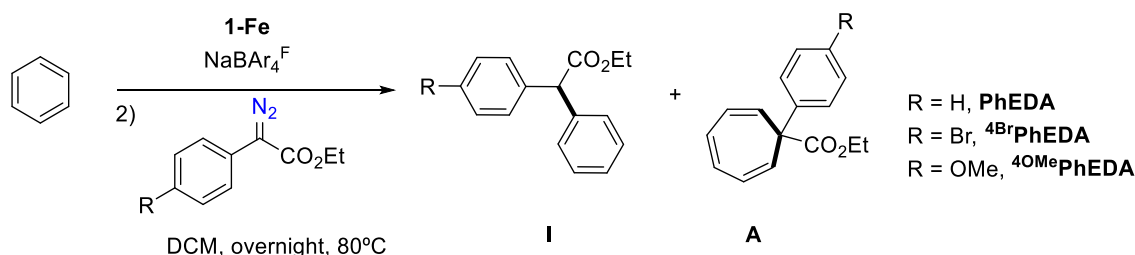


Figure IV.2. Substrate scope in the functionalization of arenes in the decomposition of EDA. Isolated yields. Isomer ratios determined by ¹H-NMR. ^aWork performed by Gerard Sabenya.

The good selectivity on this transformation encouraged us to try the same transformation with different diazoacetates in the functionalization of benzene (Scheme IV.3). Different aromatic diazoacetates were tested; moderate yields were achieved and moreover, mixtures of close 1:1 of the two isomers (insertion and addition) were obtained using ethyl phenyldiazoacetate and ethyl 4-bromophenyldiazoacetate as diazo substrates (entry 1-2, Table IV.4). Ethyl 4-metoxiphenyldiazoacetate gave a mixture of decomposition products, but no desired C-H bond functionalization product was observed (entry 3, Table IV.4). Control experiments with the diazoacetates in absence of iron complexes were made, since it has been reported that some diazo compounds

are able to insert into C-H bond by decomposition at high temperatures.¹⁷⁸ Some degree of thermal decomposition of the diazoacetates was observed. In the case of PhEDA, insertion product was observed, but in very low quantities. However, a dirty NMR spectrum was observed, with different products that could not be identified and with only a recovery of 30% of the starting material. In the case of ⁴BrPhEDA, no insertion or addition product was observed, however, two products were observed in the NMR spectrum. One of them was the starting material and accounts for 60% of the sample, and the other one presumably corresponds to the dimerization product. These blanks experiments suggest that indeed, those aryl diazoacetates are able to decompose at high reaction temperatures, but with very poor control of the reaction products, while introducing an iron complex, higher degree of selectivity in the reaction can be achieved.

The different reactivity and selectivity using aryl diazoacetates can be explained by a change on the basicity of the ester moiety of the carbene intermediate formed. As we will see in this chapter, the carbonyl group is crucial in the assistance for the formation of the insertion product. A change in the electronics of this group affects the stabilization of the intermediate responsible for an efficient insertion reaction.



Scheme IV.3. Standard conditions for the functionalization of benzene using different diazoacetates.

Table IV.4. Functionalization of benzene using different diazoacetates.

Entry	Diazoacetate	Yield (%) ^b	Selectivity (I:A) ^b
1	PhEDA	41	45:55
2	⁴ BrPhEDA	51	40:60
3	⁴ OMePhEDA	n.d.	-
4 ^c	PhEDA	5	1:>99
5 ^c	⁴ BrPhEDA	n.d.	-

^aReactions carried out at 80°C with 0.005 mmol of **1-Fe**, 8 equiv. of NaBAR₄F and 20 equiv. of the diazoacetate in 1.5 mL of benzene and 1.5 mL of dichloromethane, during 12h. ^bDetermined by ¹H-NMR using trimethoxybenzene as internal standard. ^cControl experiments in absence of the metal complex.

Also, different first row transition metals using the best ligand platform (**Me₂Pytacn**, **1**) were investigated for the reaction of benzene with EDA. All complexes were active under the same reaction conditions, although giving slightly lower yields than the obtained with **1-Fe**. Cobalt and nickel catalyst gave moderate yields (entry 3-4, Table IV.5), while Mn and Zn complexes provided good yields (entry 1, 6, Table IV.5). Interestingly, all these complexes gave excellent selectivity towards the insertion product as the Fe catalyst does. On the contrary, **1-Cu** behaved differently than the other first row metal catalysts. The yield of the reaction was moderate but it provided high selectivity towards the addition product rather than the insertion one (entry 5, Table IV.5) and also provided minor but significant amounts of dimer sub-products ($\approx 10\%$).

The use of those metals in carbene transfer reaction is not new, except for the Mn, which this was the first carbene transfer reaction reported for a manganese complex. Copper complexes are widely studied in carbene transfer reaction and specifically, in the functionalization of alkyl substituted arenes, where copper complexes had preference for the addition product.¹¹¹ Cobalt complexes are also commonly used, especially for cyclopropanation reactions.⁹⁶ On the contrary, nickel and zinc complexes remains as less explored metals. Nevertheless, nickel complexes have been used, for example, for O-H bond functionalization¹⁸⁰ and zinc complexes have been reported to catalyze the functionalization of alkanes.¹⁸¹

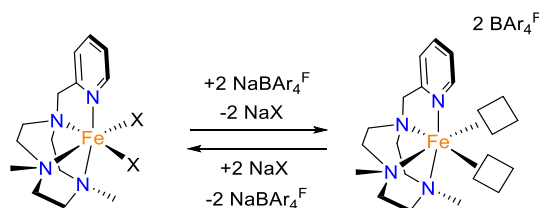
Table IV.5. Catalytic behavior of different metal complexes with **Me₂Pytacn** (**1**) ligand.

Entry	Complex	Yield (%) ^b	Selectivity (I:A) ^b
1	1-Mn	73	>99:1
2	1-Fe	83	>99:1
3	1-Co	43	>99:1
4	1-Ni	23	>99:1
5	1-Cu	52	5:95
6	1-Zn	70	>99:1

^aReaction carried out at 80°C with 0.005 mmol of the metal complex, 8 equiv. of NaBAR₄^F and 20 equiv. of the ethyl diazoacetate in 1.5 mL of benzene and 1.5 mL of dichloromethane, during 12h. ^bDetermined by ¹H-NMR using trimethoxybenzene as internal standard.

IV.1.2 Mechanistic studies

Different mechanistic information of some steps of the reaction can be extracted from the experiments described before. The large amount of NaBAR₄^F needed in the reaction accounts for an equilibrium between the initial complex and a dicationic iron species with two empty positions on the first coordination sphere (Scheme IV.4). The need for this two labile positions can be also observed in the lack of reactivity when a pentadentate ligand was used (entry 14, Table IV.3).



Scheme IV.4. Role of NaBAR₄^F in the generation of a dicationic specie.

This dicationic species has been impossible to isolate. Instead, a dimeric iron species with triflates acting as bridges, ([Fe₂(μ-OTf)₂(Me₂Pytacn)₂](BAR₄^F)₂, **20-Fe**), has been isolated and crystallographically characterized. A close comparison of the ORTEP diagram of the diiron complex (Figure IV.3, right) and the initial iron catalyst (Figure IV.3, left) shows that both complexes are coordinatively saturated and have a distorted octahedral geometry, with four sites occupied by the tetradentate ligand and the two remaining sites are filled by the oxygen atoms of the triflate ligands, which are terminally coordinated in the mononuclear complex and bridging in the dinuclear case.

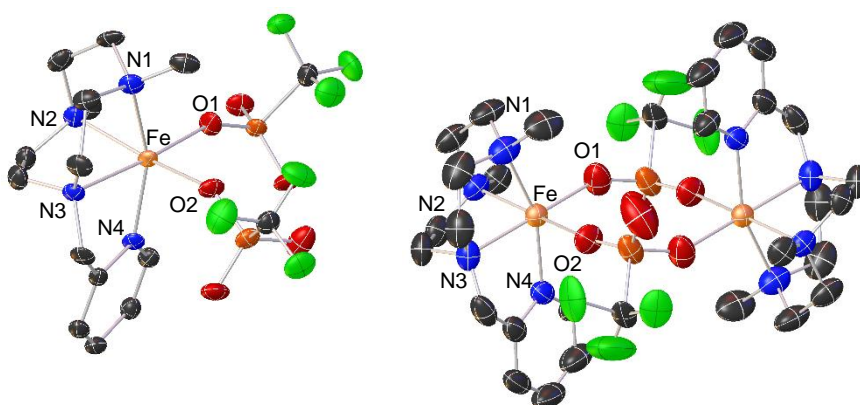
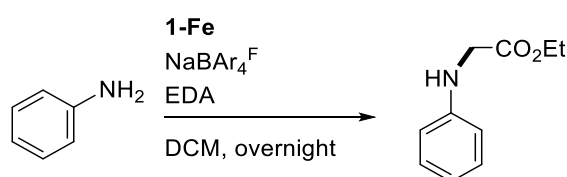


Figure IV.3. ORTEP diagram of the single crystal X-Ray structure for **1-Fe**¹³⁸ (left) and [Fe₂(μ-OTf)₂(Me₂Pytacn)₂](BAR₄^F)₂, **20-Fe** (right). 50% ellipsoid probability, H atoms have been omitted for clarity. **1-Fe** selected distances (Å): Fe-N1: 2.231, Fe-N2: 2.251, Fe-N3: 2.205, Fe-N4: 2.165, Fe-O1: 2.055, Fe-O2: 2.165. **20-Fe** selected distances (Å): Fe-N1: 2.200, Fe-N2: 2.210, Fe-N3: 2.187, Fe-N4: 2.142, Fe-O1: 2.060, Fe-O2: 2.189.

When the diiron specie (**20-Fe**) was used in the functionalization of benzene under standard conditions, but in absence of additional $\text{NaBAR}_4^{\text{F}}$, it proved to be inactive. However, upon the addition of 4 extra equivalents of $\text{NaBAR}_4^{\text{F}}$, 80% yield was observed with the insertion as the sole product. These observations suggest that we need the detachment of the two triflate anions, generating two vacant sites at the iron coordination sphere, to promote the activation of the EDA. Although the dicationic species could not be isolated neither detected by $^1\text{H-NMR}$ spectroscopy due to the paramagnetism nature of the iron complex, ions at $m/z = 152.1$, with the isotopic patterns characteristic of $[\text{Fe}(\mathbf{1})]^{2+}$, could be detected in ESI-MS spectrum, suggesting the possibility of the formation of this species in solution at room temperature.

The iron carbene species proposed to be formed during the reaction, which will be the responsible for the functionalization of the substrates, could not be isolated. Its expected high reactivity once formed complicates the possibility of its isolation. Moreover, it is proposed that the rate determining step of the reaction is the formation of the iron carbene species, and this is the reason of the high temperature needed for the reaction to proceed. Indeed, trying to functionalize X-H bonds with lower bond dissociation energies, such as amines or alcohols, using EDA as carbene source (Scheme IV.5), the temperature needed to achieve high yields was still 80°C (Table IV.6), what will suggest that the high reaction temperatures is needed to overcome a high energy barrier, independently of the strength of the bond to be functionalized. Additionally, theoretical calculations have been performed and it is estimated an energy barrier of $29.5 \text{ kcal}\cdot\text{mol}^{-1}$, a value that is only possible to overcome at high reaction temperatures.



Scheme IV.5. Functionalization of aniline using ethyl diazoacetate.

Table IV.6. Decomposition of EDA under iron complexes in the functionalization of aniline at different reaction temperatures.

Entry	Temperature (°C)	Yield (%) ^b
1	40	12
2	60	38
3	80	92

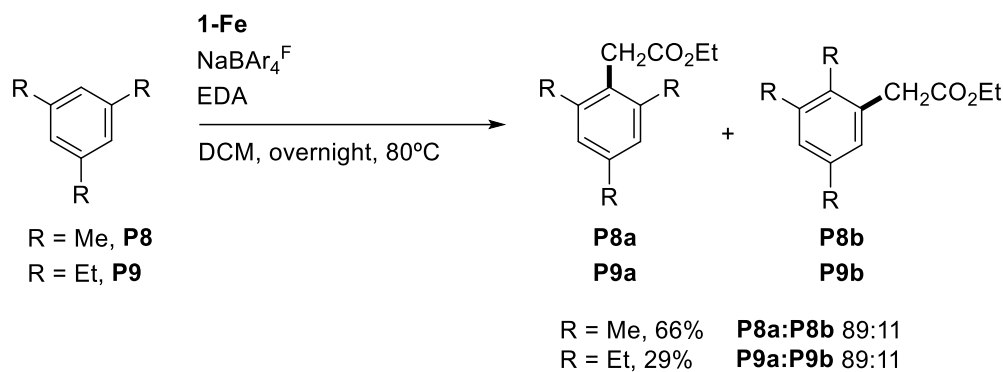
^aReaction carried out at the indicated temperature, with 0.005 mmol of **1-Fe**, 8 equiv. of NaBAR₄^F and 20 equiv. of the ethyl diazoacetate in 1.5 mL of aniline and 1.5 mL of dichloromethane, during 12h. ^bDetermined by ¹H-NMR using trimethoxybenzene as internal standard.

As the carbene intermediate could not be isolated, its nature could not be fully elucidated. However, previous Hammett analyses performed by Gerard Sabenya provide insight into its reactivity nature. Competitive experiments of pairs of monosubstituted arenes provided values of $\rho = -2.75 \pm 0.37$, which indicates the presence of an electrophilic active species, attributed to the iron carbene intermediate. This parameter suggests that the functionalization of the arenes occurs via an electrophilic aromatic substitution, as previously mentioned for the *o:m:p* ratios in the functionalization of mono-substituted arenes.

Apart from that, an inverted intramolecular KIE of 0.95 was determined in the competitive functionalization of a mixture of benzene and benzene-d₆, consistent with a change in the hybridization from sp² to sp³ in the arene functionalization step. This KIE value also suggests that the rate determining step of the reaction is not the C-H bond cleavage.

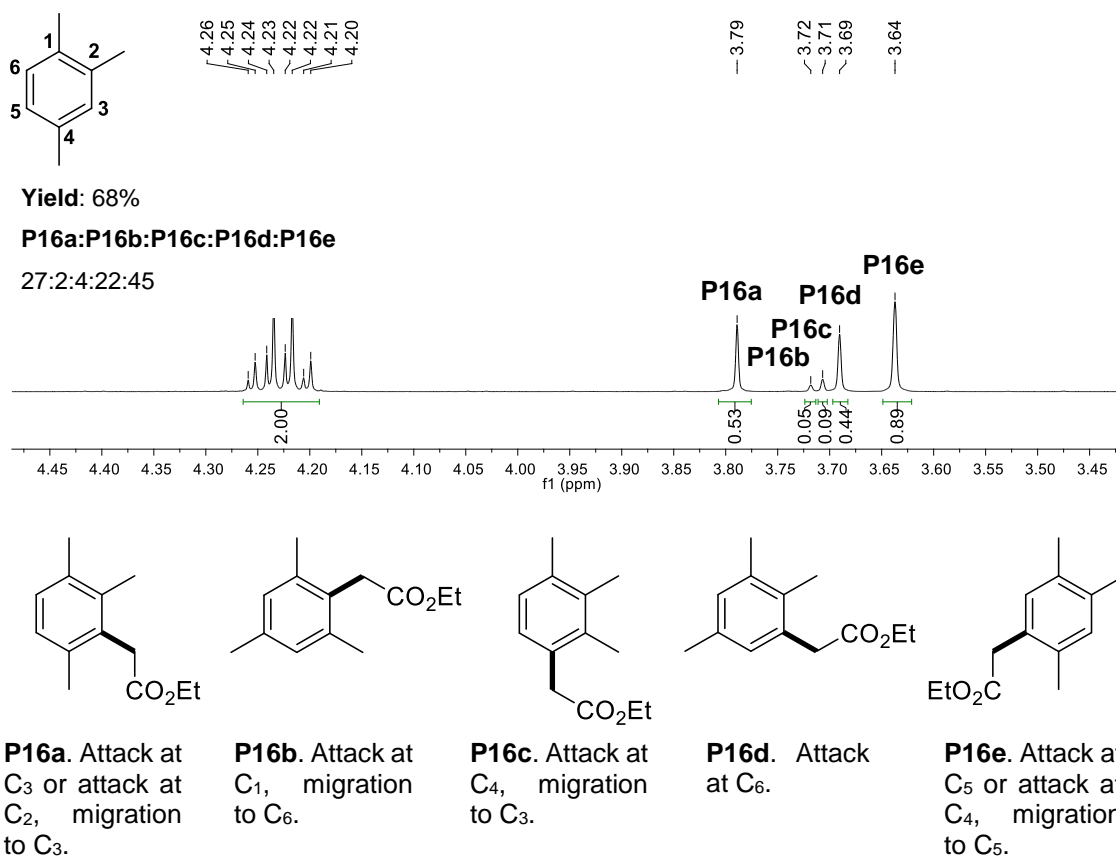
Although no intermediates could be isolated, close inspection to some results on the substrate scope and further experiments helps us to propose a reaction mechanism.

Functionalization of mesitylene and 1,3,5-triethylbenzene provided as major products ethyl esters **P8a** and **P9a** resulting from the formal insertion at the C-H bond (Scheme IV.6). However, the presence of a minor product detected in the NMR spectra of both isolated products suggested the possibility of the formation of a new regioisomer during the catalytic reaction. These minor products have been spectroscopically analyzed and assigned to a regioisomer, which can presumably come from the attack of the alkyl-substituted C to the carbene intermediate and a subsequent alkyl migration during the reaction (Scheme IV.6, **P8b** and **P9b**).



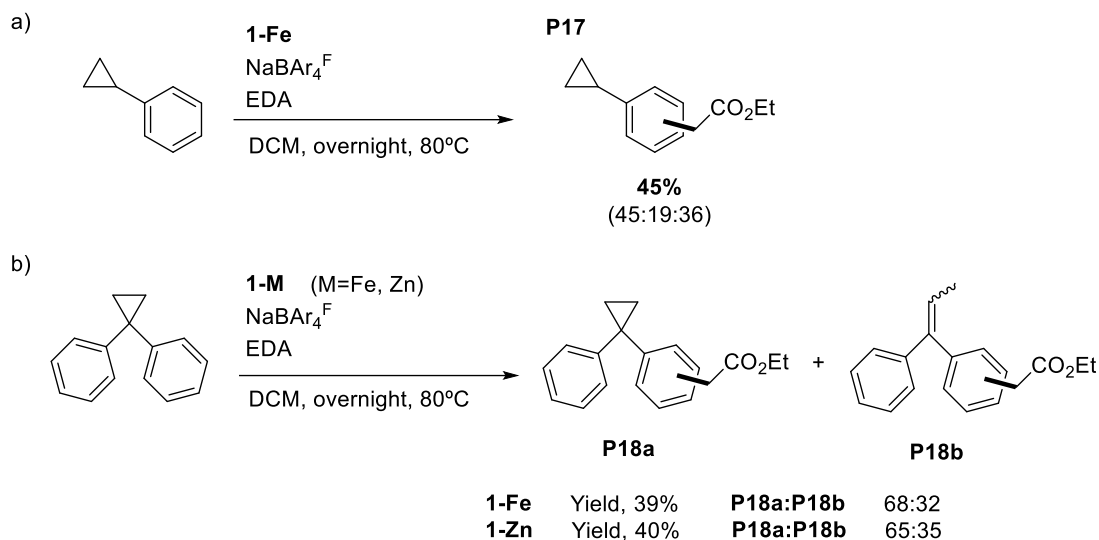
Scheme IV.6. Functionalization of mesitylene and 1,3,5-triethylbenzene under standard reaction conditions, giving a mixture of two regioisomers.

To confirm the migration of alkyl moieties during the reaction, 1,2,4-trimethylbenzene was subjected to standard reaction conditions. As expected, after isolation of the final product, 5 different isomers were observed in the $^1\text{H-NMR}$ spectrum, in concordance with the 5 possible isomers achieved in the insertion into the C-H bonds and from alkyl migrations pathways. The different isomers can be clearly distinguished by the singlet signal of the benzylic protons, appearing between 3.8 and 3.6 ppm in the $^1\text{H-NMR}$ spectrum (Scheme IV.7). Full assignment of each signal of the NMR spectrum with its corresponding isomer was done by 1-dimensional NOE experiments. From the five isomers achieved, three of them appeared as major products, which correspond to the formal insertion of the carbene moiety in C-H bonds at C_3 , C_5 and C_6 (**P16a**, **P16e**, **P16d**, respectively, Scheme IV.7), although **P16a** and **P16e** can be also originated by methyl migration pathways. From these three, the functionalization on C_5 is the preferred one (**P16e**, Scheme IV.7), presumably because is less congested than C_3 and also because is preferentially activated towards an electrophilic aromatic substitution because it is in para position with respect to the methyl group at C_2 . The two remaining isomers, the less abundant ones, can be only explained by insertions accompanied by alkyl migration (**P16b**, **P16c**, Scheme IV.7). **P16b** can be formed by an initial attack at C_1 , followed by methyl migration to C_6 , while **P16c** corresponds to an initial attack on C_4 and the migration of the methyl to C_3 .



Scheme IV.7. Different isomers achieved in the functionalization of 1,2,4-trimethylbenzene under standard conditions.

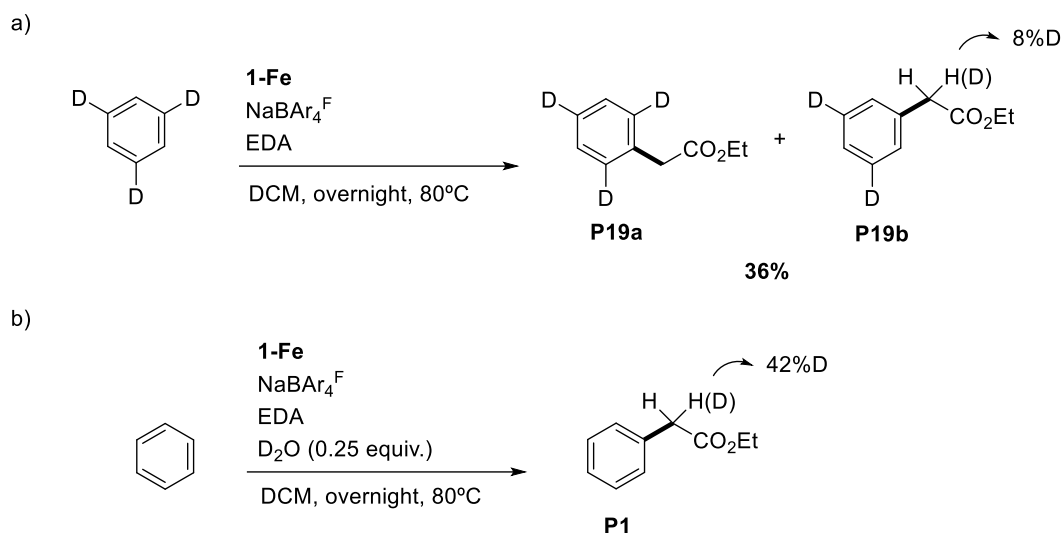
These methyl migration products can be explained considering the presence of a carbocationic intermediate. However, carbene moieties can have some degree of radical character. The presence of long lived radicals can be determined by the use of radical probes such as cyclopropylbenzene. This substrate was subjected to standard reaction conditions and no ring opening was observed (Scheme IV.8, a). This result suggests that radical intermediates are not formed, or their lifetime are very short. To further confirm this suggestion, an ultrafast radical clock was also subjected to standard reaction conditions (Scheme IV.8, b). This time, the reaction produced two products: the not rearranged cyclopropyl product **P18a** and rearranged product **P18b** in a 68:32 ratio. This result may suggest that the reaction proceeds via short-lived carbocationic or radical intermediates, the latter in contrast to the previous result. However, in the reaction of this substrate under the same reaction conditions but using the analog zinc catalyst (**1-Zn**), the two products appeared in very similar ratio, 65:35. This may suggest that the rearranged product come from carbocationic rearrangements and not a radical one, since zinc is a redox inactive metal.



Scheme IV.8. Functionalization of radical clocks under standard conditions for the determination of radical intermediates.

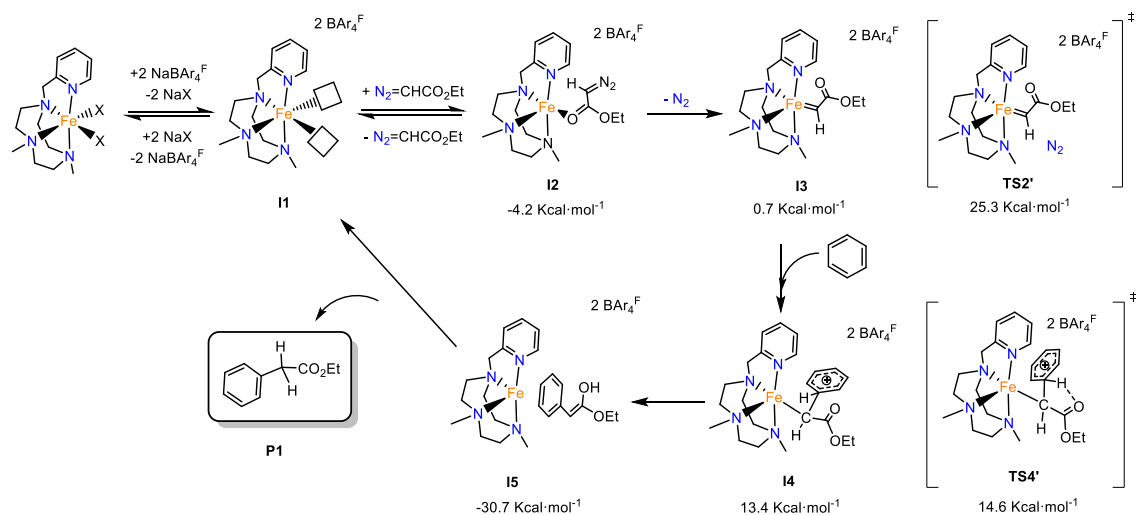
Isotopic labelling experiments were also carried out. The subjection of 1,3,5-D₃-benzene to standard reaction conditions did not lead to the migration of the deuterium atom, contrary to our initial expectations. Instead, two products coming from the formal insertion into the arene C-H bond (**P19a**, Scheme IV.9, a) and insertion into the C-D bond (**P19b**, Scheme IV.9, a) were formed. The ratio of the two mentioned products was 49:51 (extracted from the aromatic signals of the NMR spectrum), which translates into an intramolecular kinetic isotope effect, KIE=0.96, in agreement with the intermolecular KIE determined from the competitive functionalization of benzene and D₆-benzene mentioned above. Interestingly, only partially D atom from the C-D bond ends up forming the benzylic C-D bond in the **P19b**. An 8% of the D is incorporated in the final product, where the rest corresponds to the fully hydrogenated benzylic position, suggesting the possibility of the incorporation of protons from an external source.

This incorporation of protons from an external source can be observed also when benzene was submitted to the standard reaction conditions in presence of D₂O (0.25 equiv.) (Scheme IV.9, b). From this reaction, 42% of the corresponding product contained a benzylic C-D bond. Control experiments showed that the C-H bond of the product **P1** does not exchange the hydrogen atoms with D₂O, indicating that the incorporation of the deuterium atom should come from a step of the reaction mechanism. Thus, indicating that the reaction involves an intermediate species that can exchange a H atom with D₂O.



Scheme IV.9. Isotopic labelling experiments.

With all these experiments in hand, a reaction mechanism can be proposed (Scheme IV.10). The initial iron catalyst reacts with $\text{NaBAR}_4^{\text{F}}$ generating a dicationic species **I1**, which is able to coordinate the diazo compound. Calculations performed by Verónica Postils identify the O-bound adduct as the more stable species (**I2**). This intermediate should evolve to the extrusion of molecular nitrogen and the generation of the metallocarbene **I3**, upon overcoming an energy barrier of 29.5 Kcal·mol⁻¹, affordable at 80°C. An electrophilic aromatic substitution takes place forming a new C-C bond and changing the hybridization of the C from sp² to sp³, generating the carbocationic intermediate (**I4**). Thanks to the proximity, the proton of the arene is able to interact with the carbonyl group of the ester moiety through the transition state **TS4'** and promote its abstraction and generate an enol intermediate of the product (**I5**), while releasing the metal active species. This step is where the interchange with protons can occur as observed in the labelling experiments. This carbonyl assisted step is crucial for the high selectivity and reactivity, since any change in the basicity of the carbonyl group, changes completely the selectivity of the reaction, as mentioned above in the use of different aryl diazoacetates. Finally, this enol intermediate evolves to the formation of the final ester product (**P1**).



Scheme IV.10. Proposed reaction mechanism for the functionalization of benzene. Energy values were calculated by Verónica Postils (Level of theory: UB3LYP-D3BJ/cc-pVTZ/SMD(50%Bz,50%CH₂Cl₂)).

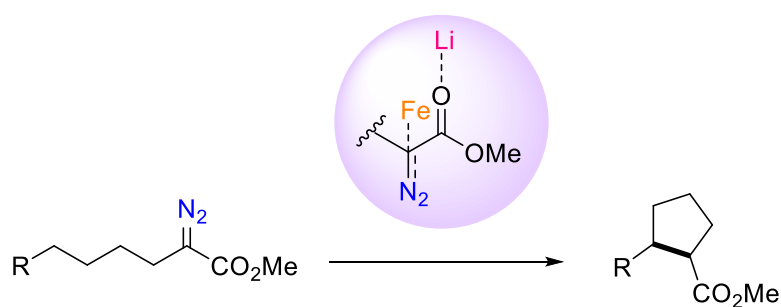
IV.2 Summary

Carbene insertion into aromatic C_{sp}²-H bonds has been accomplished by the use of non-heme iron complexes in the decomposition of ethyl diazoacetate. The novel selectivity of the system towards C_{sp}²-H bonds, avoiding C_{sp}³-H functionalization and addition products, provides an efficient transformation catalyzed by a non-precious metal complex.

Theoretical and experimental data allowed the proposal of a reaction mechanism, where the formation of the carbene intermediate is the rate determining step of the reaction. The presence of a carbocationic intermediate, in which the carbonyl group of the EDA interacts with the proton of the benzene, is the responsible of the high selectivity towards aromatic C-H bonds. This intermediate has been computational described and experimentally suggested by alkyl migration, proton interchange and radical clock experiments.

Chapter V

Intramolecular C_{sp^3} -H bond alkylation
using low-coordinate iron complexes via
carbene intermediates

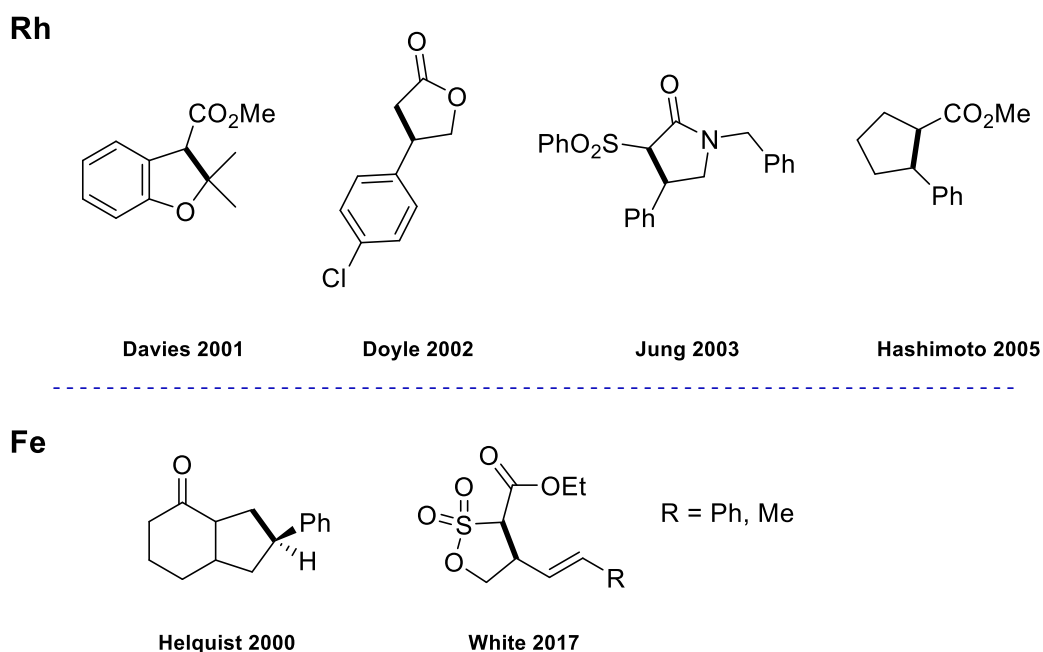


mild reaction conditions
benzylic and alkylic substrates

V.1 Results and discussion

The generation of new C_{sp}³-C_{sp}³ bonds via carbene intermediates is an interesting transformation for its high versatility. A large number of structures with different degrees of complexity can be constructed by carbene transfer reactions, either in intermolecular C-H bond functionalization or by cyclization in intramolecular reactions. Very nice examples of those transformations are mostly done using rhodium catalysts and have been mainly developed by the groups of Davies and Doyle.^{105,106}

Among all possibilities in intramolecular reactions, formation of five-membered rings is widely extended when using precious metal complexes, yet less explored for iron systems. Only two examples of five-membered ring formation have been reported using iron carbenes: the stoichiometric use of an iron carbene source to generate fused systems¹²⁰ or a catalytic system which is limited to the use of diazo sulfonate esters for the functionalization of allylic positions (Scheme V.1).¹³⁵



Scheme V.1. Resume of different 5-membered ring synthesized molecules through carbene intermediates using rhodium¹⁸²⁻¹⁸⁵ and iron^{120,135} complexes.

The great importance of this kind of cyclopentane structures as building blocks for preparing pharmaceuticals and natural products¹⁸⁶ and the scarce examples of their synthesis based on earth abundant metals via formal carbene insertion reactions, encouraged us in the seek for environmental friendly protocols allowing their construction.

In this regard, efficient carbene insertion reactions should account for an activation of the diazo substrate to form the active metalcarbene intermediate under mild reaction conditions and where the electronic nature of that metalcarbene formed should be electrophilic to enhance its ability to react with nucleophiles present in the media.

As mentioned in the introduction, different systems have been able to activate diazo compounds to form the corresponding iron-carbene. Among these systems, the use of low-coordinate iron complexes reported by Chirik¹²⁸ and Holland¹²⁹ appeared to be appealing systems for the efficient activation of diazo compounds, although the low electrophilicity of the metalcarbene formed in both works prevent their reaction with any nucleophiles.

For this reason, we propose the combination of low-coordinate iron complexes together with electron-withdrawing groups in either the ligand and the carbene fragment (coming from the diazo substrate), to increase the electrophilicity of the iron-carbene intermediate to effectively promote its reaction with nucleophiles, such as strong C-H bonds.

V.1.1 Catalytic studies

Two iron complexes with bidentate ligands based on a phenylenediamine backbone were synthesized and tested for the catalytic carbene insertion reaction, one bearing mesityl substituents as electron-donating group ($[\text{Fe}^{\text{MesPDA}}(\text{toluene})]$ **21-Fe**, Figure V.1) and the other bearing perfluorinated phenyl rings, as electron-withdrawing groups ($[\text{Fe}^{\text{FPDA}}(\text{THF})]$ **22-Fe**, Figure V.1).

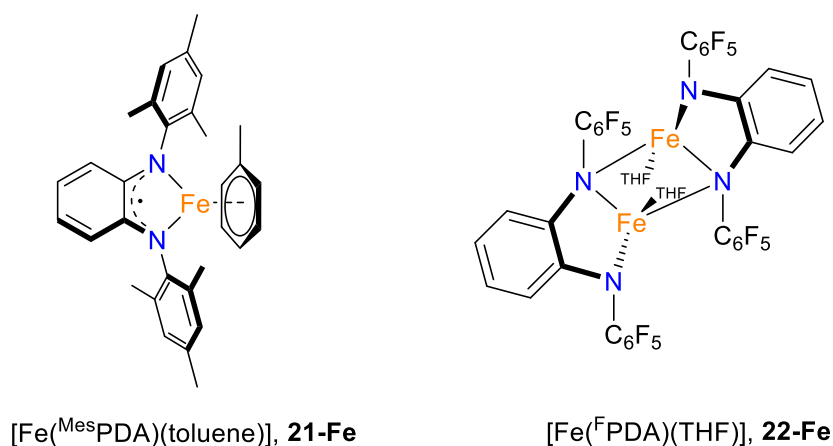


Figure V.1. Bidentate iron complexes tested for the activation of diazo compounds.

The redox non-innocent character of the ligands and their difference in the electronic properties resulted in the formation of electronically different iron complexes. The iron

complex with mesityl substituted-ligand, **21-Fe**, was isolated as a monomeric structure of a η^6 -toluene adduct. Its crystalline structure reveals a subtle dearomatization on the phenylene ring, where two sets of C-C bond distances are present (average C_α-C_α and C_α-C_β 1.42Å; C_β-C_γ_{average} 1.38Å) as well as short C-N bond distances (C-N_{average} 1.36Å), which allow the description of the complex as an iron (I) ortho-diiminosemiquinonate. On the contrary, using the perfluorinated phenyl ring, **22-Fe** was isolated as a dimeric structure with two units of [Fe(^FPDA)(THF)] in which one N of each ligand act as a bridge between the two iron centers. The C-N bond distances (C-N_{average} 1.42Å) determined in the crystal structure are consistent with single bond distances and the Fe-N distances (Fe-N_{average} 2.04Å) are comparable to those previously reported for high spin iron (II) complexes with bidentate ligands,¹⁸⁷⁻¹⁸⁹ indicating that the complex has a high spin iron (II) center.

To start with the study of the cyclization reaction, methyl 2-diazo-6-phenylhexanoate (**S20**) was used as model substrate, since the formation of a five membered-ring can be favored for the functionalization of a benzylic position (**P20**, Table V.1). However, diazoester compounds which contains protons in the β position of the diazo can undergo a metal-catalyzed β-hydride migration, giving rise to α,β-unsaturated esters (**P20'**, Table V.1), whose formation is difficult to override.^{95,190} Their elimination has only been previously accomplished in Rh based systems, and even in this case very low reaction temperatures were needed to completely avoid its formation.¹⁸⁵

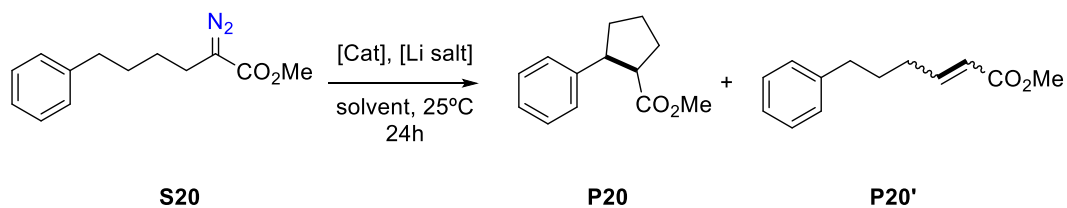
Diazo substrate **S20** was subjected to catalysis with the two mentioned iron complexes in a 24h reaction at room temperature with DCM or THF as solvent. In THF solution, no desired product **P20** was observed in neither of the two complexes; while small amounts of β-hydride migration side product **P20'** was detected in the case of **21-Fe** (entry 4, Table V.1). On the contrary, in dichloromethane solution, small quantities of **P20** were observed when using the perfluorinated **22-Fe** complex (entry 1, Table V.1). For this reason, DCM was chosen as solvent.

Although low reactivity was observed for the iron complexes, the addition of a lithium salt as Lewis acid, whose role will be disclosed later in this chapter, improved the activity of the system. Lithium tetrakis(perfluoro-tert-butoxy)aluminate ([LiAl(OC(CF₃)₃)₄]) was used as Lewis acid and interestingly, only by the addition of 5 mol% of the mentioned lithium salt respect to the substrate, the activity of **22-Fe** was significantly increased, with a conversion of almost half of the initial diazo compound and a production of 31% of the cyclized product **P20** and a corresponding 12% of **P20'** (entry 5, Table V.1). **21-Fe** complex also showed higher yields for both products compared to the results in absence

of the lithium salt, but giving worse results than the perfluorinated ligand (entry 6, Table V.1). The difference between those two complexes can be attributed for the need of a highly electrophilic iron center to generate a reactive intermediate, thus the more electron-withdrawing ligand will favor the formation of a more electrophilic metallocarbene.

Because of the higher performance of **22-Fe** compared to **21-Fe**, the optimal loading of the lithium salt was then optimized for the former complex. The addition of 15, 25, 50, 75 and 100 mol% of the lithium salt showed that the highest activity of the reaction was reached at loadings of 25 mol% or higher, when mainly all the diazo substrate was consumed (entry 8-11, Table V.1). However, the best ratio between **P20** and **P20'** product was achieved when using 25 mol% of the lithium salt, with 60% of the desired **P20** product (entry 8, Table V.1). A blank experiment in absence of the iron complex to rule out the possibility of free carbene reactivity was performed and all starting material was recovered at the end of the reaction (entry 12, Table V.1).

Moreover, the use of the iron complex used in Chapter IV, with the aminopyridine tetradentate ligand **1-Fe**, presented a negligible activity at room temperature (entry 13, Table V.1), enhancing the importance in the use of low donating ligands for a productive activation of **S20** at room temperature.

Table V.1. Reaction optimization for intramolecular cyclization via carbene intermediates using iron complexes.

Entry	Complex	Li salt(%)	Solvent	S20(%) ^b	P20(%) ^b	P20'(%) ^b
1	22-Fe	0	DCM	92	2	3
2	22-Fe	0	THF	100	0	0
3	21-Fe	0	DCM	93	0	5
4	21-Fe	0	THF	96	0	4
5	22-Fe	5	DCM	52	31	12
6	21-Fe	5	DCM	82	7	8
7	22-Fe	15	DCM	42	40	15
8	22-Fe	25	DCM	4	60	35
9	22-Fe	50	DCM	0	51	48
10	22-Fe	75	DCM	0	48	48
11	22-Fe	100	DCM	0	45	50
12	-	25	DCM	>99	0	0
13	1-Fe	25	DCM	>99	0	0

^aReactions carried out at 25°C with 0.004 mmol of **21-Fe** or 0.002 mmol of **22-Fe**, *n* mmols of [LiAl(OC(CF₃)₃)₄] and 0.08 mmol of **S20** in 1 mL of solvent, during 24h. ^bDetermined by ¹H-NMR using dibromomethane as internal standard.

Using the best reaction conditions, the scope of the reaction was tested towards the functionalization of different diazo substrates. Different aryl substituted diazo acetates were successfully functionalized in the benzylic position (entry 2-3, Table V.2). Electron-rich substituent led to a higher yield of the cyclized product rather than electron-poor substituent (73 and 53%, respectively), strengthening the proposal of the involvement of an electrophilic metalcarbene as active species. Low diastereomeric ratio between the possible *E/Z* isomers of cyclized products were observed for aryl diazo acetates derivatives.

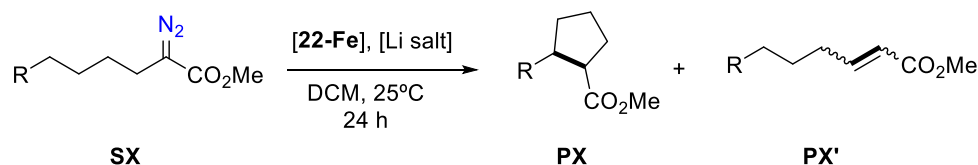
Increasing by one carbon the chain of substrate **S20**, the system was able to form selectively a 5-membered ring product rather than the 6-membered ring product, even

though the latter will correspond to the functionalization of a weaker benzylic C-H bond (entry 4, Table V.2). Nevertheless, the desired product was achieved in low yields.

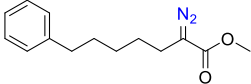
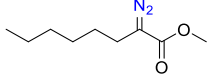
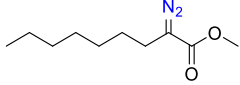
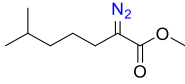
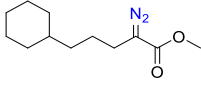
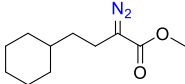
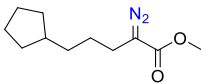
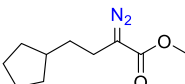
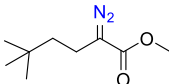
The functionalization of stronger C-H bonds, such as alkyl chains could also be performed with the Fe/Li system. Tertiary (entry 7, Table V.2) and secondary (entry 5-6, Table V.2) C-H bonds could be functionalized from moderate to good yields, observing again the preference for the formation of cyclopentane rings on substrate **S25**. In alkylic substrates, excellent diastereomeric ratio could be achieved, observing by ¹H-NMR mainly one isomer. The system was also able to generate bicyclic structures, in spiro or fused forms, in moderate to good yields (entry 8-11, Table V.2). However, low diastereoselectivity was observed in the formation of the fused ring with cyclohexyl substrate derivative **S28**, where 3 different isomers were formed. Functionalization of primary C-H bonds could also be achieved, although yields dropped completely and only 6% of the cyclopentane **P31** could be observed (entry 12, Table V.2).

In spite of the good yields obtained, always a mixture of cyclized product (**PX**) and β -hydride migration product (**PX'**) was observed.

Table V.2. Substrate scope in the intramolecular cyclization with products yields and diastereomeric ratios of the cyclized products.



Entry	X	PX (%) ^b	PX' (%) ^b	PX d:r ^c
1		60	35	76:24
	S20			
2		73	24	77:23
	S21			
3		53	43	77:23
	S22			

4		26	71	>99:1
	S23			
5		59	39	95:5
	S24			
6		68	30	91:6
	S25			
7		70	26	-
	S26			
8		68	31	-
	S27			
9		56	31	63:25:12
	S28			
10		71	20	-
	S29			
11		76	10	>99:1
	S30			
12		6	93	-
	S31			

^aReactions carried out at 25°C with 0.002 mmol of **22-Fe**, 0.02 mmol of [LiAl(OC(CF₃)₃)₄] and 0.08 mmol of **SX** in 1 mL of dichloromethane, during 24h. ^bDetermined by ¹H-NMR using dibromomethane as internal standard. ^cDetermined by ¹H-NMR.

The isolation of the desired cyclized products was performed at 1 mmol scale of the substrate. Purification by chromatographic column resulted in the isolation of an inseparable mixture between the cyclized product (**PX**) and the β -hydride migration product (**PX'**), with no possibility of obtaining pure samples. For this reason, a post-functionalization of the olefin was carried out. After the catalytic reaction with the Fe/Li system, the reaction mixture was submitted to oxidizing conditions with KMnO_4 for the oxidation of the undesired olefin product (see experimental section), allowing the purification by chromatographic column of the cyclized product as pure material. All products were isolated with similar yields as the ones determined by $^1\text{H-NMR}$ at small scale (Figure V.2). Diastereomeric ratios could be better determined by GC-MS, since in some cases the minor isomer could not be observed by ^1H or $^{13}\text{C-NMR}$. In case of all monocyclic products, the major isomer always corresponds to the trans isomer.

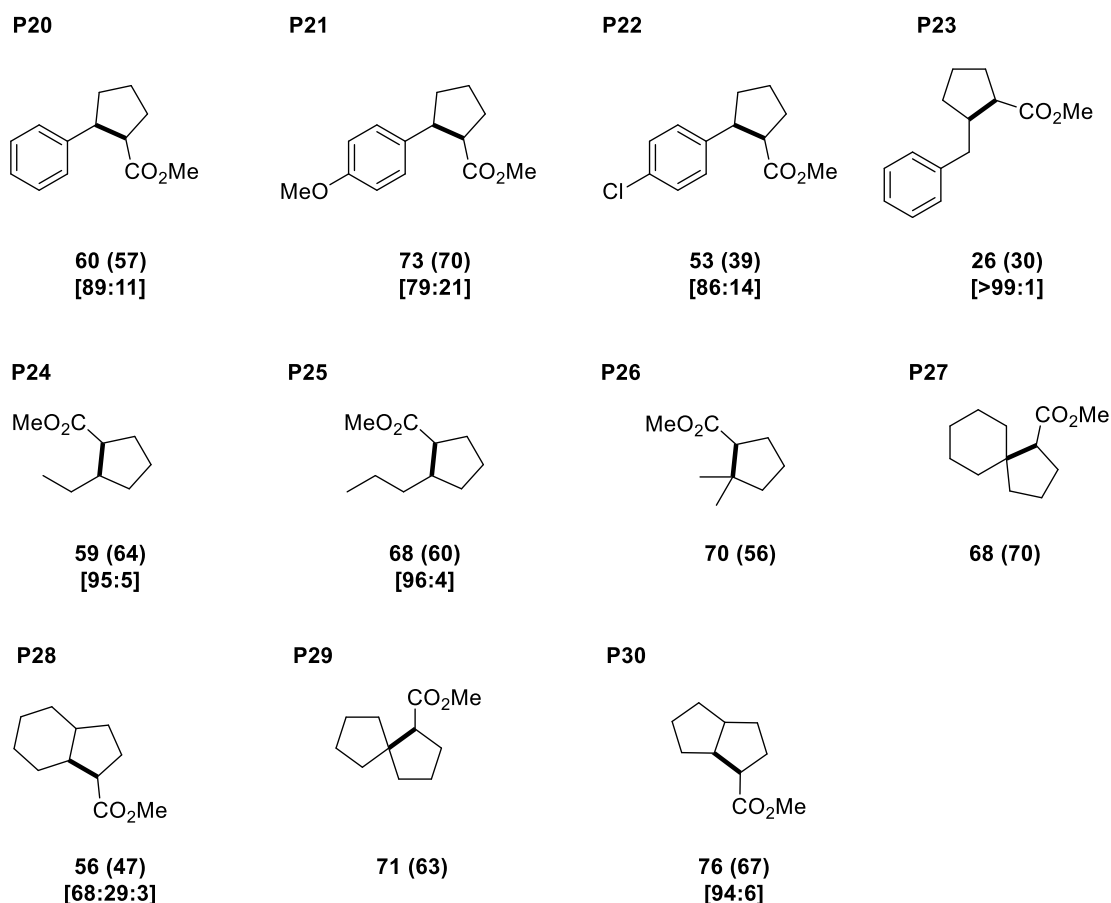
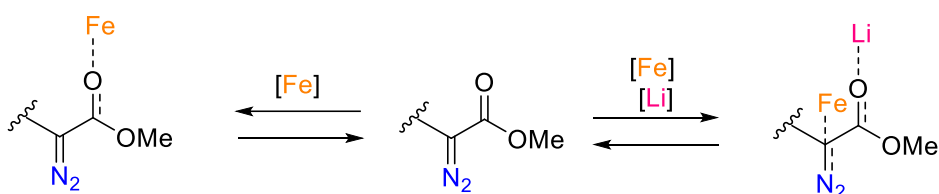


Figure V.2. Substrate scope with the yield determined by $^1\text{H-NMR}$ and the isolated yield in parenthesis. Diastereomeric ratio of isolated samples determined by GC-MS in brackets. Reactions carried out at 25°C with 0.025 mmol of **22-Fe**, 0.25 mmol of $[\text{LiAl}(\text{OC}(\text{CF}_3)_3)_4]$ and 1 mmol of **SX** in 12.5 mL of dichloromethane, during 24h.

V.1.2 Mechanistic studies

Different collection of experiments has been carried out in order to disclose some key mechanistic points of this system. Firstly, since [LiAl(OC(CF₃)₃)₄] plays a key role in the activation of the diazo compound, the elucidation of its function is needed.

The addition of the diazo substrate **S20** over a solution of the iron complex **22-Fe** in dichloromethane produces an immediate color change from orange to dark brown, suggesting a possible coordination of the diazo substrate to the iron complex. This possible interaction was studied by means of FT-IR spectroscopy. Interestingly, analyzing the oil formed after mixing equimolar amounts of **S20** and **22-Fe**, the band corresponding to the C=O functional group of **S20** was shifted 13 cm⁻¹ to lower frequencies from the one corresponding to the free diazo compound. This shift may suggest a possible coordination of **S20** to the iron complex through the O atom of the carbonyl group. This behavior is not surprising as it was previously observed by computational studies in the system from Chapter IV.¹⁹¹ For the formation of the metallocarbene, the O-bound adduct should evolve to the C-bound adduct to finally extrude the N₂ molecule. In the previous system, to overcome this energetic barrier, heat was needed. On the contrary, in this present system, we hypothesized that the undesired O-coordination can be override by the addition of a stronger Lewis acid than the iron center, thus the O atom will preferentially coordinate to the added Lewis acid, leaving iron to freely form the C-bound adduct (Scheme V.2).



Scheme V.2. Coordination of Lewis acids into the O atom of the diazo substrate.

Among the different Lewis acid possible, alkali metal salts with weakly coordinating anions were proposed to be a proper choice for their high solubility in organic solvents. In particular, [LiAl(OC(CF₃)₃)₄] was proven to be efficient for the present catalytic system as we have seen during this chapter. The same IR study previously done with the iron complex was done with the lithium salt. The addition of 5 mol% of lithium salt in the diazo compound **S20** produced a split in two of the C=O band, which are assigned as the free diazo (1690 cm⁻¹) and the lithium-bound adduct (1656 cm⁻¹) (Figure V.3, a). Increasing the amount of lithium salt up to 25 mol% favored the apparition of the new band while disappears the band of the free diazo (Figure V.3, b and c). At 25 mol% of lithium, the

band of the free substrate was completely gone and the new band remained invariable under higher concentrations of lithium salt. This experiment suggests that, indeed, lithium is able to coordinate substrate **S20** through the O atom as it was proposed. And the higher activity achieved in the system upon the addition of the lithium salt points towards the hypothesis of the formation of a strong Li-O adduct, preventing the coordination of the iron center to the O atom and favoring its coordination into the C center.

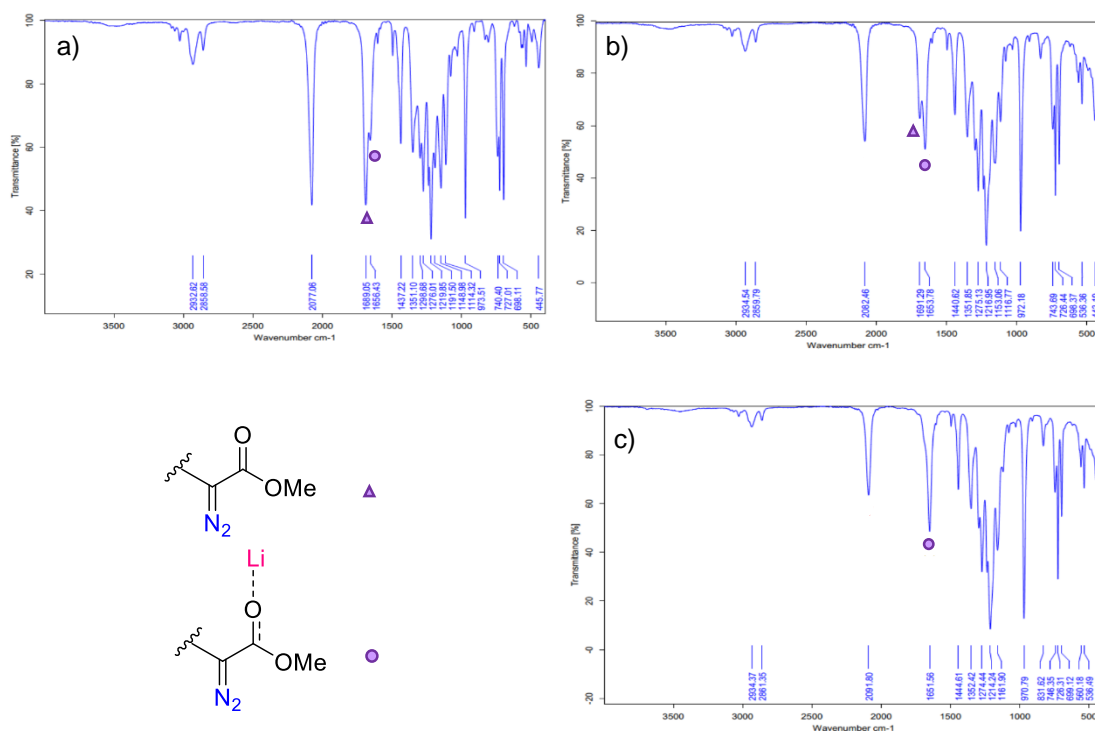


Figure V.3. IR spectra of different molar mixtures of **S20**: $[\text{LiAl}(\text{OC}(\text{CF}_3)_3)_4]$. a) 1:0.05; b) 1:0.15; c) 1:0.25.

The identification of the rate determining step of the reaction is another important issue that needs to be address. For this reason, the monitoring of the consumption of **S20** under the optimized reaction conditions along time showed a first order dependence on the diazo acetate (Figure V.4), indicating that the rate determining step of the reaction is the formation of the metallocarbene specie, as it happens in the iron system of Chapter IV.

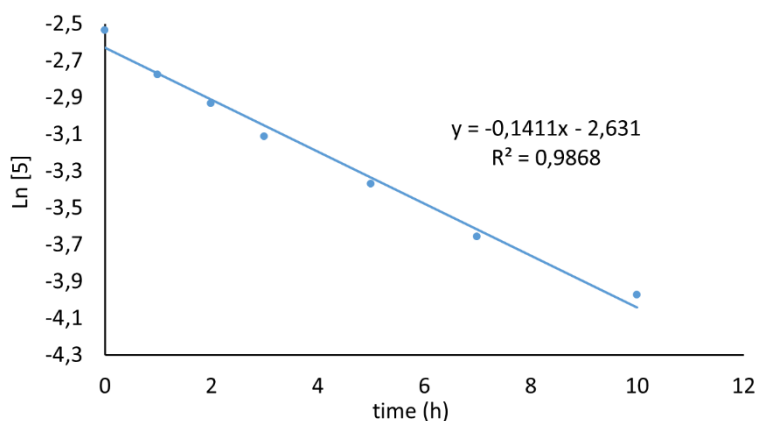
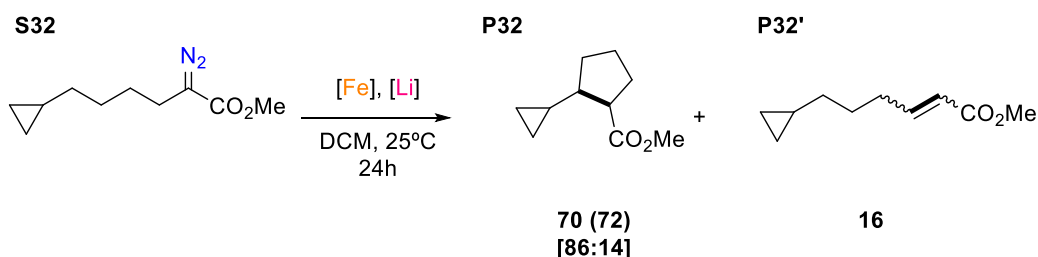


Figure V.4. Plot of Ln[S20] vs time (h) for C-H functionalization of **S20** under optimized reaction conditions.

After the formation of the metalcarbene species, two different pathways can occur to promote the product formation: a stepwise mechanism, which involves the homolytic C-H bond cleavage followed by the recombination of the carbene with the generated carbon radical center to form the new C-C bond; or a concerted mechanism in which an insertion of the carbene to the C-H bond takes place. To discern between these two scenarios, two different experiments were conducted.

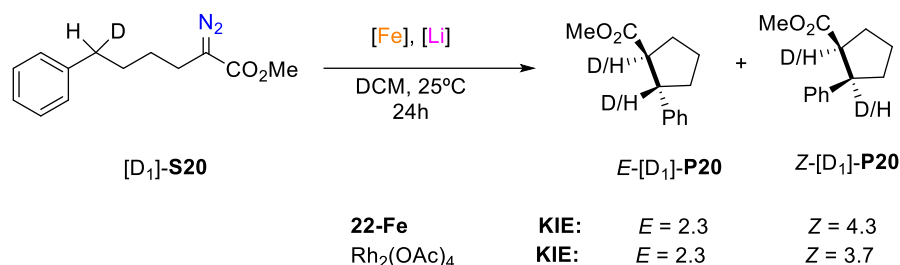
Firstly, the functionalization of cyclopropyl derivative diazo acetate (**S32**) as radical clock was performed under standard reaction conditions. A 68% of product yield could be achieved as cyclopentane without opening of the cyclopropyl ring, while the rest of the sample corresponds to β -hydride migration product (Scheme V.3). This results may suggest that either, no radicals are involved in the reaction or if they are present, their lifetime is very short and rapidly recombine.



Scheme V.3. Functionalization of a radical clock substrate. Isolated yield in parenthesis. Diastereomeric ratio of isolated samples determined by GC-MS in brackets.

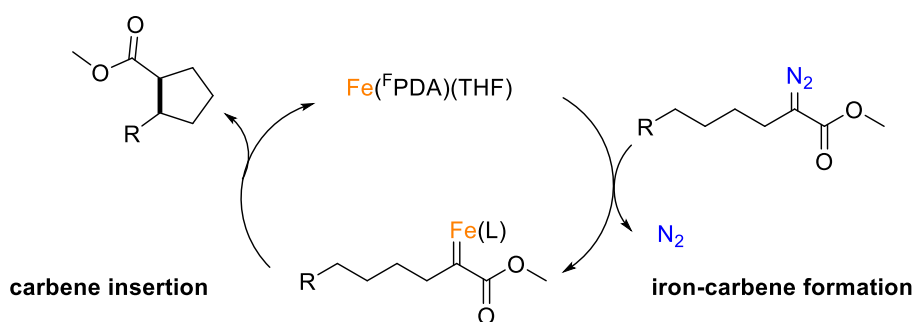
Additionally, the intramolecular kinetic isotopic effect (KIE) was determined. The partially deuterated diazo reagent [D₁]-**S20** was submitted under standard catalytic conditions and the KIE was determined by relative integration on the ¹H-NMR spectrum. A KIE value of 2.3 for the major *trans* isomer was obtained, while a higher value of 4.3 was calculated for the *Z* isomer. Although those values may suggest a possible involvement of a radical center, a control experiment using the same substrate, but

applying $\text{Rh}_2(\text{OAc})_4$ complex as catalyst was performed, since it is known that rhodium carboxylates complexes are capable of functionalizing those substrates through carbene insertion mechanism.^{185,192} Close KIE values to the Fe system were obtained for both isomers (Scheme V.4), indicating a carbene insertion mechanism for the Fe/Li system.



Scheme V.4. Functionalization of [D₁]-20 for the determination of the KIE using iron and rhodium complexes.

With all these results in hand, a preliminary mechanism can be proposed. First, the formation of the metallocarbene takes place, being the rate determining step of the reaction. The addition of the lithium salt prevents the unfruitful coordination of the iron center to the carbonyl group, helping the formation of the metallocarbene species to proceed under mild reaction conditions. Then, a concerted carbene insertion step occurs, which involve the simultaneous formation of the new C-H and C-C bonds with the final regeneration of the active catalyst and the releasing of the product (Scheme V.5).



Scheme V.5. Proposed reaction mechanism for the catalytic functionalization of $\text{C}_{\text{sp}^3}\text{-H}$ bonds.

V.2 Summary

A new system for the selective formation of cyclopentane products by iron-carbene intermediates has been described. The combination of an iron complex with ligand of low coordination number and electron-withdrawing properties and a lithium salt acting as strong Lewis acid, allowed the performance of the system under mild reaction conditions.

Mechanistic studies reveal that the lithium cation plays an important role preventing the unproductive coordination of the iron complex to the carbonyl group of the diazo

acetate, allowing its coordination into the carbenic carbon, promoting an efficient extrusion of the N₂ molecule, possible at room temperature. Moreover, a concerted carbene insertion mechanism can be proposed based on the no-detection of radical intermediates and for the similar performance as a rhodium carboxylate complex.

Chapter VI

General Conclusions

The use of first row transition metals in metal-carbene chemistry is limited in the literature when compared to the presence of noble metals. For this reason, the main goal of this thesis has been the description of new NHC complexes with first row transition metal ions, and also by the use of iron-based catalytic systems for the formation of new C-C bonds.

Specifically, in **Chapter III**, the design of a new ligand, which is composed by a macrocyclic structure, the *tacn*, and a triazolium salt, acting as a mesoionic carbene, is described. Iron, zinc, copper(I) and silver complexes from the corresponding ligand were synthesized and characterized in solid and solution state, and their properties compared with those of the complexes bearing the analog pyridine based ligand. Preliminary reactivities of those complexes have been studied. Interestingly, the copper(I) complex have shown ability for the reversible binding and activation O₂, generating a copper-superoxide species which is able to perform HAT reactivity. This complex is the first organometallic copper-superoxide species described to date.

In **Chapter IV**, a system for the functionalization of aromatic C-H bonds by carbene transfer reaction from a commercially available diazo compound (EDA) is described, by using a combination of iron complexes with tetradentate aminopyridine based ligands and NaBAR₄^F, acting as halide scavenger. Harsh reaction conditions are needed (80°C in an overnight reaction). However, unprecedented selectivity towards Csp²-H bonds, avoiding Csp³-H bond functionalization and addition reactions, was observed. Full description of the mechanism has been studied by means of experimental evidences and theoretical calculations. Key point in the reaction selectivity comes from the formation of carbocationic intermediates in which a carbonyl-metal binding assisted step takes place, directing the high selectivity of the reaction.

Finally, in **Chapter V**, intramolecular functionalization of Csp³-H bonds, by forming cyclopentane rings, using diazoacetates as carbene transfer agents is reported. The use of a bidentate redox active ligand as supporting ligand for iron complexes, and its combination with a lithium salt acting as Lewis acid has allowed the description of a system which is able to operate under very mild reaction conditions. FT-IR spectroscopy provides evidences that the addition of the Lewis acid salt prevents the unproductive coordination of the carbonyl group of the starting diazoacetate to the metal center, allowing a favorable formation of the carbene intermediate by directing the coordination of the iron center into the carbenic carbon.

Chapter VII

Experimental Section

VII.1 Experimental Section Chapter III

VII.1.1 Instrumentation

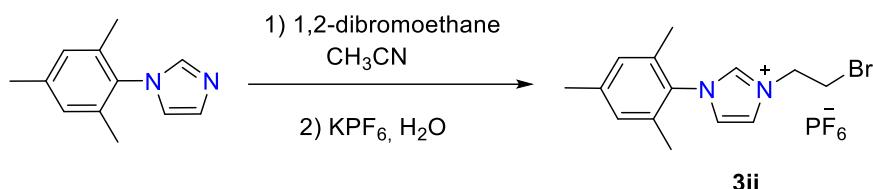
^1H and ^{13}C NMR spectra were taken on Bruker DPZ300 and DPX400 spectrometers at 25°C and referenced to residual solvent peaks. High resolution mass spectra (HRMS) were recorded on a Bruker MicroTOF-Q IITM instrument with a ESI source at Serveis Tècnics of the University of Girona. Samples were introduced into the mass spectrometer ion source by direct infusion through a syringe pump and were externally calibrated using sodium formate. GC-MS analyses were performed on an Agilent 7890A gas chromatograph equipped with an HP-5 capillary column interfaced with an Agilent 5975C mass spectrometer. The X-ray intensity data were measured on a Bruker D8 QUEST ECO three-circle diffractometer system equipped with a Ceramic x-ray tube ($\text{Mo K}\alpha$, $\lambda = 0.71073 \text{ \AA}$), a doubly curved silicon crystal monochromator, and a CPAD detector (PHOTON II) and on a Apex DUO Kappa 4-axis goniometer equipped with an APPEX 2 4K CCD area detector, a Microfocus Source E025 IuS using $\text{MoK}\alpha$ radiation, Quazar MX multilayer Optics as monochromator and an Oxford Cryosystems low temperature device Cryostream 700 plus ($T = -173 \text{ }^\circ\text{C}$). UV-Vis spectroscopy was performed on a Cary 50 Scan (Varian) UV-Vis spectrophotometer or on an Agilent 8453 diode array spectrophotometer with 1 cm quartz cells. Low temperature control was achieved with a cryostat from Unisoku Scientific Instruments, Japan.

VII.1.2 Materials

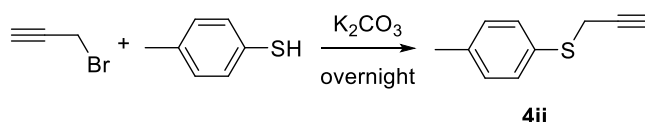
All air- and moisture- sensitive materials were manipulated with standard Schlenk techniques under argon atmosphere or in a glovebox. Reagents were purchased from commercial sources and used as received, without any further purification unless stated otherwise. Solvents were purchased from SDS and Scharlab, purified and dried by passing through an activated alumina purification system (M-Braun SPS-800) or by conventional distillation techniques. 2,2,6,6-Tetramethylpiperidinoxy (TEMPO-H)¹⁹³ was synthesized as previously reported.

VII.1.3 Synthesis of ligands

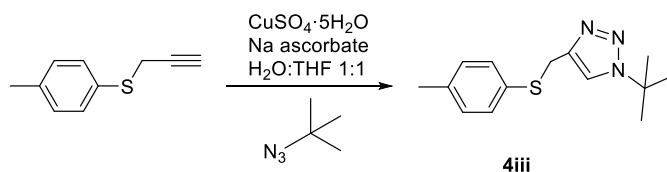
Me_2tacn ,¹⁹⁴ **3i**¹⁴¹ and *tert*-butyl azide (**4i**)¹⁹⁵ were synthesized as previously reported.



3ii: 1,2-Dibromoethane (25.5 mL, 295 mmols, 19 equiv.) was added into a solution of 1-mesityl-1H-imidazole (**3i**) (2.9 gr, 15.56 mmols) in acetonitrile and the solution was stirred under reflux overnight. Then, the solvent was removed under vacuum and the residue was dissolved in water. KPF_6 (2.9 gr, 15.56 mmols, 1 equiv.) was added and a precipitate was formed. The mixture was filtered and the resulting solid was cleaned with Et_2O , to give the final product as a brown pale solid (90% yield). $^1\text{H-NMR}$ (CD_3CN , 400 MHz, 300K): 8.69 (t, $J = 1.6\text{Hz}$, 1H), 7.73 (t, $J = 1.8\text{Hz}$, 1H), 7.52 (t, $J = 1.8\text{Hz}$, 1H), 7.15 (s, 2H), 4.70 (t, $J = 5.8\text{Hz}$, 2H), 3.92 (t, $J = 5.8\text{Hz}$, 2H), 2.38 (s, 3H), 2.07 (s, 6H). $^{13}\text{C-NMR}$ (CD_3CN , 100 MHz): 141.4, 136.9, 134.8, 129.5, 124.4, 123.1, 51.1, 30.6, 20.2, 16.4.

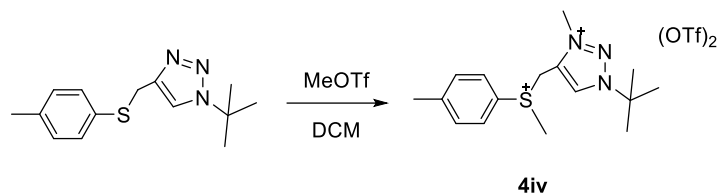


4ii: A solution of propargyl bromide (2.14 mL, 19.32 mmol, 1.2 equiv.), *p*-toluenethiol (2 gr, 16.1 mmol, 1 equiv.) and K_2CO_3 (2670 mg, 19.32 mmol, 1.2 equiv.) in acetonitrile was stirred at r.t. overnight. Then, the solution is filtered and the filtrates were strongly dried to give the desired product as a yellow oil (97% yield). $^1\text{H-NMR}$ (CDCl_3 , 400 MHz, 300K): 7.42 (d, $J = 8\text{Hz}$, 2H), 7.18 (d, $J = 8\text{Hz}$, 2H), 3.60 (d, $J = 2.6\text{Hz}$, 2H), 2.38 (s, 3H), 2.26 (t, $J = 2.6\text{Hz}$, 3H). $^{13}\text{C-NMR}$ (CDCl_3 , 100 MHz): 137.4, 131.1, 129.8, 80.1, 71.5, 23.3, 21.1.

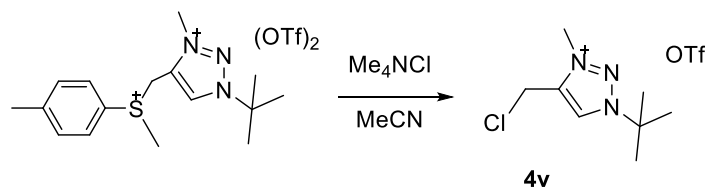


4iii: **4ii** (2000 mg, 12.3 mmol, 1 equiv.), $\text{CuSO}_4 \cdot 5\text{H}_2\text{O}$ (154 mg, 0.62 mmol, 0.05 equiv.) and sodium ascorbate (487 mg, 2.46 mmol, 0.2 equiv) were suspended in a mixture of H_2O (20 mL) and THF (20 mL). *tert*-butyl azide (1463 mg, 14.76 mmol, 1.2 equiv.) was added and the mixture was heated at 100°C overnight. Then, the mixture was allowed to cool down. The solvent was evaporated and the residue was dissolved in CH_2Cl_2 . The solution was filtered through Celite[®]. The filtrate was extracted three times with H_2O . All organic layers were combined, dried over MgSO_4 and evaporated to

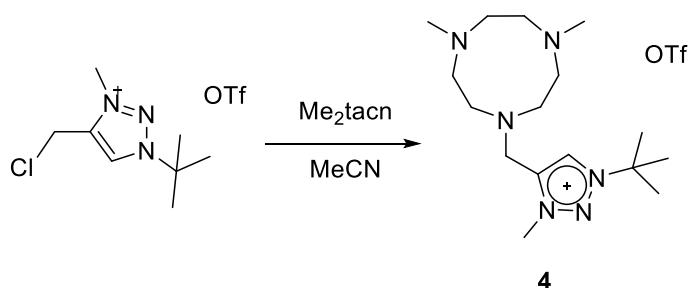
dryness to give the final product as a brown oil (86% yield). $^1\text{H-NMR}$ (CDCl_3 , 400 MHz, 300K): 7.35 (s, 1H), 7.26 (d, $J = 8\text{Hz}$, 2H), 7.09 (d, $J = 8\text{Hz}$, 2H), 4.20 (s, 2H), 2.32 (s, 3H), 1.62 (s, 9H). $^{13}\text{C-NMR}$ (CDCl_3 , 100 MHz): 136.7, 132.0, 130.7, 129.7, 119.2, 59.3, 29.9, 21.0.



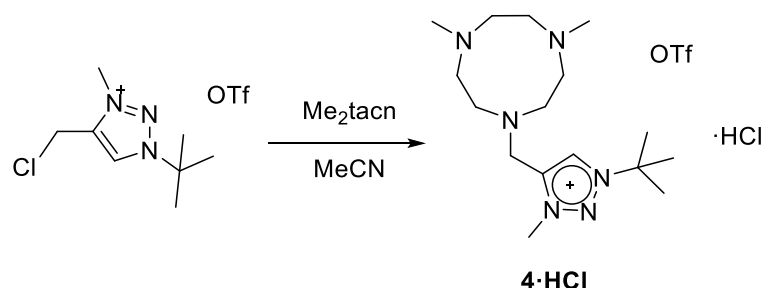
4iv: **4iii** (2000 mg, 7.65 mmol, 1 equiv.) was dissolved in CH_2Cl_2 in a pressure flask and cooled down to 0°C . MeOTf (6mL, 53.5 mmol, 7 equiv.) was added, while stirring at 0°C . After 15 minutes, the mixture was heated at 50°C for 16h. After that reaction time, all volatiles were evaporated and strongly dried to give the final product as a brown oil (95% yield). $^1\text{H-NMR}$ (CD_3CN , 400 MHz, 300K): 8.36, 7.88 (d, $J = 8.3\text{Hz}$, 2H), 7.61 (d, $J = 8.3\text{Hz}$, 2H), 5.22 (d, $J = 14.7\text{Hz}$, 1H), 5.06 (d, $J = 14.7\text{Hz}$, 1H), 4.18 (s, 3H), 3.43 (s, 3H), 2.52 (s, 3H), 1.68 (s, 9H). $^{13}\text{C-NMR}$ (CD_3CN , 100 MHz): 147.8, 132.0, 132.0, 131.2, 129.6, 67.3, 38.7, 37.9, 28.1, 26.1, 20.8.



4v: **4iv** (4270 mg, 7.25 mmol, 1 equiv.) and Me_4NCl (1192 mg, 10.9 mmol, 1.5 equiv.) were dissolved in acetonitrile and stirred at r.t. for 3 hours. The solvent was evaporated and the residue was dissolved in the minimum amount of dichloromethane and filtered through Celite[®]. The product is precipitated with hexane, while stirring. The solution is poured and the precipitation procedure is repeated two more times. Complete purification of the product is achieved by alumina column (DCM:MeOH, 100:1) to give the final product as a pale brown solid (73% yield). $^1\text{H-NMR}$ (CDCl_3 , 400 MHz, 300K): 8.92 (s, 1H), 4.99 (s, 2H), 4.37 (s, 3H), 1.78 (s, 9H). $^{13}\text{C-NMR}$ (CDCl_3 , 100 MHz): 140.5, 127.7, 66.7, 38.4, 31.0, 29.1.



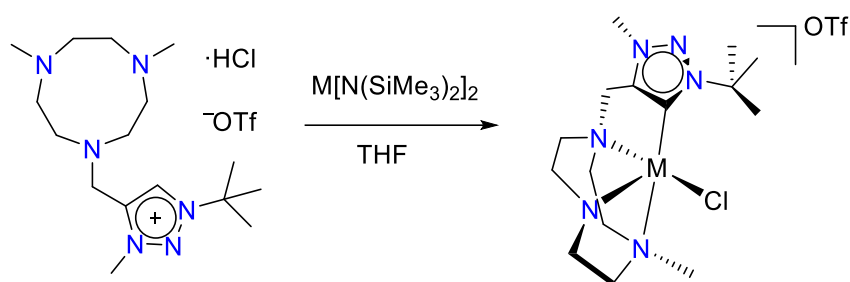
4: **4v** (530 mg, 1.57 mmols, 1 equiv.) and Me₂tacn (494 mg, 3.14 mmols, 2 equiv.) were dissolved in acetonitrile and refluxed for 18h. Then, the reaction was cooled down and the solvent was evaporated. The residue was dissolved in dichloromethane, basified with NaOH 2M for the removal of HCl salt and extracted with dichloromethane. The organic layer was concentrated and the residue was dissolved in the minimum amount of dichloromethane and precipitated with the addition of an excess of hexane, while stirring. The solution is poured and the precipitation procedure is repeated two more times. The product is thoroughly dried to give the final product as a brown oil (45% yield) and stored under moisture free conditions. ¹H-NMR (CDCl₃, 400 MHz, 300K): 9.07 (s, 1H), 4.36 (s, 3H), 4.09 (s, 2H), 2.87 - 2.85 (m, 4H), 2.71 - 2.69 (m, 8H), 2.39 (s, 6H), 1.78 (s, 9H). ¹³C-NMR (CDCl₃, 100 MHz): 143.5, 127.5, 65.8, 57.1, 56.7, 55.2, 50.3, 46.5, 38.3, 29.2.



4·HCl: **4v** (530 mg, 1.57 mmols, 1 equiv.) and Me₂tacn (494 mg, 3.14 mmols, 2 equiv.) were dissolved in acetonitrile and refluxed for 18h. Then, the reaction was cooled down and the solvent was evaporated. The residue was dissolved in the minimum amount of dichloromethane and precipitated with the addition of an excess of hexane, while stirring. The solution is poured and the precipitation procedure is repeated two more times. The product is thoroughly dried to afford an orange-brown powder (60% yield) as the final product and stored under moisture free conditions. ¹H-NMR (CD₃CN, 400 MHz, 300K): 9.03 (s, 1H), 4.23 (s, 3H), 4.10 (s, 2H), 3.30 - 3.20 (m, 4H), 3.06 - 3.01 (m, 4H), 2.87 - 2.79 (m, 4H), 2.64 (s, 6H), 1.77 (s, 9H). ¹³C-NMR (CD₃CN, 100 MHz): 141.2, 127.6, 65.8, 54.7, 52.4, 51.9, 49.5, 43.8, 37.9, 28.3. ESI-HRMS calcd. for C₁₆H₃₃N₆ [M-OTf-HCl]⁺: 309.2761, found 309.2768.

VII.1.4 Synthesis of complexes

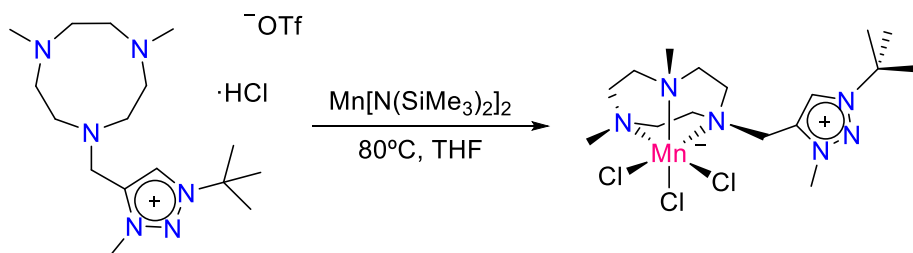
Fe[N(SiMe₃)₂]₂,¹⁹⁶ Mn[N(SiMe₃)₂]₂,¹⁹⁶ Cu[N(SiMe₃)₂]₂,¹⁹⁷ Zn[N(SiMe₃)₂]₂¹⁹⁸ were synthesized as previously reported.



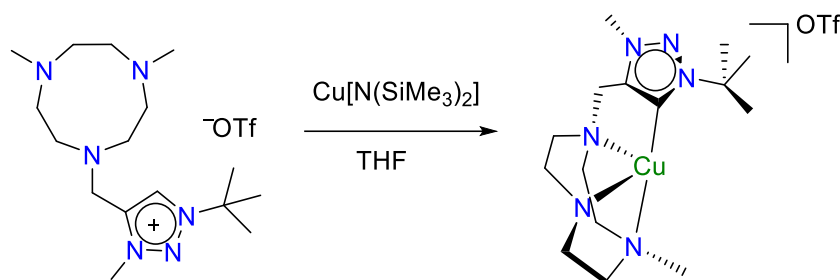
4-M (M=Fe, Zn): To a suspension of **4-HCl** in THF, $M[N(\text{SiMe}_3)_2]_2$ was added as a solid and stirred overnight, while the ligand gets solubilized. Then, the solution was filtered and the filtrate was submitted to crystallization conditions.

4-Fe: Single crystals for X-Ray diffraction were achieved by double layer crystallization of THF/*n*-pentane at -40°C . 35% yield of yellow crystals. $^1\text{H-NMR}$ (CD_2Cl_2 , 400 MHz, 300K): 158.1 (s, 3H), 126.8 (s, 3H), 93.2 (s, 2H), 85.5 (s, 2H), 43.6 (s, 5H), 32.3 (s, 2H), 22.8 (s, 9H), 13.0 (s, 3H), -2.3 (s, 3H). ESI-HRMS calcd. for $\text{C}_{16}\text{H}_{32}\text{N}_6\text{FeCl}$ $[\text{M-OTf}]^+$: 399.1721, found 399.1743.

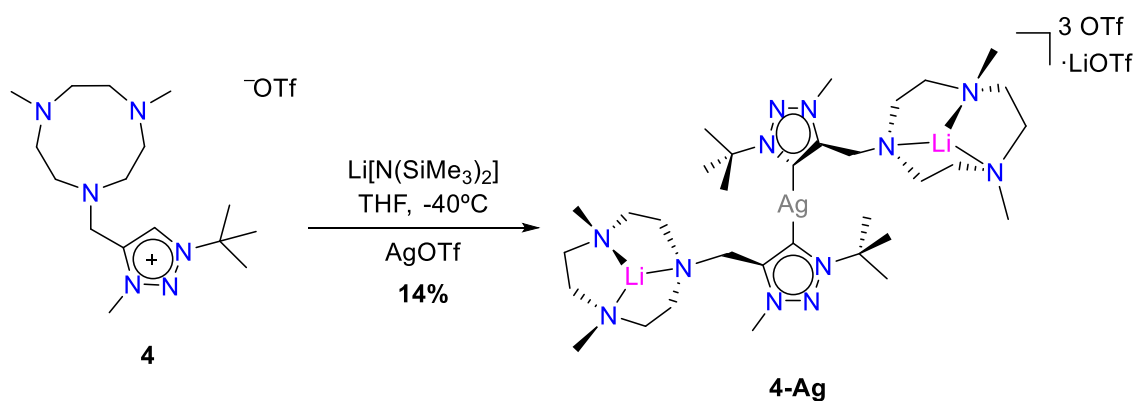
4-Zn: Single crystals for X-Ray diffraction were achieved by double layer crystallization of acetone/*n*-pentane at room temperature. 47% yield of colorless crystals. $^1\text{H-NMR}$ (acetone- d_6 , 400 MHz, 300K): 4.27 (s, 2H), 4.16 (s, 3H), 3.30 - 3.17 (m, 4H), 3.06 - 2.95 (m, 8H), 2.82 (s, 6H), 1.87 (s, 9H). $^{13}\text{C-NMR}$ (acetone- d_6 , 100 MHz): 154.3, 150.6, 64.6, 55.3, 54.2, 50.6, 49.5, 47.9, 35.4, 29.4. ESI-HRMS calcd. for $\text{C}_{16}\text{H}_{32}\text{N}_6\text{ZnCl}$ $[\text{M-OTf}]^+$: 407.1663, found 407.1678.



4-Mn: To a suspension of **4-HCl** in THF, $\text{Mn}[N(\text{SiMe}_3)_2]_2$ was added as a solid and stirred overnight at 80° . Then, the solution was filtered and the filtrate was dried. X-Ray crystals were obtained by double layer crystallization with dichloromethane/pentane at -40°C . 12% yield of colorless crystals. ESI-HRMS calcd. for $\text{C}_{16}\text{H}_{33}\text{N}_6\text{MnCl}_2$ $[\text{M-Cl}]^+$: 434.1519, found 434.1532.



4-Cu: To a solution of **4** in THF, previously dried overnight with molecular sieves, $\text{Cu}[\text{N}(\text{SiMe}_3)_2]$ was added as a solid and stirred overnight. Then, the solution was filtered off and the filtrate was crystallized by double layer crystallization of THF/*n*-pentane at -40°C . 50% yield of yellow crystals. $^1\text{H-NMR}$ (acetone- d_6 , 400 MHz, 300K): 4.12 (s, 2H), 4.05 (s, 3H), 3.21 - 3.18 (m, 2H), 2.95 - 2.94 (m, 8H), 2.81 (m, 8H), 1.73 (s, 9H). ESI-HRMS calcd. for $\text{C}_{16}\text{H}_{32}\text{N}_6\text{Cu}$ $[\text{M-OTf}]^+$: 371.1979, found 371.1973.



4-Ag: To a solution of **4** in THF at -40°C , a solution of $\text{Li}[\text{N}(\text{SiMe}_3)_2]$ in THF (1M) was added and the mixture was stirred for 30 minutes while warming at room temperature. Then, AgOTf was added directly as solid and the mixture was stirred for 2 hours. Afterwards, the solution was dried, dissolved in dichloromethane and finally crystallized by double layer with *n*-hexane at -40°C to afford colorless crystals (14% yield). $^1\text{H-NMR}$ (CD_2Cl_2 , 400 MHz, 300K): 4.32 (s, 2H), 4.29 (s, 3H), 2.94 - 2.57 (m, 12H), 2.46 (s, 6H), 1.79 (s, 9H). $^7\text{Li-NMR}$ (CD_2Cl_2 , 155 MHz, 300K): 0.63 (s).

VII.1.5 Crystal data

Table VII.1. Crystal data for **4-Fe**

Empirical formula	C ₁₇ H ₃₂ ClF ₃ FeN ₆ O ₃ S	
Formula weight	548.84	
Temperature	100(2) K	
Wavelength	0.71073 Å	
Crystal system	Monoclinic	
Space group	P2(1)/c	
Unit cell dimensions	a = 10.7138(6) Å	α = 90°.
	b = 12.8019(7) Å	β = 90.491(2)°.
	c = 17.4038(9) Å	γ = 90°
Volume	2387.0(2) Å ³	
Z	4	
Density (calculated)	1.527 Mg/m ³	
Absorption coefficient	0.886 mm ⁻¹	
F(000)	1144	
Crystal size	0.05 x 0.04 x 0.01 mm ³	
Theta range for data collection	1.975 to 31.522°.	
Index ranges	?<=h<=? , ?<=k<=? , ?<=l<=?	
Reflections collected	7656	
Independent reflections	7656[R(int) =?]	
Completeness to theta =31.522°	96.100006%	
Absorption correction	Multi-scan	
Max. and min. transmission	0.991 and 0.762	
Refinement method	Full-matrix least-squares on F ²	
Data / restraints / parameters	7656/ 0/ 295	
Goodness-of-fit on F ²	0.971	
Final R indices [I>2sigma(I)]	R1 = 0.0455, wR2 = 0.1068	
R indices (all data)	R1 = 0.0692, wR2 = 0.1146	
Largest diff. peak and hole	0.798 and -0.726 e.Å ⁻³	

Table VII.2. Crystal data for **4-Zn**

Empirical formula	C ₁₇ H ₃₂ ClF ₃ N ₆ O ₃ SZn	
Formula weight	558.36 g/mol	
Temperature	100(2) K	
Wavelength	0.71073 Å	
Crystal size	0.120 x 0.140 x 0.220 mm	
Crystal habit	colorless block	
Crystal system	Monoclinic	
Space group	P 1 21/c 1	
Unit cell dimensions	a = 10.604(9) Å	α = 90°

	$b = 12.707(12) \text{ \AA}$	$\beta = 92.35(3)^\circ$
	$c = 17.513(15) \text{ \AA}$	$\gamma = 90^\circ$
Volume	2358.(4) \AA^3	
Z	4	
Density (calculated)	1.573 g/cm^3	
Absorption coefficient	1.299 mm^{-1}	
F(000)	1160	
Theta range for data collection	2.50 to 27.57°	
Index ranges	-13<=h<=13, -16<=k<=16, -22<=l<=22	
Reflections collected	62493	
Independent reflections	5430 [R(int) = 0.0500]	
Coverage of independent reflections	99.5%	
Absorption correction	Multi-scan	
Max. and min. transmission	0.7456 and 0.6892	
Structure solution technique	direct methods	
Structure solution program	SHELXT 2014/5 (Sheldrick, 2014)	
Refinement method	Full-matrix least-squares on F^2	
Refinement program	SHELXL-2017/1 (Sheldrick, 2017)	
Data / restraints / parameters	5430 / 0 / 295	
Goodness-of-fit on F^2	1.042	
Final R indices [$I > 2\sigma(I)$]	4562 data; $I > 2\sigma(I)$ R1 = 0.0277, wR2 = 0.0553	
	all data R1 = 0.0399, wR2 = 0.0599	
Largest diff. peak and hole	0.353 and -0.387 e\AA^{-3}	
R.M.S. deviation from mean	0.064 e\AA^{-3}	

Table VII.3. Crystal data for 4-Mn

Empirical formula	$\text{C}_{19}\text{H}_{39}\text{Cl}_9\text{MnN}_6$	
Formula weight	725.55 g/mol	
Temperature	100(2) K	
Wavelength	0.71073 \AA	
Crystal size	0.250 x 0.250 x 0.300 mm	
Crystal habit	Clear colourless block	
Crystal system	Monoclinic	
Space group	P 1 21/c 1	
Unit cell dimensions	$a = 16.6327(8) \text{ \AA}$	$\alpha = 90^\circ$
	$b = 17.4212(8) \text{ \AA}$	$\beta = 95.300(2)^\circ$
	$c = 22.4913(10) \text{ \AA}$	$\gamma = 90^\circ$
Volume	6489.3(5) \AA^3	
Z	8	

Density (calculated)	1.485 g/cm ³
Absorption coefficient	1.169 mm ⁻¹
F(000)	2984
Theta range for data collection	2.51 to 27.62°
Index ranges	-21 ≤ h ≤ 21, -22 ≤ k ≤ 22, -29 ≤ l ≤ 29
Reflections collected	125981
Independent reflections	14942 [R(int) = 0.0392]
Coverage of independent reflections	99.0%
Absorption correction	Multi-scan
Max. and min. transmission	0.7590 and 0.7210
Structure solution technique	direct methods
Structure solution program	SHELXT 2014/5 (Sheldrick, 2014)
Refinement method	Full-matrix least-squares on F ²
Refinement program	SHELXL-2017/1 (Sheldrick, 2017)
Data / restraints / parameters	14942 / 0 / 643
Goodness-of-fit on F ²	1.080
Final R indices [I > 2σ(I)]	12410 data; I > 2σ(I) R1 = 0.0618, wR2 = 0.1477 all data R1 = 0.0761, wR2 = 0.1587
Largest diff. peak and hole	1.851 and -1.774 eÅ ⁻³
R.M.S. deviation from mean	0.115 eÅ ⁻³

Table VII.4. Crystal data for **4-Cu**

Empirical formula	C ₂₁ H ₄₀ CuF ₃ N ₆ O ₄ S	
Formula weight	593.19 g/mol	
Temperature	100(2) K	
Wavelength	0.71073 Å	
Crystal size	0.080 x 0.200 x 0.200 mm	
Crystal habit	pale yellow-green block	
Crystal system	triclinic	
Space group	P -1	
Unit cell dimensions	a = 10.2299(7) Å	α = 88.948(3)°
	b = 11.5233(7) Å	β = 74.247(3)°
	c = 12.0696(9) Å	γ = 81.259(3)°
Volume	1353.06(16) Å ³	
Z	2	
Density (calculated)	1.456 g/cm ³	
Absorption coefficient	0.943 mm ⁻¹	

F(000)	624
Theta range for data collection	2.77 to 28.00°
Index ranges	-13<=h<=13, -15<=k<=15, -15<=l<=15
Reflections collected	35059
Independent reflections	6417 [R(int) = 0.1465]
Coverage of independent reflections	98.3%
Absorption correction	Multi-scan
Max. and min. transmission	0.9280 and 0.8340
Structure solution technique	direct methods
Structure solution program	SHELXT 2014/5 (Sheldrick, 2014)
Refinement method	Full-matrix least-squares on F ²
Refinement program	SHELXL-2017/1 (Sheldrick, 2017)
Data / restraints / parameters	6417 / 18 / 331
Goodness-of-fit on F ²	1.177
Final R indices [I>2σ(I)]	4762 data; I>2σ(I) R1 = 0.0834, wR2 = 0.1523 all data R1 = 0.1230, wR2 = 0.1665
Largest diff. peak and hole	1.288 and -0.747 eÅ ⁻³
R.M.S. deviation from mean	0.117 eÅ ⁻³

Table VII.5. Crystal data for **4-Ag**

Empirical formula	C ₄₀ H ₇₂ AgCl ₈ F ₁₂ Li ₃ N ₁₂ O ₁₂ S ₄	
Formula weight	1681.62 g/mol	
Temperature	100(2) K	
Wavelength	0.71076 Å	
Crystal system	monoclinic	
Space group	C 1 2/c 1c	
Unit cell dimensions	a = 21.691(16) Å	α = 90°
	b = 16.239(12) Å	β = 104.72(2)°
	c = 20.698(14) Å	γ = 90°
Volume	7051.(9) Å ³	
Z	4	
Density (calculated)	1.584 g/cm ³	
Absorption coefficient	0.798 mm ⁻¹	
F(000)	3424	
Theta range for data collection	2.43 to 25.87°	
Index ranges	-26<=h<=26, -19<=k<=19, -25<=l<=25	
Reflections collected	82645	
Independent reflections	6792 [R(int) = 0.0682]	
Coverage of independent reflections	99.3%	
Absorption correction	Multi-scan	
Structure solution technique	direct methods	

Structure solution program	SHELXT 2014/5 (Sheldrick, 2014)
Refinement method	Full-matrix least-squares on F ²
Refinement program	SHELXL-2017/1 (Sheldrick, 2017)
Data / restraints / parameters	6792 / 0 / 422
Goodness-of-fit on F ²	1.128
Final R indices [I>2σ(I)]	5239 data; I>2σ(I) R1 = 0.0540, wR2 = 0.1361 all data R1 = 0.0786, wR2 = 0.1534
Largest diff. peak and hole	1.440 and -0.939 eÅ ⁻³
R.M.S. deviation from mean	0.106 eÅ ⁻³

VII.1.6 Copper-superoxide experiments

Formation of copper-superoxide

A stock solution at 0.9mM of **4-Cu** in acetone was prepared inside the glovebox and 2 mL of this solution was transferred in a UV-Vis cuvette. The cuvette was capped with a septum and taken out of the glovebox, placed in a Unisoku cryostat coupled in a UV-Vis spectrophotometer and the temperature was decreased down to -90°C. After reaching thermal equilibrium, dry dioxygen was bubbled for 1 minute and then the spectrum was recorded. Full formation of the copper-superoxide species takes 15 minutes.

Reaction of copper-superoxide with 2,6-di-*tert*-butyl-4-methoxyphenol

After the formation of the copper-superoxide specie, vacuum/N₂ cycles were repeated 3 times into the cuvette, maintaining its temperature at -90°C. Then, 10 equiv. of a stock solution of 2,6-di-*tert*-butyl-4-methoxyphenol in acetone was added and the reaction was stirred for 30 minutes to ensure the total consumption of the copper-superoxide. Afterwards, the cuvette was removed from UV-Vis spectrophotometer and 1 equiv. respect to the initial **4-Cu** of trimethoxybenzene as internal standard was added. The final solution was filtered through a silica plug and subsequently rinsed with 2 mL of DCM. The resulting solution was analyzed by GC. Yields were calculated based on the initial **4-Cu** complex.

VII. 2 Experimental Section Chapter IV

VII.2.1 Instrumentation

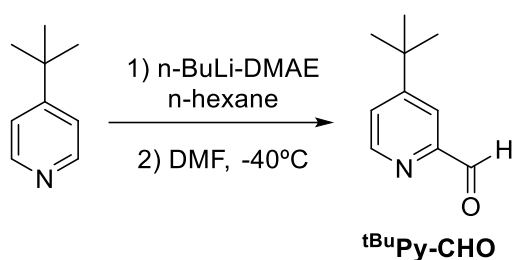
IR spectra were taken in a Mattson-Galaxy Satellite FT-IR spectrophotometer using a MKII Golden Gate single reflection ATR system. Elemental analyses were performed using a CHNS-O EA-1108 elemental analyzer from Fisons. ^1H and ^{13}C NMR spectra were taken on Bruker DPZ300 and DPX400 spectrometers at 25°C and referenced to residual solvent peaks. Electrospray ionization mass spectrometry (ESI-MS) experiments were performed on a Bruker Daltonics Esquire 3000 Spectrometer using a 1 mM solution of the analyzed compound. High resolution mass spectra (HRMS) were recorded on a Bruker MicroTOF-Q IITM instrument with a ESI source at Serveis Tècnics of the University of Girona. Samples were introduced into the mass spectrometer ion source by direct infusion through a syringe pump and were externally calibrated using sodium formate. GC-MS analyses were performed on an Agilent 7890A gas chromatograph equipped with an HP-5 capillary column interfaced with an Agilent 5975C mass spectrometer. X-ray structure determination was measured on a BRUKER SMART APEX CCD diffractometer using graphite-monochromated Mo K α radiation ($\lambda = 0.71073 \text{ \AA}$) from an x-Ray Tube. The structure was solved by direct methods and refined by full-matrix least-squares methods on F2. The non-hydrogen atoms were refined anisotropically. The H-atoms were placed in geometrically optimized positions and forced to ride on the atom to which they are attached.

VII.2.2 Materials

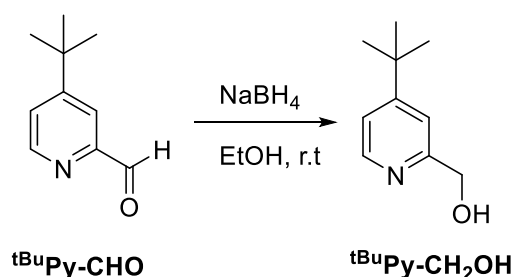
All air- and moisture- sensitive materials were manipulated with standard Schlenck techniques under nitrogen atmosphere or in a glovebox. All commercially available reagents were purchased from commercial sources and used as received, without any further purification unless stated otherwise. Solvents were purchased from SDS and Scharlab, purified and dried by passing through an activated alumina purification system (M-Braun SPS-800). Ethyldiazoacetate was purchased from Sigma-Aldrich and its concentration was determined by ^1H -NMR upon the addition of an internal standard.

VII.2.3 Synthesis of ligands

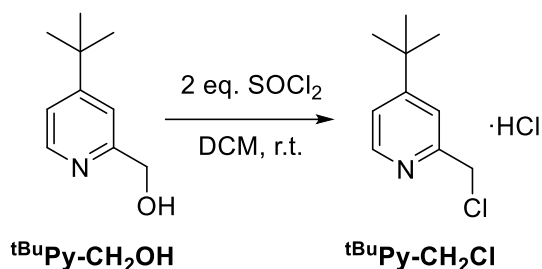
$^{199}\text{Tpa}^{(*,Br)}$ (**18**) and $^{200}\text{Tp}^{\text{Mes}}$ (**19**) ligands were synthesized as previously reported.

Synthesis of Me₂^{tBu}Pytacn (5):

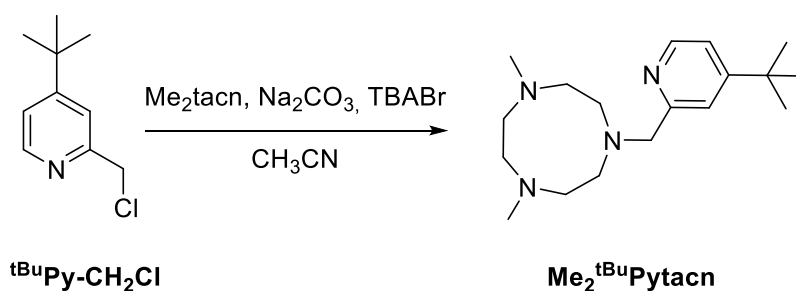
²⁰¹tBuPy-CHO: *n*-BuLi (1.6M in *n*-hexane, 28 mL, 48 mmol) was added dropwise to a cooled (-10°C) solution of 2-dimethylaminoethanol (2.4 mL, 24 mmol) in dry *n*-hexane (30 mL). The mixture was stirred at this temperature for 30 min, and then the 4-*tert*-butylpyridine (12 mmol) was added at once as a solid. After stirring at 0°C for 1h, the reaction was cooled to -40°C and a solution of dry DMF (1.39 mL, 18 mmol) in dry THF (45 mL) was added. After 30 minutes at -40°C, the mixture was quenched with 60 mL of 1 M HCl, the organic layer was separated and the aqueous phase was extracted with Et₂O (3 x 30 mL). The combined organic phases were dried (MgSO₄) and concentrated to dryness and the resulting residue was purified by flash chromatography (*n*-hexane:AcOEt, 10:1) affording the product as a yellow oil with some impurities (48% yield). The product was used without further purification. ¹H-NMR (CDCl₃, 400 MHz, 300K): δ 10.07 (s, 1H), 8.67 (d, *J* = 5.2Hz, 1H), 7.96 (d, *J* = 2.2Hz, 1H), 7.50 (dd, *J* = 5.2, 2.2Hz, 1H), 1.34 (s, 9H).



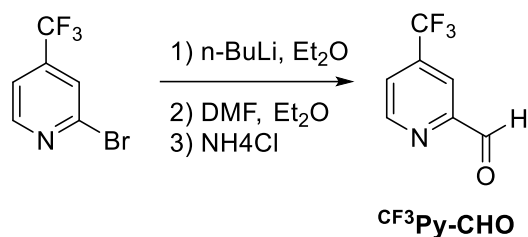
^{tBu}Py-CH₂OH: ^{tBu}Py-CHO (12.5 mmols) was dissolved in absolute ethanol (30 mL) and NaBH₄ (1g, 25 mmols) was directly added as a solid in little portions. The mixture was stirred overnight at room temperature and then 10 mL of water were cautiously added in order to destroy the unreacted NaBH₄. After 10 minutes of stirring, the solvent was removed under reduced pressure and 10 mL of water were added to the resulting white residue. The mixture was extracted with 3 x 20 mL DCM, the combined organic phases were dried with anhydrous MgSO₄ and the solvent was removed under reduced pressure. The residue was purified by silica chromatographic column (AcOEt) to yield the desired product as a colorless oil (39% yield). ¹H-NMR (CDCl₃, 400 MHz, 300K): δ 8.41 (d, *J* = 5.4Hz, 1H), 7.25 (s, 1H), 7.17 (d, *J* = 5.4Hz, 1H), 4.73 (s, 2H), 1.29 (s, 9H).



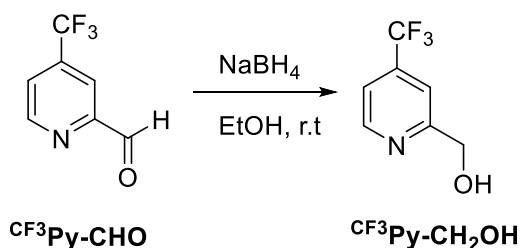
tBuPy-CH₂Cl: tBuPy-CH₂OH (11.7 mmols) was dissolved in DCM (20 mL). SOCl₂ (1.7 mL, 23.3 mmols) was cautiously added dropwise and the mixture was stirred overnight at room temperature under N₂. The solvent was removed under reduced pressure (gaseous HCl is formed during this process and extreme caution must be taken) and a brown residue was obtained. This residue was suspended in 20 mL of diethyl ether and stirred for two hours to give a fine white precipitate which was filtered and dried under vacuum (84% yield). ¹H-NMR (CDCl₃, 400 MHz, 300K): δ 8.64 (s, 1H), 8.00 (s, 1H), 7.83 (s, 1H), 5.21 (s, 2H), 1.46 (s, 9H).



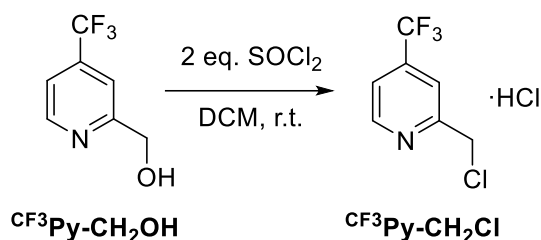
Me₂tBuPytacn: tBuPy-CH₂Cl (2.6 mmols), Me₂tacn·3HBr (1.02g, 2.6 mmols) and anhydrous acetonitrile (35 mL) were mixed in a 50 mL flask. Na₂CO₃ (1.90 g) and tetrabutylammonium bromide (TBABr) (0.04g) were added directly as solids and the resulting mixture was heated at reflux under N₂ for 20 hours. After cooling at room temperature, the resulting yellow mixture was filtered and the filter cake was washed with CH₂Cl₂. The combined filtrates were evaporated under reduced pressure. To the resulting residue, 1M NaOH (30 mL) was added and the mixture was extracted with CH₂Cl₂ (3x20 mL). The combined organic layers were dried over anhydrous MgSO₄ and the solvent was removed under reduced pressure. The resulting residue was treated with hexane (50 mL) and stirred for 12 hours. The mixture was filtered and the solution was removed under reduced pressure to yield the product (45% yield) as a yellow oil. ¹H-NMR (CDCl₃, 400 MHz, 300K): 8.40 (d, *J* = 4Hz, 1H), 7.55 (s, 1H), 7.12 (d, *J* = 4Hz, 1H), 3.82 (s, 2H), 2.82 (s, 4H), 2.80 - 2.78 (m, 4H), 2.68 - 2.65 (m, 4H), 2.35 (s, 6H), 1.31 (s, 9H).

Synthesis of Me₂^{CF₃}Pytacn (**9**):

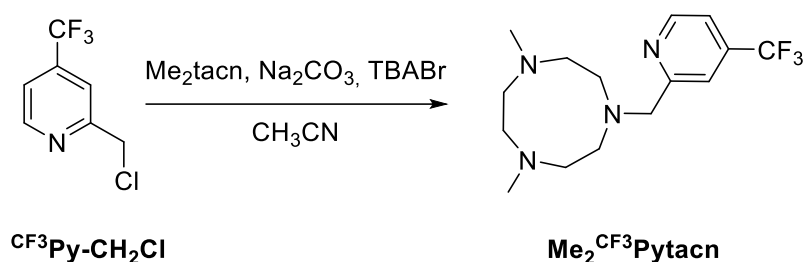
CF₃Py-CHO: To a solution of 2-bromo-2-(trifluoromethyl)pyridine (0.3 mL, 2.42 mmols) in diethyl ether (20 mL) at -78°, *n*-BuLi (1.6M in *n*-hexane, 1.66mL, 2.66 mmols) was added. After 40 min, DMF (0.281 mL, 3.63 mmols) was added and the reaction mixture was stirred at -78°C for further 45 minutes and the reaction mixture was allowed to warm to r.t. over a period of 1h. Then the reaction mixture was quenched with a solution of water in ammonium chloride. The organic layers were extracted, dried with MgSO₄ and evaporated to provide the product with impurities. The residue was used in the next reaction step without further purification.



CF₃Py-CH₂OH: CF₃Py-CHO (12.5 mmols) was dissolved in absolute ethanol (30 mL) and NaBH₄ (1g, 25 mmols) was directly added as a solid in little portions. The mixture was stirred overnight at room temperature and then 10 mL of water were cautiously added in order to destroy the unreacted NaBH₄. After 10 minutes of stirring, the solvent was removed under reduced pressure and 10 mL of water were added to the resulting white residue. The mixture was extracted with 3 x 20 mL DCM, the combined organic phases were dried with anhydrous MgSO₄ and the solvent was removed under reduced pressure. The residue was purified by silica chromatographic column (*n*-hexane:AcOEt, 1:1) to yield the desired product as a colorless oil (23% combined yield). ¹H-NMR (CDCl₃, 400 MHz, 300K): δ 8.75 (d, *J* = 5Hz, 1H), 7.55 (s, 1H), 7.44 (d, *J* = 5Hz, 1H), 4.86 (s, 2H).



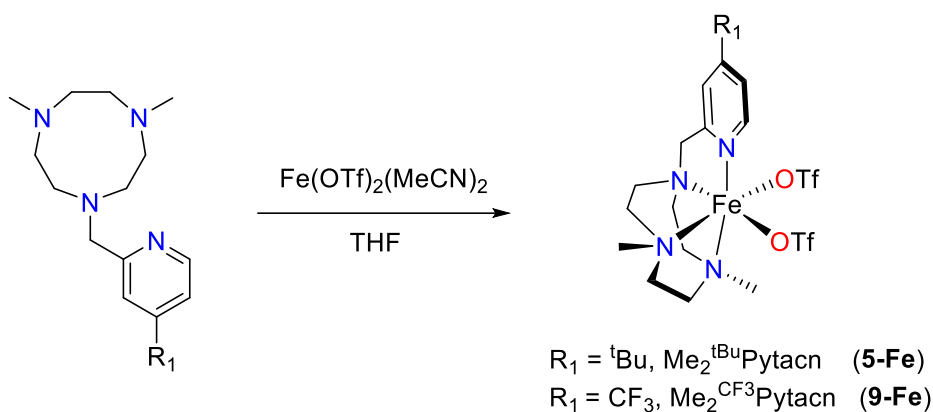
CF₃Py-CH₂Cl: CF₃Py-CH₂OH (11.7 mmols) was dissolved in DCM (20 mL). SOCl₂ (1.7 mL, 23.3 mmols) was cautiously added dropwise and the mixture was stirred overnight at room temperature under N₂. The solvent was under reduced pressure (gaseous HCl is formed during this process and extreme caution must be taken) and a brown residue was obtained which is used without further purification.



Me₂CF₃Pytacn: CF₃Py-CH₂Cl (2.6 mmols), Me₂tacn-3HBr (1.02g, 2.6 mmols) and anhydrous acetonitrile (35 mL) were mixed in a 50 mL flask. Na₂CO₃ (1.90 g) and tetrabutylammonium bromide (TBABr) (0.04g) were added directly as solids and the resulting mixture was heated at reflux under N₂ for 20 hours. After cooling at room temperature, the resulting yellow mixture was filtered and the filter cake was washed with CH₂Cl₂. The combined filtrates were evaporated under reduced pressure. To the resulting residue, 1M NaOH (30 mL) was added and the mixture was extracted with CH₂Cl₂ (3x20 mL). The combined organic layers were dried over anhydrous MgSO₄ and the solvent was removed under reduced pressure. The resulting residue was treated with hexane (50 mL) and stirred for 12 hours. The mixture was filtered and the solution was removed under reduced pressure to yield the product (32% combined yield) as a yellow oil. ¹H-NMR (CDCl₃, 400 MHz, 300K): 8.67 (d, *J* = 5Hz, 1H), 7.85 (s, 1H), 7.34 (d, *J* = 5Hz, 1H), 3.92 (s, 2H), 2.82 - 2.80 (m, 4H), 2.74 (s, 4H), 2.66 - 2.64 (m, 4H), 2.34 (s, 6H).

VII.2.4 Synthesis of complexes

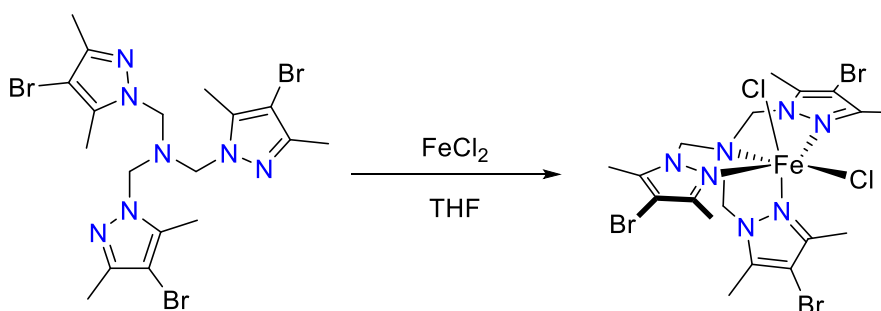
1-Fe,¹³⁸ **8-Fe,**²⁰² **6-Fe,**²⁰³ **10-Fe,**²⁰⁴ **11-Fe,**²⁰⁵ **12-Fe,**²⁰⁵ **13-Fe,**²⁰⁶ **14-Fe,**²⁰⁷ **15-Fe,**²⁰⁸ **16-Fe,**²⁰⁹ **17-Fe,**²⁰⁸ **1-Mn,**¹⁶¹ **1-Co,**²¹⁰ **1-Ni**²¹¹ were synthesized as previously reported.



[Fe(OTf)₂(Me₂^{R1}Pytacn)]: In a glovebox, a suspension of Fe(OTf)₂(MeCN)₂ in THF was added into a solution of the ligand in THF. The reaction mixture was stirred at room temperature overnight. The solvent was removed, and dichloromethane was added into the residue and the solution was filtered off through Celite©. Slow diethyl ether diffusion over the resultant solution afforded, in one night, the final complex.

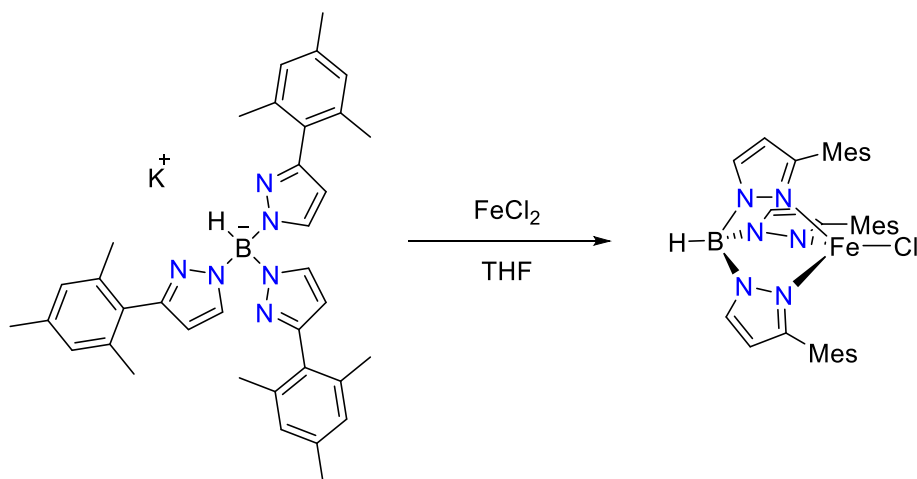
5-Fe: 63% yield, of a yellow powder. Anal. Calcd for C₂₀H₃₂F₆FeN₄O₆S₂: C, 36.48; N, 8.51; H, 4.90. Found: C, 36.19; N, 8.15; H, 4.69. ¹H-NMR (CD₃CN, 400 MHz, 300K): 13.9 (s), 10.6 (s), 9.0 (s), 6.6 (s), 4.5 (s). FT-IR (ATR) ν , cm⁻¹: 2971–2875, 1615, 1295, 1213, 1162, 1029, 633, 510. ESI-MS calcd. for C₁₉H₃₂F₃FeN₄O₃S [M – OTf]⁺: 509.1491, found 509.1483; calcd. for C₁₈H₃₂FeN₄ [M – 2OTf]²⁺: 180.0982, found 180.0986.

9-Fe: 20% yield of a yellow powder. Anal. Calcd for C₁₇H₂₃F₉FeN₄O₆S₂: C, 30.46; N, 8.36; H, 3.46. Found: C, 29.99; N, 8.03; H, 3.21. ¹H-NMR (CD₃CN, 400 MHz, 300K): 11.1 (s), 8.7 (s), 6.0 (s), 5.1 (s), 4.3 (s), 3.2 (s). FT-IR (ATR) ν , cm⁻¹: 3442–2877, 1643, 1223, 1155, 1025, 633, 515. ESI-MS calcd. for C₁₆H₂₃F₆FeN₄O₃S [M – OTf]⁺: 521.0739, found 521.0747; calcd. for C₁₅H₂₃F₃FeN₄ [M – 2OTf]²⁺: 186.0607, found 186.0615.

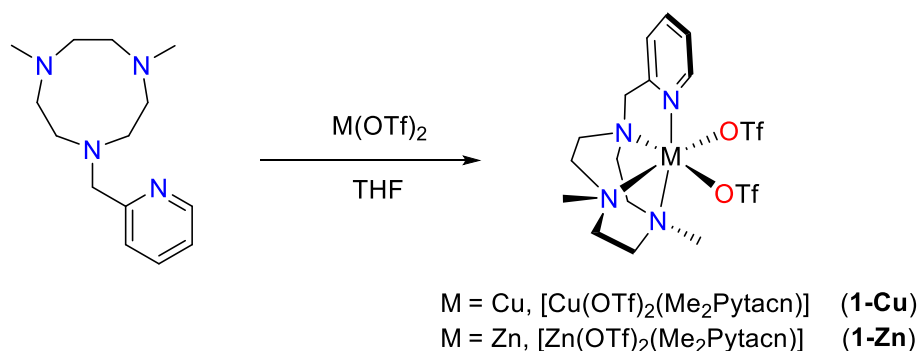


18-Fe: In a glovebox, a solution of the ligand in THF was slowly added to a suspension of FeCl₂ in THF. The reaction mixture was stirred at room temperature overnight. The solvent was removed, and dichloromethane was added into the residue and the solution was filtered off through Celite©. Slow diethyl ether diffusion over the

resultant solution afforded, in one night, the product as a white powder (51% yield). Anal. Calcd for $C_{18}H_{24}Br_3Cl_2FeN_7$: C, 30.67; N, 13.91; H, 3.43. Found: C, 30.40; N, 13.47; H, 2.23. 1H -NMR (CD_3CN , 400 MHz, 300K): 13.5 (s), 10.1 (s). FT-IR (ATR) ν , cm^{-1} : 2956-2914, 1544, 1474, 1392, 1315, 1271, 1245, 1083, 995, 876, 578, 495. ESI-HRMS calcd. for $C_{18}H_{24}Br_3N_7FeCl$ $[M-Cl]^+$: 669.8635, found: 669.8652.



19-Fe: In a glovebox, a solution of the ligand in THF was slowly added to a suspension of $FeCl_2$ in THF. The reaction mixture was stirred at room temperature overnight. The solvent was removed, and dichloromethane was added into the residue and the solution was filtered off through Celite®. Slow diethyl ether diffusion over the resultant solution afforded, in one night, the product as a white powder (61% yield). Anal. Calcd for $C_{36}H_{40}BClFeN_6$: C, 65.63; N, 12.76; H, 6.12. Found: C, 65.26; N, 12.33; H, 6.02. 1H -NMR (C_6D_6 , 400 MHz, 300K): 65.9 (s), 56.5 (s), 4.2 (s), 2.1 (s), -29.8 (s). FT-IR (ATR) ν , cm^{-1} : 2916-2854, 2473, 1480, 1349, 1178, 1045, 846, 779, 743, 702. ESI-HRMS calcd. for $C_{36}H_{40}BN_6Fe(CH_3CN)$ $[M - Cl + CH_3CN]^+$: 664.3024, found: 664.3036.

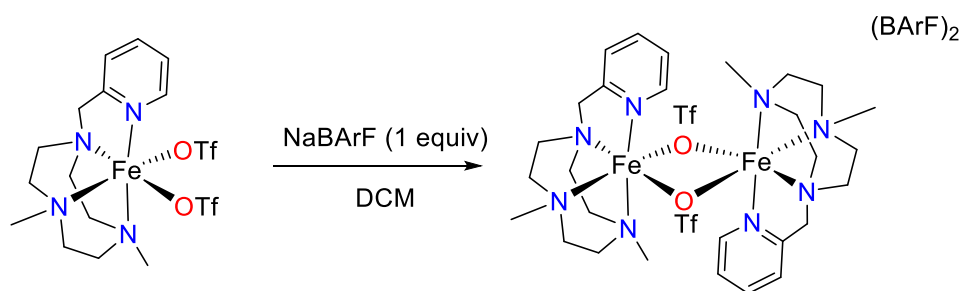


1-M: In a glovebox, to a suspension of $M(OTf)_2$ in THF was added into a solution of the ligand in THF. The reaction mixture was stirred at room temperature overnight. The solvent was removed, and dichloromethane was added into the residue (for Cu complex additional drops of acetonitrile were needed) and the solution was filtered off through

Celite©. Slow diethyl ether diffusion over the resultant solution afforded, in one night, the desired product.

1-Cu: 72% yield of a blue powder. Anal. Calcd for $C_{16}H_{24}CuF_6N_4O_6S_2$: C, 31.50; N, 9.18; H, 3.97. Found: C, 31.23; 8.67; H, 3.60. FT-IR (ATR) ν , cm^{-1} : 3210-2190, 1476, 1459, 1280, 1218, 1156, 1023, 632, 575, 516. ESI-MS calcd. for $C_{15}H_{24}CuF_3N_4O_3S$ [M – OTf] $^+$: 460.0812, found 460.0823; calcd. for $C_{14}H_{24}CuN_4$ [M – 2OTf] $^{2+}$: 155.5643, found 155.5644.

1-Zn: 68% yield of colorless crystals suitable for X-Ray analysis. Anal. Calcd for $C_{16}H_{24}F_6N_4O_6S_2Zn$: C, 31.41; N, 9.16; H, 3.95. Found: C, 30.94; N, 8.66; 3.48. 1H -NMR (CD_3CN , 400 MHz, 300K): 8.65 (d, $J = 3.6$ Hz, 1H), 8.13 (td, $J = 1.6, 8$ Hz, 1H), 7.68 - 7.65 (m, 1H), 7.59 (d, $J = 8$ Hz, 1H), 4.29 (s, 2H), 3.08 - 3.03 (m, 2H), 2.93 - 2.87 (m, 6H), 2.81 - 2.74 (m, 2H), 2.62 (s, 6H), 2.39 - 2.36 (m, 2H). FT-IR (ATR) ν , cm^{-1} : 3249-2883, 1293, 1219, 1158, 1083, 1024, 630, 575, 514. ESI-MS calcd. for $C_{15}H_{24}F_3N_4O_3SZn$ [M – OTf] $^+$: 461.0807, found 461.0811; calcd. for $C_{14}H_{24}N_4Zn$ [M – 2OTf] $^{2+}$: 156.0641, found 156.0632.

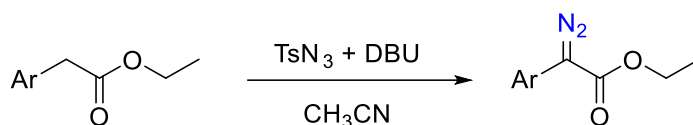


[Fe₂(μ-OTf)₂(Me₂Pytacn)₂](BARF)₂, 20-Fe: In a glovebox, **1-Fe** was dissolved in dichloromethane and NaBARF^F (1 equiv) was added and stirred at room temperature for 4 hours. Afterwards, the solution was filtered off through Celite©. Slow diethyl ether diffusion over the resultant solution afforded, in one night, colorless crystals (59% yield). Anal. Calcd for $C_{94}H_{72}B_2F_{54}Fe_2N_8O_6S_2$: C, 42.88; N, 4.26; H, 2.76. Found: C, 42.82; N, 4.22; H, 2.68. 1H -NMR (CD_3CN , 400 MHz, 300K): 13.0 (s), 9.9 (s), 9.8 (s), 7.7 (s), 6.6 (s), 5.8 (s), 3.9 (s). FT-IR (ATR) ν , cm^{-1} : 2963-2872, 1353, 1274, 1234, 1117, 1024, 887, 839, 712, 682, 670, 628. ESI-HRMS calcd. for $C_{15}H_{24}F_3FeN_4O_3S$ [M/2 – BARF] $^+$: 453.0865, found 453.0858; calcd. for $C_{96}H_{78}B_2F_{48}Fe_2N_{10}$ [M- 2OTf + 2CH₃CN] $^{2+}$: 1208.2264, found: 1208.2230.

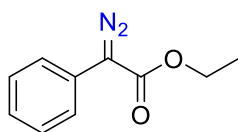
VII.2.5 Synthesis of substrates

VII.2.5.1 Synthesis of diazo acetates

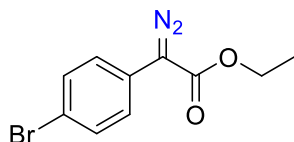
The following diazo acetates were synthesized according to previously reported procedures.²¹² Ethyl 2-(4-methoxyphenyl)acetate was synthesized as previously reported.²¹³



At room temperature, a solution of 1,8-diazabicyclo-[5.4.0]-undec-7-ene (DBU) (947 μ L, 6.32 mmol, 1.5 equiv) in anhydrous CH_3CN was added dropwise to a solution of ethyl aryl acetate (4.21 mmols, 1 equiv) and *p*-toluenesulfonyl azide (TsN_3) (1g, 5.05 mmols, 1.2 equiv) in anhydrous CH_3CN . Then, the reaction mixture was stirred at room temperature for 15 hours. At this point, water was added and the resulting mixture was extracted with diethyl ether and the organic layers were combined. The organic layer was washed with brine and dried over anhydrous MgSO_4 . After the removal of the solvent under reduced pressure, the residue was purified by flash chromatography over silica.

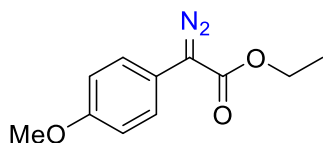


Ethyl 2-diazo-2-phenylacetate: The reaction crude was purified by flash chromatography over silica using hexane:ethyl acetate (30:1) to give the final product as a red oil (82% yield). $^1\text{H-NMR}$ (CDCl_3 , 400 MHz, 300K): 7.51 (d, $J = 8.4\text{Hz}$, 2H), 7.41 (t, $J = 8\text{Hz}$, 2H), 7.21 (t, $J = 8\text{Hz}$, 1H), 4.37 (q, $J = 7.2\text{Hz}$, 2H), 1.37 (t, $J = 7.2\text{Hz}$, 3H). $^{13}\text{C-NMR}$ (CDCl_3 , 100 MHz): 165.3, 128.9, 125.8, 124.0, 61.0, 14.5. FT-IR (ATR) ν , cm^{-1} : 3061-2982, 2078, 1698, 1498, 1370, 1336, 1241, 1149, 1048, 1027, 752, 689, 668, 495.



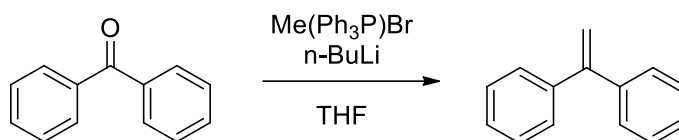
Ethyl 2-(4-bromophenyl)-2-diazoacetate: The reaction crude was purified by flash chromatography over silica using hexane:ethyl acetate (30:1) to give the final product as an orange oil (84% yield). $^1\text{H-NMR}$ (CDCl_3 , 400 MHz, 300K): 7.52 (d, $J = 8\text{Hz}$, 2H), 7.39 (d, $J = 8\text{Hz}$, 2H), 4.36 (q, $J = 8\text{Hz}$, 2H), 1.36 (t, $J = 8\text{Hz}$, 3H). $^{13}\text{C-NMR}$ (CDCl_3 , 100 MHz):

164.9, 132.0, 125.3, 124.9, 119.3, 61.2, 14.5. FT-IR (ATR) ν , cm^{-1} : 2985-2911, 2091, 1692, 1486, 1369, 1336, 1273, 1161, 1045, 628, 613, 738, 494.

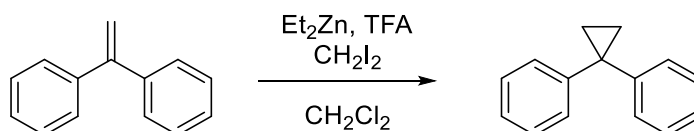


Ethyl 2-(4-methoxyphenyl)2-diazoacetate: The reaction crude was purified by flash chromatography over silica using hexane:ethyl acetate (30:1) to give the final product as a red oil (63% yield). $^1\text{H-NMR}$ (CDCl_3 , 400 MHz, 300K): 7.38 (d, $J = 9.0\text{Hz}$, 2H), 6.94 (d, $J = 9\text{Hz}$, 2H), 4.32 (q, $J = 7.1\text{Hz}$, 2H), 3.80 (s, 3H), 1.33 (t, $J = 7.1\text{Hz}$, 3H). $^{13}\text{C-NMR}$ (CDCl_3 , 100 MHz): 165.8, 158.0, 125.9, 117.0, 114.6, 60.9, 55.3, 14.5. FT-IR (ATR) ν , cm^{-1} : 2982-1836, 2087, 1691, 1608, 1509, 1477, 1367, 1343, 1294, 1236, 1160, 1029, 827, 734, 639, 614, 531, 508.

VII.2.5.2 Synthesis of fast radical clock



Ethene-1,1-diyl dibenzene: To a suspension of methyltriphenylphosphonium bromide (8.6g, 24 mmol, 1.1 equiv.) in THF was added dropwise a solution of $n\text{-BuLi}$ (16 mL, 1.6 M in hexane, 26 mmols, 1.2 equiv) at 0°C during 30 minutes. After the addition, the solution is stirred at 0°C for 90 min. A solution of benzophenone (4 g, 22 mmols, 1 equiv.) in THF was then added and warmed to 70°C and stirred overnight. Afterwards, the reaction was quenched with water. The aqueous layer was extracted with diethyl ether, dried over MgSO_4 , and the solvent was removed under reduced pressure. The residue was purified by flash chromatography over silica using hexane:ethyl acetate 9:2 to give the final product as a colorless oil (86% yield). $^1\text{H-NMR}$ (CDCl_3 , 400 MHz, 300K): 7.39 - 7.36 (m, 10H), 5.50 (s, 2H). $^{13}\text{C-NMR}$ (CDCl_3 , 100 MHz): 150.1, 141.5, 128.3, 128.2, 127.7, 114.3.



Cyclopropane-1,1-diyl dibenzene: A solution of Et_2Zn (26 mL, 1M in hexane, 26 mmols, 1.5 equiv.) in dichloromethane was cooled in an ice bath. A solution of trifluoroacetic acid (TFA) (2 mL, 26 mmols, 1.5 equiv.) in dichloromethane was then added dropwise. Upon

stirring for 20 min, a solution of CH_2I_2 (2.1 mL, 26 mmols, 1.5 equiv.) in dichloromethane was added to the reaction mixture. After an additional 20 min of stirring, a solution of the olefin (3.1g, 17.3 mmols, 1 equiv.) in dichloromethane was added and the ice bath was removed. The reaction was stirred for 3 days at room temperature. After the completion of the reaction, it was quenched with 0.1N HCl and extracted. The organic layer was washed with NaHCO_3 aq., H_2O and brine, dried over MgSO_4 and concentrated to dryness. The residue was purified by flash chromatography over silica using hexane:ethyl acetate 50:1 to give a colorless oil (94% yield). $^1\text{H-NMR}$ (CDCl_3 , 400 MHz, 300K): 7.47 - 7.35 (m, 10H), 1.49 (s, 4H). $^{13}\text{C-NMR}$ (CDCl_3 , 100 MHz): 145.9, 128.6, 128.4, 126.1, 30.1, 16.7.

VII.2.6 Catalytic procedures

VII.2.6.1 Reaction protocol for catalysis

In a crimp vial was mixed 0.005 mmol of the catalyst, 0.04 mmol of NaBARF_4 and a mixture of 1.5 mL of dichloromethane and 1.5 mL of the arene substrate under N_2 (for solid substrates, 3 mL of DCM was mixed with 100 equiv. of the arene). The solution was stirred at room temperature for 20 min and then 0.1 mmol of ethyl diazoacetate was added and heated for 12h at 80°C . After that time, the reaction was cooled down and internal standard trimethoxybenzene was added. The solution was filtered through a silica plug and subsequently rinsed with 2 mL of DCM. The resulting solution was analyzed by GC and NMR spectroscopy.

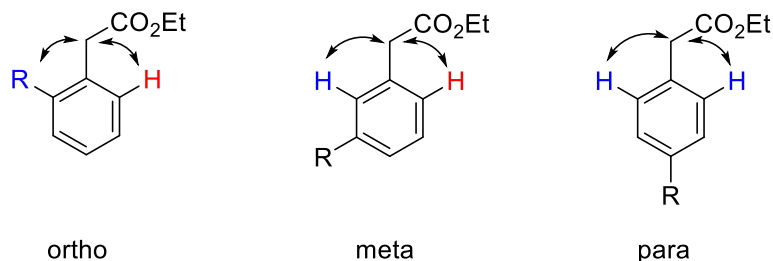
VII.2.6.2 General procedure for product isolation

A Schlenk flask was charged with 0.05 mmol of catalyst, 0.4 mmol of NaBARF_4 and a mixture of 15 mL of dichloromethane and 15 mL of the arene substrate under N_2 (for solid substrates, 30 mL of DCM was mixed with 100 equiv. of the arene). The solution was stirred at room temperature for 20 min and then 1 mmol of ethyl diazoacetate was added and heated for 12h at 80°C . After that reaction time, the reaction mixture was cooled down and purified by flash chromatography over silica using hexane to elute the substrate and then hexane:ethyl acetate 10:1 to elute the final product.

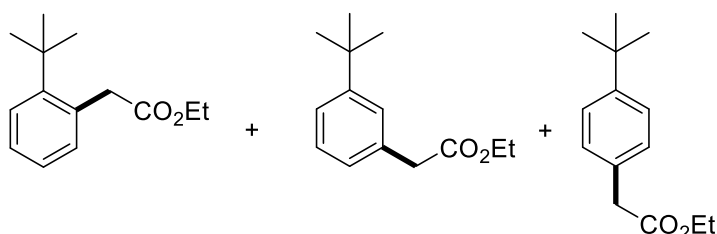
VII.2.7 Characterization of isolated products

All non-symmetric substrates were isolated as mixture of product regioisomers. Spectroscopic data have been compared to previously reported products when possible. The assignment of the *ortho*, *meta* and *para* isomers has been done by 2-D NOESY

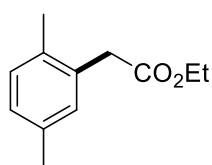
experiments. The CH_2COEt_2 signal of the *ortho* isomer show NOE with the benzylic protons of the corresponding substituent and with the aromatic proton on the α -position (Scheme VII.1). The *meta* isomer show NOE with two different aromatic signals, while the *para* isomer has only NOE with one aromatic signal (because of the symmetry).



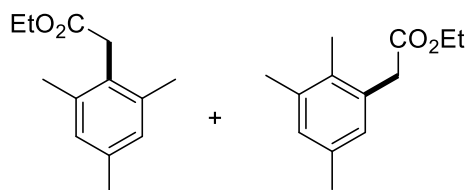
Scheme VII.1. NOE of the different isomers for its assignment.



²¹⁴**P5a + P5b + P5c**: colorless oil (60% yield). ¹H-NMR (CDCl_3 , 400 MHz, 300K): 7.46 - 7.14 (m, 4H), 4.22 - 4.17 (m, 2H), 3.96 (s), 3.65 (s), 3.62 (s), 1.45 (s), 1.37 (s), 1.36 (s), 1.32 - 1.28 (m, 3H). ¹³C-NMR (CDCl_3 , 100 MHz): 172.3, 171.9, 171.8, 151.4, 149.9, 147.9, 113.8, 132.9, 132.4, 131.1, 130.9, 128.9, 128.2, 127.1, 126.3, 126.1, 125.5, 124.0, 60.8, 41.7, 40.9, 40.4, 31.6, 31.4, 14.2.

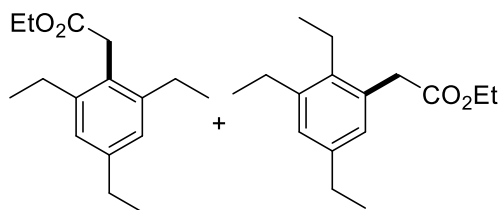


²¹⁵**P7**: colorless oil (66% yield). ¹H-NMR (CDCl_3 , 400 MHz, 300K): 7.13 - 6.99 (m, 3H), 4.19 (q, $J = 7.1\text{Hz}$, 2H), 3.62 (s, 2H), 2.34 (s, 3H), 2.31 (s, 3H), 1.29 (t, $J = 7.1\text{Hz}$, 3H). ¹³C-NMR (CDCl_3 , 100 MHz): 170.4, 134.3, 132.4, 131.4, 129.6, 129.0, 126.8, 59.5, 38.0, 19.7, 17.9, 13.0.

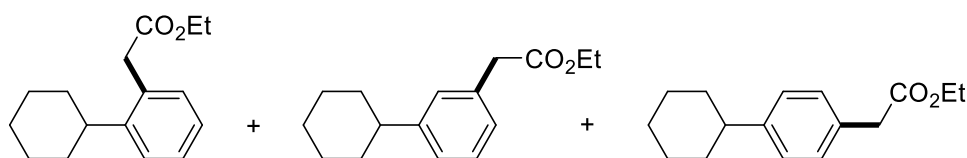


P8a + P8b, colorless oil (66% yield). ¹H-NMR (CDCl_3 , 400 MHz, 300K): 6.97 (s) 6.92 (s), 4.25 - 4.17 (m, 2H), 3.70 (s), 3.67 (s), 2.35 (s), 2.32 (s), 2.22 (s), 1.33 - 1.28 (m, 3H).

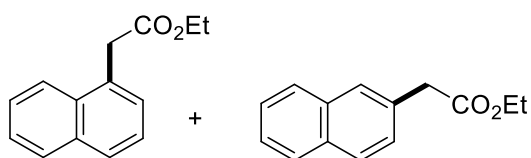
^{13}C -NMR (CDCl_3 , 100 MHz): 171.9, 171.6, 137.0, 136.9, 136.4, 134.9, 132.7, 132.3, 130.0, 128.9, 128.8, 60.8, 60.7, 39.9, 35.1, 20.9, 20.8, 20.6, 20.2, 15.1, 14.3.



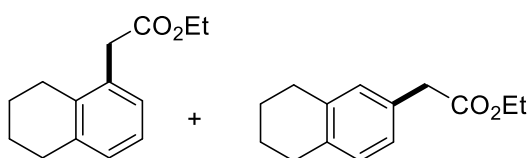
P9a + P9b: colorless oil (29% yield). ^1H -NMR (CDCl_3 , 400 MHz, 300K): 6.95 (s, 2H), 4.18 (q (x2), $J = 9.5\text{Hz}$, 2H), 3.73 (s), 3.67 (s), 2.72 - 2.63 (m, 6H), 1.31 - 1.21 (m, 12H). ^{13}C -NMR (CDCl_3 , 100 MHz): 175.3, 172.1, 143.1, 143.0, 127.9, 127.4, 125.9, 125.6, 60.9, 60.7, 34.0, 28.6, 28.5, 26.5, 15.8, 15.5, 15.2, 14.2.



P11a + P11b + P11c: colorless oil (53% yield). ^1H -NMR (CDCl_3 , 400 MHz, 300K): 7.30 - 7.13 (m, 4H), 4.21 - 4.16 (m, 2H), 3.71 (s), 3.62 (s), 3.61 (s), 2.77 - 2.72 (m), 2.52 - 2.50 (m), 1.89 - 1.77 (m, 5H), 1.45 - 1.40 (m, 5H), 1.31 - 1.27 (m, 3H). ^{13}C -NMR (CDCl_3 , 100 MHz): 171.9, 171.9, 171.7, 148.4, 146.9, 146.4, 134.0, 131.6, 131.5, 130.6, 129.1, 128.5, 127.9, 127.6, 127.0, 126.7, 126.3, 125.8, 125.5, 60.8, 60.8, 44.5, 44.2, 41.5, 41.0, 40.2, 39.0, 34.5, 34.4, 34.1, 27.1, 26.9, 26.3, 26.2, 14.2.

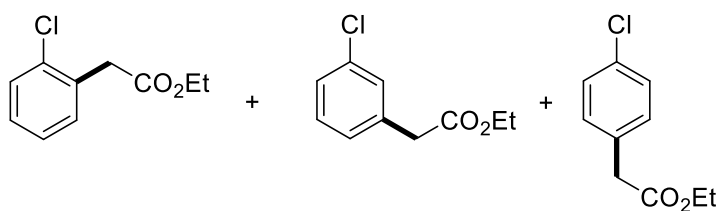


$^{216}\text{P12a} + \text{P12b}$: colorless oil (42% yield). ^1H -NMR (CDCl_3 , 400 MHz, 300K): 8.07 - 8.05 (m, 1H), 7.92 - 7.78 (m, 3H), 7.60 - 7.45 (m, 3H), 4.21 (m, 2H), 4.11 (s), 3.82 (s), 1.29 (m, 3H). ^{13}C -NMR (CDCl_3 , 100 MHz): 170.4, 132.6, 132.2, 131.2, 130.9, 130.4, 129.5, 127.5, 127.0, 126.8, 126.7, 126.7, 126.4, 126.4, 126.2, 125.1, 124.9, 124.6, 124.5, 124.3, 122.6, 59.7, 40.4, 38.0, 13.0, 12.9.

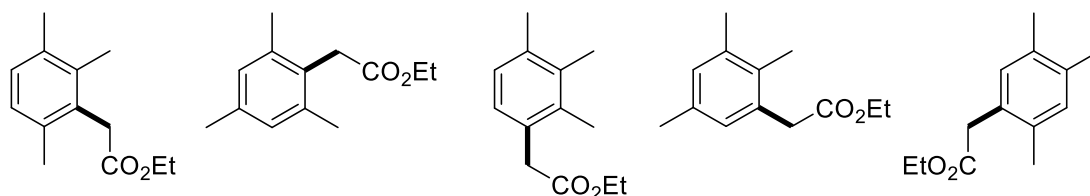


P13a + P13b: colorless oil (67% yield). ^1H -NMR (CDCl_3 , 400 MHz, 300K): 7.13 - 7.03 (m, 3H), 4.22 - 4.16 (m, 2H), 3.64 (s), 3.58 (s), 2.85 - 2.71 (m, 4H), 1.84 - 1.81 (m, 4H), 1.32

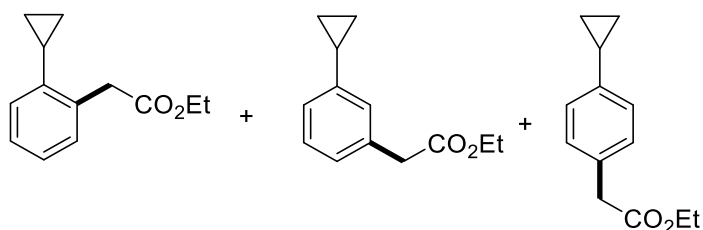
- 1.28 (m, 3H). ^{13}C -NMR (CDCl_3 , 100 MHz): 172.0, 171.4, 137.7, 137.3, 135.9, 135.8, 132.9, 131.1, 129.9, 129.4, 128.6, 127.7, 126.3, 125.4, 60.8, 60.8, 41.1, 38.9, 30.1, 29.4, 29.1, 26.5, 23.3, 23.3, 23.2, 22.8, 14.3.



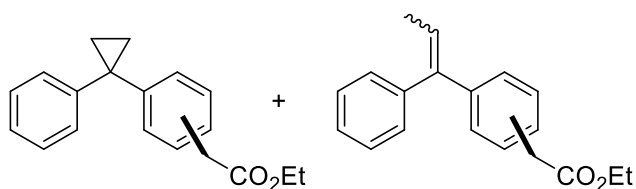
$^{216}\text{P15a} + \text{P15b} + \text{P15c}$: colorless oil (27% yield). ^1H -NMR (CDCl_3 , 400 MHz, 300K): 7.39 - 7.20 (m, 4H), 4.21 - 4.14 (m, 2H), 3.76 (s), 3.58 (s), 3.57 (s), 1.28 - 1.23 (m, 3H). ^{13}C -NMR (CDCl_3 , 100 MHz): 171.2, 171.0, 170.6, 134.6, 133.0, 132.6, 132.5, 131.5, 130.6, 129.8, 129.5, 129.5, 128.7, 128.7, 127.5, 127.3, 126.9, 61.1, 61.0, 41.0, 40.7, 39.2, 14.2.



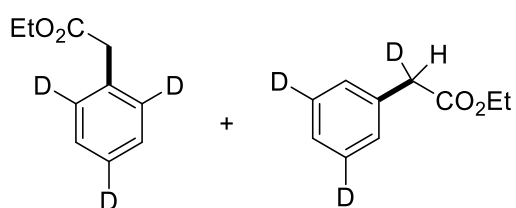
P16a + P16b + P16c + P16d + P16e: colorless oil (67% yield). ^1H -NMR (CDCl_3 , 400 MHz, 300K): 7.07 - 6.95 (m, 2H), 4.26 - 4.20 (m, 2H), 3.79 (s), 3.72 (s), 3.71 (s), 3.69 (s), 3.64 (s), 2.39 - 2.24 (m, 9H), 1.35 - 1.31 (m, 3H). ^{13}C -NMR (CDCl_3 , 100 MHz): 172.0, 171.9, 171.9, 171.6, 137.0, 136.9, 136.4, 135.7, 135.6, 135.6, 135.5, 135.3, 134.9, 134.7, 134.4, 134.1, 134.0, 132.7, 132.3, 131.8, 131.7, 131.5, 130.1, 130.0, 128.9, 128.7, 127.6, 127.5, 127.4, 60.8, 60.7, 40.2, 39.9, 38.9, 35.8, 35.1, 20.8, 20.8, 20.6, 20.5, 20.3, 19.3, 19.2, 19.0, 16.0, 15.1, 14.3.



P17a + P17b + P17c: colorless oil (45% yield). ^1H -NMR (CDCl_3 , 400 MHz, 300K): 7.28 - 7.01 (m, 4H), 4.23 - 4.15 (m, 2H), 3.87 (s), 3.61 (s), 3.60 (s), 2.00 - 1.90 (m, 1H), 1.31 - 1.27 (m, 3H), 0.98 - 0.95 (m, 2H), 0.72 - 0.68 (m, 2H). ^{13}C -NMR (CDCl_3 , 100 MHz): 171.9, 171.8, 171.7, 144.3, 142.8, 141.5, 134.4, 134.1, 131.1, 130.0, 129.1, 128.5, 127.3, 126.8, 126.4, 126.3, 126.0, 125.9, 124.3, 60.8, 60.8, 60.8, 41.5, 41.0, 39.1, 15.3, 15.1, 14.2, 14.2, 13.4, 9.2, 9.1, 6.9, 6.9.



P18a + P18b: colorless oil (39% yield). $^1\text{H-NMR}$ (CDCl_3 , 400 MHz, 300K): 7.40 - 7.14 (m, 9H), 6.39 (q, $J = 7\text{Hz}$), 4.20 - 4.15 (m), 4.07 - 4.05 (m), 3.70 (s), 3.61 (s), 3.60 (s), 3.52 (s), 3.46 (s), 3.46 (s), 1.63 (d, $J = 7\text{Hz}$, 3H), 1.34 - 1.16 (m, 7H). $^{13}\text{C-NMR}$ (CDCl_3 , 100 MHz): 171.8, 171.7, 171.6, 171.6, 146.0-125.2 (69 s), 60.9, 60.8, 60.6, 60.6, 41.5, 41.1, 41.0, 38.6, 38.1, 37.8, 35.0, 29.9, 29.6, 29.6, 29.5, 28.1, 28.0, 27.9, 18.0, 17.9, 16.9, 16.5, 16.5, 16.4, 16.4, 14.2, 14.2, 14.2.



P19a + P19b: colorless oil (36% yield). $^1\text{H-NMR}$ (CDCl_3 , 400 MHz, 300K): 7.32 - 7.26 (m, 2H), 4.15 (q, $J = 7.1\text{Hz}$, 2H), 3.61 (s, 2H), 1.25 (t, $J = 7.1\text{Hz}$, 3H). $^{13}\text{C-NMR}$ (CDCl_3 , 100 MHz): 171.7, 129.2, 128.3, 126.8, 60.9, 41.4 (m), 14.2.

VII.2.5 Crystal data

Table VII.6. Crystal data for **1-Zn**

Empirical formula	$\text{C}_{16}\text{H}_{24}\text{F}_6\text{N}_4\text{O}_6\text{S}_2\text{Zn}$	
Formula weight	611.88 g/mol	
Temperature	100(2) K	
Wavelength	0.71073 Å	
Crystal size	0.250 x 0.250 x 0.120 mm	
Crystal system	Monoclinic	
Space group	P 21/n	
Unit cell dimensions	$a = 8.9462(9)$ Å	$\alpha = 90^\circ$
	$b = 17.3922(19)$ Å	$\beta = 93.804(2)^\circ$
	$c = 15.2554(17)$ Å	$\gamma = 90^\circ$
Volume	2368.4(4) Å ³	
Z	4	
Density (calculated)	1.716 g/cm ³	
Absorption coefficient	1.301 mm ⁻¹	

F(000)	1248
Theta range for data collection	2.342 to 26.998°
Index ranges	-11 ≤ h ≤ 11, -22 ≤ k ≤ 22, -18 ≤ l ≤ 19
Reflections collected	33957
Independent reflections	5146 [R(int) = 0.0394]
Coverage of independent reflections	99.8%
Absorption correction	Empirical
Max. and min. transmission	1.0 and 0.799018
Refinement method	Full-matrix least-squares on F ²
Data / restraints / parameters	5146 / 0 / 318
Goodness-of-fit on F ²	1.164
Final R indices [I > 2σ(I)]	I > 2σ(I) R1 = 0.0608, wR2 = 0.1292 all data R1 = 0.0659, wR2 = 0.1317
Largest diff. peak and hole	0.946 and -0.649 eÅ ⁻³

Table VII.7. Crystal data for **20-Fe**

Empirical formula	C ₄₈ H ₃₈ BCl ₂ F ₂₇ FeN ₄ O ₃ S	
Formula weight	1401.44 g/mol	
Temperature	143(2) K	
Wavelength	0.71073 Å	
Crystal size	0.350 x 0.220 x 0.150 mm	
Crystal system	Triclinic	
Space group	P -1	
Unit cell dimensions	a = 12.6950(11) Å	α = 102.363(2)°
	b = 13.3351(11) Å	β = 97.011(2)°
	c = 17.1823(15) Å	γ = 92.487(2)°
Volume	2812.8(4) Å ³	
Z	2	
Density (calculated)	1.655 g/cm ³	
Absorption coefficient	0.535 mm ⁻¹	
F(000)	1404	
Theta range for data collection	2.159 to 28.285°	
Index ranges	-16 ≤ h ≤ 16, -17 ≤ k ≤ 17, -22 ≤ l ≤ 22	
Reflections collected	43857	
Independent reflections	13585 [R(int) = 0.0462]	

Coverage of independent reflections	99.6%
Absorption correction	Empirical
Max. and min. transmission	1 and 0.765601
Refinement method	Full-matrix least-squares on F ²
Data / restraints / parameters	13585 / 90 / 975
Goodness-of-fit on F ²	1.037
Final R indices [$I > 2\sigma(I)$]	$I > 2\sigma(I)$ R1 = 0.0726, wR2 = 0.1656
	all data R1 = 0.1055, wR2 = 0.1860
Largest diff. peak and hole	0.734 and -0.380 eÅ ⁻³

VII.3 Experimental Section Chapter V

VII.3.1 Instrumentation

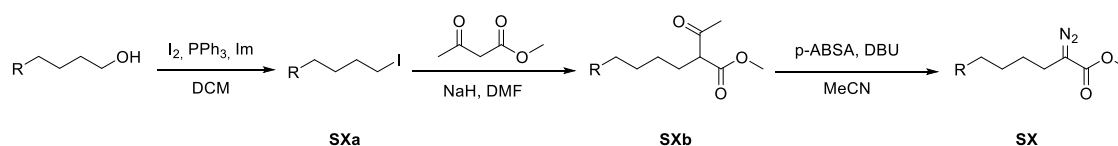
IR spectra were taken in a Mattson-Galaxy Satellite FT-IR spectrophotometer using a MKII Golden Gate single reflection ATR system. ^1H and ^{13}C NMR spectra were taken on BrukerDPZ300 and DPX400 spectrometers at 25°C referenced to residual solvent peaks. High resolution mass spectra (HRMS) were recorded on a Bruker MicroTOF-Q IITM instrument with a ESI source at Serveis Tècnics of the University of Girona. Samples were introduced into the mass spectrometer ion source by direct infusion through a syringe pump and were externally calibrated using sodium formate. GC-MS analyses were performed on an Agilent 7890A gas chromatograph equipped with an HP-5 capillary column interfaced with an Agilent 5975C mass spectrometer.

VII.3.2 Materials

All air- and moisture- sensitive materials were manipulated with standard Schlenk techniques under argon atmosphere or in a glovebox. All commercially available reagents were purchased from commercial sources and used as received, without any further purification unless stated otherwise. Solvents were purchased from SDS and Scharlab. Solvents were purified and dried by passing through an activated alumina purification system (M-Braun SPS-800) or by conventional distillation techniques. 4-(4-chlorophenyl)butan-1-ol was synthesized as previously reported.²¹⁷

VII.3.3 Synthesis of diazo acetates

The following diazo acetates were synthesized following previously reported procedures.²¹⁸

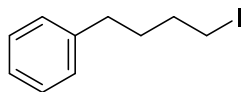


SXa: A solution of triphenylphosphine (3.93 gr, 15 mmols, 1.5 equiv.) and I_2 (3.8 gr, 15 mmols, 1.5 equiv.) in dichloromethane (100 mL) was allowed to stir for 10 minutes at room temperature. Imidazole (1.7 gr, 25 mmols, 2.5 equiv.) was added to the resulting mixture. After 10 minutes, the corresponding alcohol (10 mmols) was added and the resulting mixture was stirred for 3 hours. Then, the mixture was quenched with an aqueous solution of sodium metabisulfite (50 mL). The aqueous and organic layers were

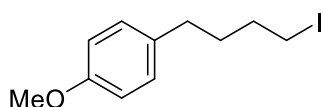
separated and the aqueous solution was extracted with dichloromethane (3 x 100mL). The combined organic layers were dried with MgSO₄ and concentrated under reduced pressure. The residue was purified by flash chromatography (hexane for alkyl substrates, 95:5 hexane:ethyl acetate for aryl substrates).

SXb: To a suspension of sodium hydride (173 mg, 7.2 mmols, 1.2 equiv.) in DMF (5 mL) was added methyl acetoacetate (0.78 mL, 7.2 mmols, 1.2 equiv.) dropwise at 0°C. The solution was stirred at 0°C for 30 minutes. Then, **SXa** (6 mmols) was added and the reaction was stirred at 80°C for 3 hours. The reaction was quenched with HCl 1M. The aqueous layer was extracted with dichloromethane (3 x 100mL). The combined organic layers were dried over MgSO₄ and concentrated under reduced pressure. The residue was purified by flash chromatography (90:10 hexane:ethyl acetate).

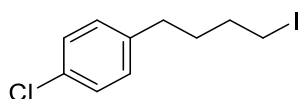
SX: To a solution of DBU (0.9 mL, 6 mmols, 1.5 equiv.) and *p*-acetamidobenzenesulfonyl azide (*p*-ABSA) (1.4 gr, 6 mmols, 1.5 equiv.) in MeCN, was added **SXb** (4 mmols) and the reaction was stirred at room temperature overnight. The reaction was concentrated under reduced pressure and the residue was purified by flash chromatography (90:10 hexane:ethyl acetate) to give the pure product.



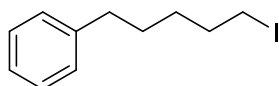
S20a: colorless oil (95% yield). ¹H-NMR (CDCl₃, 400 MHz, 300K): δ 7.35 - 7.21 (m, 5H), 3.24 (t, *J* = 6.6Hz, 2H), 2.68 (t, *J* = 7.5Hz, 2H), 1.94 - 1.86 (m, 2H), 1.82 - 1.74 (m, 2H). ¹³C-NMR (CDCl₃, 100 MHz): 141.8, 128.4, 126.0, 34.8, 33.0, 32.3, 6.9.



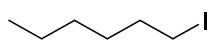
S21a: colorless oil (98% yield). ¹H-NMR (CDCl₃, 400 MHz, 300K): δ 7.11 (d, *J* = 8.7Hz, 2H), 6.86 (d, *J* = 8.7Hz, 2H), 3.80 (s, 3H), 3.21 (t, *J* = 6.9Hz, 2H), 2.60 (t, *J* = 7.6Hz, 2H), 1.90 - 1.83 (m, 2H), 1.79 - 1.70 (m, 2H). ¹³C-NMR (CDCl₃, 100 MHz): 157.9, 133.9, 129.3, 113.9, 113.8, 55.3, 33.9, 33.0, 32.5, 6.9.



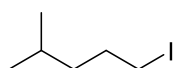
S22a: colorless oil (70% yield). ¹H-NMR (CDCl₃, 400 MHz, 300K): δ 7.28 (d, *J* = 8.4Hz, 2H), 7.13 (d, *J* = 8.4Hz, 2H), 3.22 (t, *J* = 6.8Hz, 2H), 2.63 (t, *J* = 7.5Hz, 2H), 1.89 - 1.83 (m, 2H), 1.78 - 1.72 (m, 2H). ¹³C-NMR (CDCl₃, 100 MHz): 140.2, 131.6, 129.8, 128.5, 34.1, 32.8, 32.1, 6.7.



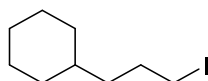
S23a: colorless oil (88% yield). $^1\text{H-NMR}$ (CDCl_3 , 400 MHz, 300K): δ 7.36 - 7.33 (m, 2H), 7.26 - 7.23 (m, 3H), 3.23 (t, $J = 7.1\text{Hz}$, 2H), 2.68 (t, $J = 8\text{Hz}$, 2H), 1.93 - 1.88 (m, 2H), 1.73 - 1.67 (m, 2H), 1.57 - 1.48 (m, 2H). $^{13}\text{C-NMR}$ (CDCl_3 , 100 MHz): 142.4, 128.5, 128.4, 125.9, 35.8, 33.5, 30.5, 30.3, 7.0.



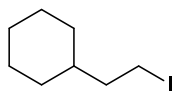
S24a: colorless oil (94% yield). $^1\text{H-NMR}$ (CDCl_3 , 400 MHz, 300K): δ 3.18 (t, $J = 7.1\text{Hz}$, 2H), 1.85 - 1.78 (m, 2H), 1.30 - 1.27 (m, 6H), 0.90 - 0.87 (m, 3H). $^{13}\text{C-NMR}$ (CDCl_3 , 100 MHz): 33.5, 30.7, 30.2, 22.5, 14.0, 7.4.



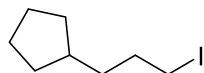
S26a: colorless oil (66% yield). $^1\text{H-NMR}$ (CDCl_3 , 400 MHz, 300K): δ 3.15 (t, $J = 7.1\text{Hz}$, 2H), 1.85 - 1.78 (m, 2H), 1.58 - 1.53 (m, 1H), 1.29 - 1.23 (m, 2H), 0.87 (d, $J = 4\text{Hz}$, 6H). $^{13}\text{C-NMR}$ (CDCl_3 , 100 MHz): 39.8, 31.6, 27.3, 22.5, 7.5.



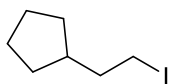
S27a: colorless oil (95% yield). $^1\text{H-NMR}$ (CDCl_3 , 400 MHz, 300K): δ 3.16 (t, $J = 7.2\text{Hz}$, 2H), 1.86 - 1.79 (m, 2H), 1.69 - 1.66 (m, 5H), 1.29 - 1.14 (m, 6H), 0.92 - 0.87 (m, 2H). $^{13}\text{C-NMR}$ (CDCl_3 , 100 MHz): 38.3, 36.9, 33.3, 31.2, 26.6, 26.3, 7.7.



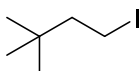
S28a: colorless oil (87% yield). $^1\text{H-NMR}$ (CDCl_3 , 400 MHz, 300K): δ 3.20 (t, $J = 7.2\text{Hz}$, 2H), 1.76 - 1.63 (m, 7H), 1.37 - 1.33 (m, 1H), 1.26 - 1.12 (m, 3H), 0.94 - 0.86 (m, 2H). $^{13}\text{C-NMR}$ (CDCl_3 , 100 MHz): 41.2, 38.5, 32.5, 26.5, 26.1, 5.1.



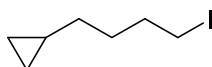
S29a: colorless oil (67% yield). $^1\text{H-NMR}$ (CDCl_3 , 400 MHz, 300K): δ 3.19 (t, $J = 7.1\text{Hz}$, 2H), 1.89 - 1.77 (m, 5H), 1.61 - 1.52 (m, 4H), 1.44 - 1.40 (m, 2H), 1.12 - 1.07 (m, 2H). $^{13}\text{C-NMR}$ (CDCl_3 , 100 MHz): 39.3, 37.0, 33.0, 32.7, 25.2, 7.6.



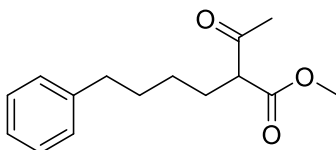
S30a: colorless oil (75% yield). $^1\text{H-NMR}$ (CDCl_3 , 400 MHz, 300K): δ 3.18 (t, $J = 7\text{Hz}$, 2H), 1.88 - 1.80 (m, 5H), 1.61 - 1.54 (m, 4H), 1.12 - 1.07 (m, 2H). $^{13}\text{C-NMR}$ (CDCl_3 , 100 MHz): 40.9, 40.2, 31.9, 25.1, 6.1.



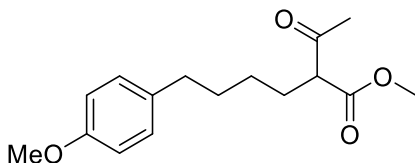
S31a: colorless oil (66% yield). $^1\text{H-NMR}$ (CDCl_3 , 400 MHz, 300K): δ 3.20 - 3.16 (m, 2H), 1.95 - 1.90 (m, 2H), 0.92 (s, 9H). $^{13}\text{C-NMR}$ (CDCl_3 , 100 MHz): 49.4, 33.3, 28.8, 1.6.



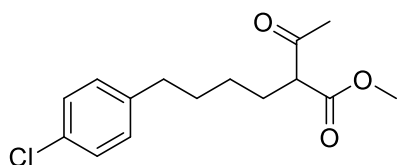
S32a: colorless oil (59% yield). $^1\text{H-NMR}$ (CDCl_3 , 400 MHz, 300K): δ 3.21 (t, $J = 7\text{Hz}$, 2H), 1.91 - 1.84 (m, 2H), 1.53 - 1.48 (m, 2H), 1.26 - 1.20 (m, 2H), 0.71 - 0.62 (m, 1H), 0.45 - 0.40 (m, 2H), 0.04 - 0.01 (m, 2H). $^{13}\text{C-NMR}$ (CDCl_3 , 100 MHz): 33.6, 33.4, 30.6, 10.7, 7.3, 4.5.



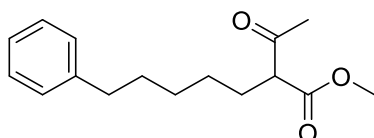
S20b: colorless oil (86% yield). $^1\text{H-NMR}$ (CDCl_3 , 400 MHz, 300K): δ 7.29 - 7.25 (m, 2H), 7.19 - 7.15 (m, 3H), 3.72 (s, 3H), 3.41 (t, $J = 7.2\text{Hz}$, 1H), 2.60 (t, $J = 7.6\text{Hz}$, 2H), 2.20 (s, 3H), 1.90 - 1.84 (m, 2H), 1.66 - 1.61 (m, 2H), 1.35 - 1.30 (m, 2H). $^{13}\text{C-NMR}$ (CDCl_3 , 100 MHz): 203.2, 170.3, 142.2, 128.4, 128.3, 125.8, 59.6, 52.4, 35.5, 31.1, 28.9, 28.1, 27.0.



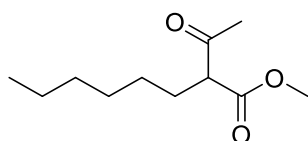
S21b: colorless oil (84% yield). $^1\text{H-NMR}$ (CDCl_3 , 400 MHz, 300K): δ 7.09 (d, $J = 8.6\text{Hz}$, 2H), 6.83 (d, $J = 8.6\text{Hz}$, 2H), 3.80 (s, 3H), 3.74 (s, 3H), 3.43 (t, $J = 7.3\text{Hz}$, 1H), 2.56 (t, $J = 7.6\text{Hz}$, 2H), 2.23 (s, 3H), 1.91 - 1.87 (m, 2H), 1.64 - 1.59 (m, 2H), 1.35 - 1.30 (m, 2H). $^{13}\text{C-NMR}$ (CDCl_3 , 100 MHz): 203.2, 170.3, 157.7, 134.3, 129.2, 113.7, 59.6, 55.2, 52.4, 34.6, 31.3, 28.9, 28.1, 26.9.



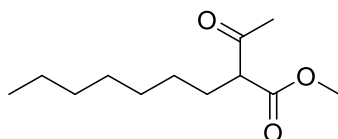
S22b: colorless oil (79% yield). $^1\text{H-NMR}$ (CDCl_3 , 400 MHz, 300K): δ 7.20 (d, $J = 8.3\text{Hz}$, 2H), 7.06 (d, $J = 8.3\text{Hz}$, 2H), 3.70 (s, 3H), 3.40 (t, $J = 7.3\text{Hz}$, 1H), 2.55 (t, $J = 7.6\text{Hz}$, 2H), 2.19 (s, 3H), 1.87 - 1.81 (m, 2H), 1.61 - 1.55 (m, 2H), 1.31 - 1.26 (m, 2H). $^{13}\text{C-NMR}$ (CDCl_3 , 100 MHz): 203.0, 170.2, 140.6, 131.4, 129.7, 128.3, 59.5, 52.4, 34.8, 31.0, 28.9, 27.9, 26.8.



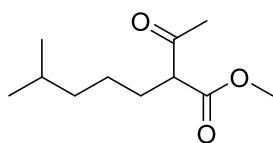
S23b: colorless oil (73% yield). $^1\text{H-NMR}$ (CDCl_3 , 400 MHz, 300K): δ 7.29 - 7.25 (m, 2H), 7.19 - 7.15 (m, 3H), 3.73 (s, 3H), 3.41 (t, $J = 7.2\text{Hz}$, 1H), 2.60 (t, $J = 7.6\text{Hz}$, 2H), 2.21 (s, 3H), 1.86 - 1.82 (m, 2H), 1.64 - 1.60 (m, 2H), 1.36 - 1.31 (m, 4H). $^{13}\text{C-NMR}$ (CDCl_3 , 100 MHz): 203.2, 170.4, 142.5, 128.4, 128.3, 125.7, 59.7, 52.3, 35.8, 31.1, 28.9, 28.8, 28.2, 27.3.



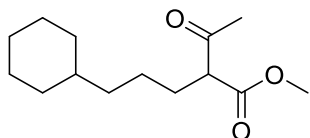
S24b: colorless oil (68% yield). $^1\text{H-NMR}$ (CDCl_3 , 400 MHz, 300K): δ 3.68 (s, 3H), 3.37 (t, $J = 7.2\text{Hz}$, 1H), 2.16 (s, 3H), 1.82 - 1.75 (m, 2H), 1.23 - 1.21 (m, 8H), 0.84 - 0.80 (m, 3H). $^{13}\text{C-NMR}$ (CDCl_3 , 100 MHz): 203.1, 170.3, 59.6, 52.2, 31.4, 28.9, 28.6, 28.2, 27.3, 22.4, 13.9.



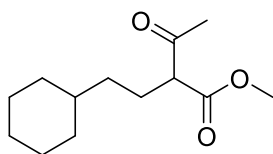
S25b: colorless oil (75% yield). $^1\text{H-NMR}$ (CDCl_3 , 400 MHz, 300K): δ 3.66 (s, 3H), 3.35 (t, $J = 7.2\text{Hz}$, 1H), 2.15 (s, 3H), 1.78 - 1.76 (m, 2H), 1.22 - 1.20 (m, 10H), 0.82 - 0.78 (m, 3H). $^{13}\text{C-NMR}$ (CDCl_3 , 100 MHz): 203.1, 170.3, 59.6, 52.2, 31.6, 29.2, 28.9, 28.6, 28.2, 27.4, 22.5, 14.0.



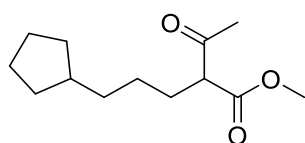
S26b: colorless oil (53% yield). $^1\text{H-NMR}$ (CDCl_3 , 400 MHz, 300K): δ 3.72 (s, 3H), 3.41 (t, $J = 7.2\text{Hz}$, 1H), 2.21 (s, 3H), 1.83 - 1.77 (m, 2H), 1.51 - 1.46 (m, 1H), 1.27 - 1.22 (m, 2H), 1.20 - 1.16 (m, 2H), 0.85 (s, 3H), 0.83 (s, 3H). $^{13}\text{C-NMR}$ (CDCl_3 , 100 MHz): 203.3, 170.4, 59.8, 52.3, 38.5, 28.7, 28.5, 27.7, 25.2, 22.5, 22.4.



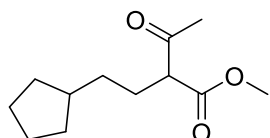
S27b: colorless oil (67% yield). $^1\text{H-NMR}$ (CDCl_3 , 400 MHz, 300K): δ 3.70 (s, 3H), 3.40 (t, $J = 7.3\text{Hz}$, 1H), 2.19 (s, 3H), 1.83 - 1.75 (m, 2H), 1.65 - 1.59 (m, 5H), 1.26 - 1.11 (m, 8H), 0.83 - 0.80 (m, 2H). $^{13}\text{C-NMR}$ (CDCl_3 , 100 MHz): 203.2, 170.4, 59.7, 52.2, 37.3, 37.0, 33.3, 33.2, 28.7, 28.5, 26.6, 26.3, 24.7.



S28b: colorless oil (52% yield). $^1\text{H-NMR}$ (CDCl_3 , 400 MHz, 300K): δ 3.72 (s, 3H), 3.37 (t, $J = 7.5\text{Hz}$, 1H), 2.20 (s, 3H), 1.86 - 1.80 (m, 2H), 1.69 - 1.65 (m, 5H), 1.22 - 1.10 (m, 6H), 0.91 - 0.80 (m, 2H). $^{13}\text{C-NMR}$ (CDCl_3 , 100 MHz): 203.3, 170.4, 59.9, 52.3, 37.5, 35.0, 33.1, 28.7, 26.5, 26.2, 25.6.

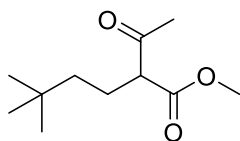


S29b: colorless oil (67% yield). $^1\text{H-NMR}$ (CDCl_3 , 400 MHz, 300K): δ 3.70 (s, 3H), 3.39 (t, $J = 7.3\text{Hz}$, 1H), 2.19 (s, 3H), 1.82 - 1.79 (m, 2H), 1.71 - 1.67 (m, 3H), 1.56 - 1.46 (m, 4H), 1.27 - 1.21 (m, 4H), 1.01 - 0.98 (m, 2H). $^{13}\text{C-NMR}$ (CDCl_3 , 100 MHz): 203.3, 170.4, 59.7, 52.3, 39.8, 35.8, 32.6, 32.6, 28.8, 28.5, 26.6, 25.1.

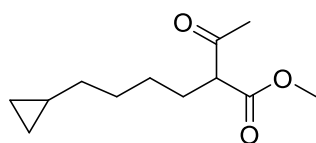


S30b: colorless oil (61% yield). $^1\text{H-NMR}$ (CDCl_3 , 400 MHz, 300K): δ 3.73 (s, 3H), 3.40 (t, $J = 7.4\text{Hz}$, 1H), 2.22 (s, 3H), 1.87 - 1.83 (m, 2H), 1.75 - 1.72 (m, 3H), 1.60 - 1.50 (m,

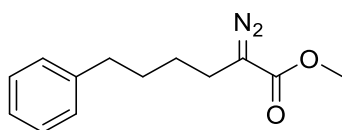
4H), 1.27 - 1.26 (m, 2H), 1.07 - 1.06 (m, 2H). $^{13}\text{C-NMR}$ (CDCl_3 , 100 MHz): 203.3, 170.4, 59.9, 52.3, 39.8, 33.8, 32.5, 32.4, 28.8, 27.5, 25.1.



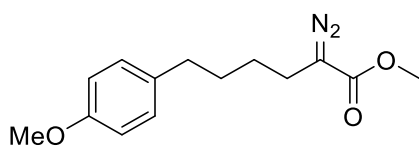
S31b: colorless oil (46% yield). $^1\text{H-NMR}$ (CDCl_3 , 400 MHz, 300K): δ 3.73 (s, 3H), 3.35 (t, $J = 7.4\text{Hz}$, 1H), 2.22 (s, 3H), 1.85 - 1.77 (m, 2H), 1.16 - 1.09 (m, 2H), 0.88 (s, 9H). $^{13}\text{C-NMR}$ (CDCl_3 , 100 MHz): 203.3, 170.4, 60.3, 52.3, 41.5, 30.3, 29.1, 28.9, 23.7.



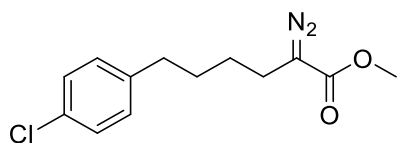
S32b: colorless oil (64% yield). $^1\text{H-NMR}$ (CDCl_3 , 400 MHz, 300K): δ 3.66 (s, 3H), 3.36 (t, $J = 9.8\text{Hz}$, 1H), 2.15 (s, 3H), 1.82 - 1.73 (m, 2H), 1.37 - 1.18 (m, 4H), 1.14 - 1.06 (m, 2H), 0.60 - 0.50 (m, 1H), 0.33 - 0.27 (m, 2H), -0.08 - -0.13 (m, 2H). $^{13}\text{C-NMR}$ (CDCl_3 , 100 MHz): 203.1, 170.3, 59.6, 52.2, 34.3, 29.2, 28.7, 28.2, 27.2, 10.6, 4.3, 4.3.



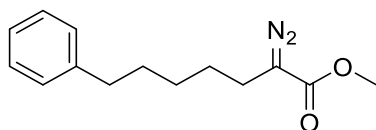
S20: yellow oil (52% yield). $^1\text{H-NMR}$ (CDCl_3 , 400 MHz, 300K): δ 7.35 - 7.30 (m, 2H), 7.25 - 7.20 (m, 3H), 3.79 (s, 3H), 2.69 (t, $J = 7.5\text{Hz}$, 2H), 2.38 (t, $J = 7.5\text{Hz}$, 2H), 1.78 - 1.68 (m, 2H), 1.68 - 1.57 (m, 2H). $^{13}\text{C-NMR}$ (CDCl_3 , 100 MHz): 168.0, 142.1, 128.4, 128.4, 125.9, 51.9, 35.6, 30.5, 27.3, 23.0. FT-IR (ATR) ν , cm^{-1} : 2932, 2858, 2076, 1690, 1436, 1350, 1306, 1190, 1149, 1115, 740, 699.



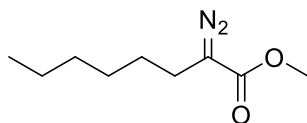
S21: yellow oil (43% yield). $^1\text{H-NMR}$ (CDCl_3 , 400 MHz, 300K): δ 7.08 (d, $J = 8.8\text{Hz}$, 2H), 6.83 (d, $J = 8.8\text{Hz}$, 2H), 3.79 (s, 3H), 3.75 (s, 3H), 2.58 (t, $J = 7.6\text{Hz}$, 2H), 2.32 (t, $J = 7.2\text{Hz}$, 2H), 1.67 - 1.61 (m, 2H), 1.57 - 1.51 (m, 2H). $^{13}\text{C-NMR}$ (CDCl_3 , 100 MHz): 168.1, 157.8, 134.2, 129.3, 113.8, 55.3, 51.9, 34.6, 30.7, 27.2, 23.0. FT-IR (ATR) ν , cm^{-1} : 2932, 2857, 2836, 2075, 1686, 1612, 1511, 1462, 1436, 1349, 1200, 1243, 1176, 1148, 1116, 1034, 809, 735, 559, 521.



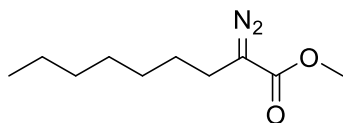
S22: yellow oil (47% yield). $^1\text{H-NMR}$ (CDCl_3 , 400 MHz, 300K): δ 7.24 (d, $J = 8.4\text{Hz}$, 2H), 7.09 (d, $J = 8.4\text{Hz}$, 2H), 3.75 (s, 3H), 2.60 (t, $J = 7.6\text{Hz}$, 2H), 2.32 (t, $J = 7.2\text{Hz}$, 2H), 1.69 - 1.61 (m, 2H), 1.57 - 1.49 (m, 2H). $^{13}\text{C-NMR}$ (CDCl_3 , 100 MHz): 168.1, 140.5, 131.5, 129.7, 128.4, 51.9, 34.8, 30.3, 27.1, 23.0. FT-IR (ATR) ν , cm^{-1} : 2933, 2859, 2075, 1686, 1492, 1435, 1349, 1305, 1189, 1114, 1091, 1014, 836, 803, 738, 660, 627, 522.



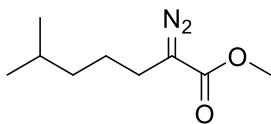
S23: yellow oil (47% yield). $^1\text{H-NMR}$ (CDCl_3 , 400 MHz, 300K): δ 7.28 - 7.26 (m, 2H), 7.18 - 7.16 (m, 3H), 3.76 (s, 3H), 2.62 (t, $J = 8\text{Hz}$, 2H), 2.30 (t, $J = 7.6\text{Hz}$, 2H), 1.68 - 1.62 (m, 2H), 1.56 - 1.51 (m, 2H), 1.44 - 1.38 (m, 2H). $^{13}\text{C-NMR}$ (CDCl_3 , 100 MHz): 168.1, 142.5, 128.4, 128.3, 125.7, 51.9, 35.8, 31.1, 28.4, 27.5, 23.0. FT-IR (ATR) ν , cm^{-1} : 2930, 2857, 2075, 1688, 1436, 1347, 1189, 1145, 1114, 910, 731, 698.



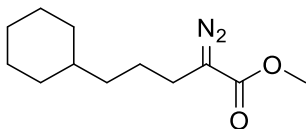
S24: yellow oil (48% yield). $^1\text{H-NMR}$ (CDCl_3 , 400 MHz, 300K): δ 3.78 (s, 3H), 3.32 (t, $J = 7.2\text{Hz}$, 2H), 1.52 - 1.48 (m, 2H), 1.35 - 1.31 (m, 6H), 0.92 - 0.89 (m, 3H). $^{13}\text{C-NMR}$ (CDCl_3 , 100 MHz): 168.0, 51.8, 31.4, 28.4, 27.5, 23.0, 22.5, 14.0. FT-IR (ATR) ν , cm^{-1} : 2955, 2927, 2858, 2075, 1691, 1436, 1347, 1304, 1188, 1132, 1085, 738.



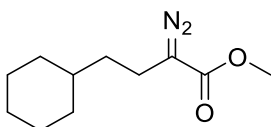
S25: yellow oil (55% yield). $^1\text{H-NMR}$ (CDCl_3 , 400 MHz, 300K): δ 3.75 (s, 3H), 3.29 (t, $J = 7.2\text{Hz}$, 2H), 1.51 - 1.47 (m, 2H), 1.33 - 1.27 (m, 8H), 0.87 (t, $J = 6.8\text{Hz}$, 3H). $^{13}\text{C-NMR}$ (CDCl_3 , 100 MHz): 168.6, 52.3, 32.2, 29.4, 29.2, 28.1, 23.5, 23.1, 14.5. FT-IR (ATR) ν , cm^{-1} : 2954, 2926, 2856, 2075, 1692, 1436, 1347, 1282, 1188, 1132, 1089, 738.



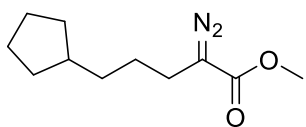
S26: yellow oil (51% yield). $^1\text{H-NMR}$ (CDCl_3 , 400 MHz, 300K): δ 3.76 (s, 3H), 2.29 (t, $J = 7.2\text{Hz}$, 2H), 1.56 - 1.48 (m, 3H), 1.26 - 1.22 (m, 2H), 0.88 (d, $J = 6.4\text{Hz}$, 6H). $^{13}\text{C-NMR}$ (CDCl_3 , 100 MHz): 168.0, 51.8, 37.9, 27.7, 25.4, 23.2, 22.5. FT-IR (ATR) ν , cm^{-1} : 2954, 2903, 2870, 2074, 1689, 1436, 1359, 1322, 1302, 1279, 1189, 1135, 1088, 737.



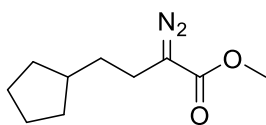
S27: yellow oil (63% yield). $^1\text{H-NMR}$ (CDCl_3 , 400 MHz, 300K): δ 3.73 (s, 3H), 2.26 (t, $J = 7.6\text{Hz}$, 2H), 1.68 - 1.60 (m, 5H), 1.48 - 1.44 (m, 2H), 1.22 - 1.12 (m, 6H), 0.89 - 0.86 (m, 2H). $^{13}\text{C-NMR}$ (CDCl_3 , 100 MHz): 168.1, 51.8, 37.4, 36.5, 33.3, 26.6, 26.3, 24.9, 23.3. FT-IR (ATR) ν , cm^{-1} : 2921, 2850, 2074, 1692, 1435, 1345, 1308, 1280, 1188, 1138, 737.



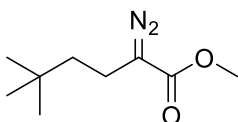
S28: yellow oil (52% yield). $^1\text{H-NMR}$ (CDCl_3 , 400 MHz, 300K): δ 3.73 (s, 3H), 2.29 (t, $J = 7.7\text{Hz}$, 2H), 1.71 - 1.65 (m, 5H), 1.39 - 1.33 (m, 2H), 1.22 - 1.16 (m, 4H), 0.94 - 0.84 (m, 2H). $^{13}\text{C-NMR}$ (CDCl_3 , 100 MHz): 168.1, 51.8, 36.8, 34.9, 33.0, 26.5, 26.2, 20.3. FT-IR (ATR) ν , cm^{-1} : 2921, 2851, 2074, 1692, 1435, 1341, 1317, 1300, 1189, 1165, 1139, 1108, 1074, 737.



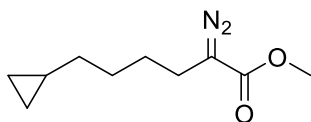
S29: yellow oil (48% yield). $^1\text{H-NMR}$ (CDCl_3 , 400 MHz, 300K): δ 3.78 (s, 3H), 2.31 (t, $J = 7.4\text{Hz}$, 2H), 1.80 - 1.72 (m, 3H), 1.66 - 1.49 (m, 6H), 1.39 - 1.35 (m, 2H), 1.12 - 1.09 (m, 2H). $^{13}\text{C-NMR}$ (CDCl_3 , 100 MHz): 168.1, 51.8, 39.9, 35.2, 32.7, 26.8, 25.1, 23.2. FT-IR (ATR) ν , cm^{-1} : 2948, 2862, 2075, 1692, 1624, 1435, 1346, 1306, 1280, 1189, 1141, 737.



S30: yellow oil (59% yield). $^1\text{H-NMR}$ (CDCl_3 , 400 MHz, 300K): δ 3.77 (s, 3H), 2.34 - 2.31 (m, 2H), 1.82 - 1.79 (m, 3H), 1.63 - 1.51 (m, 6H), 1.14 - 1.10 (m, 2H). $^{13}\text{C-NMR}$ (CDCl_3 , 100 MHz): 168.1, 51.8, 39.2, 33.8, 32.5, 25.2, 22.2. FT-IR (ATR) ν , cm^{-1} : 2949, 2866, 2074, 1690, 1624, 1435, 1335, 1302, 1189, 1145, 1117, 1074, 738.



S31: yellow oil (50% yield). $^1\text{H-NMR}$ (CDCl_3 , 400 MHz, 300K): δ 3.76 (s, 3H), 2.30 - 2.26 (m, 2H), 1.41 - 1.37 (m, 2H), 0.94 (s, 9H). $^{13}\text{C-NMR}$ (CDCl_3 , 100 MHz): 168.1, 51.8, 41.2, 30.2, 29.1, 18.4. FT-IR (ATR) ν , cm^{-1} : 2954, 2907, 2869, 2075, 1692, 1471, 1436, 1333, 1274, 1239, 1190, 1157, 1107, 735.



S32: yellow oil (69% yield). $^1\text{H-NMR}$ (CDCl_3 , 400 MHz, 300K): δ 3.77 (s, 3H), 2.32 (t, $J = 7.3\text{Hz}$, 2H), 1.59 - 1.44 (m, 4H), 1.25 - 1.20 (m, 2H), 0.68 - 0.62 (m, 1H), 0.43 - 0.39 (m, 2H), 0.02 - -0.01 (m, 2H). $^{13}\text{C-NMR}$ (CDCl_3 , 100 MHz): 168.1, 51.9, 34.3, 28.8, 27.4, 23.1, 10.7, 4.4. FT-IR (ATR) ν , cm^{-1} : 3076, 2999, 2925, 2855, 2075, 1690, 1436, 1348, 1189, 1136, 1014, 821, 739.

VII.3.4 Catalytic procedures

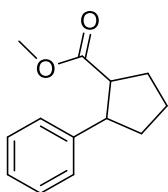
VII.3.4.1 Reaction protocol for catalysis

Under N_2 atmosphere, to a solution of the iron complex (0.004 or 0.002 mmols) in dichloromethane (1 mL), was added **S20** (18.6 mg, 0.08 mmols). Then, the corresponding amount of $[\text{LiAl}(\text{OC}(\text{CF}_3)_3)_4]$ was added as solid and the reaction was stirred at room temperature for 16 hours. After that, the solution was passed through a silica plug and eluted with 2 mL of dichloromethane and 1 mL of ethyl acetate. The solvent was removed under reduced pressure. At this point, 0.7 mL of deuterated chloroform and dibromomethane as internal standard (5.6 μL , 0.08 mmols) were added. The products yields were analyzed by $^1\text{H-NMR}$ spectroscopy.

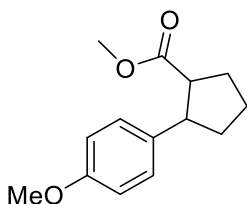
VII.3.4.2 General procedure for product isolation

A Schlenck flask was charged with **22-Fe** (28.3 mg, 0.025 mmols) in dichloromethane (12.5 mL) and **S20** mmol of the corresponding diazo acetate was added. $[\text{LiAl}(\text{OC}(\text{CF}_3)_3)_4]$ (244 mg, 0.25 mmols) was added as a solid and the reaction was stirred under N_2 atmosphere for 24 hours at 25°C . After the completion of the reaction, the solvent was removed and the residue was dissolved in acetone. This solution was added into a previously stirred solution of KMnO_4 and BnEt_3NCl as previously described²¹⁹ for the oxidation of the olefin. The reaction was stirred for 30 minutes at 0°C and it was finally quenched with an aqueous solution of NaHSO_3 . The acetone was evaporated under reduced pressure and the aqueous phase was extracted with ethyl acetate (3 x 50 mL). The organic layers were removed under reduced pressure and the residue was purified by flash chromatography (20:1 hexane:ethyl acetate) to give the pure product.

VII.3.5 Characterization of isolated products

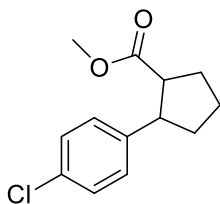


P20: Pure product was isolated as a colorless oil in a 89:11 mixture of diastereomers (57% yield). $^1\text{H-NMR}$ (CDCl_3 , 400 MHz, 300K): δ 7.34 - 7.20 (m, 5H), 3.64 (s, 3H), 3.47 - 3.35 (m, 1H), 3.26 (s, 3H), 3.19 - 3.16 (m, 1H), 2.91 - 2.84 (m, 1H), 2.22 - 1.76 (m, 6H). $^{13}\text{C-NMR}$ (CDCl_3 , 100 MHz): 176.4, 175.1, 143.9, 141.7, 128.4, 128.0, 127.9, 127.2, 126.4, 126.3, 52.0, 51.6, 50.9, 49.8, 49.8, 49.2, 35.1, 31.2, 30.9, 28.6, 25.1, 24.8. HRSM (ESI+) m/z calculated for $\text{C}_{13}\text{H}_{16}\text{O}_2$ $[\text{M}+\text{Na}]^+$ 227.1043, found 227.1045.

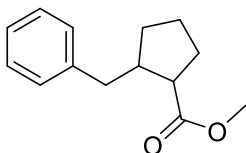


P21: Pure product was isolated as a white solid in a 79:21 mixture of diastereomers (70% yield). $^1\text{H-NMR}$ (CDCl_3 , 400 MHz, 300K): δ 7.19 - 7.13 (m, 2H), 6.88 - 6.82 (m, 2H), 3.79 (s, 3H), 3.63 (s, 3H), 3.40 - 3.31 (m, 1H), 3.29 (s, 3H), 3.17 - 3.11 (m, 1H), 2.85 - 2.78 (m, 1H), 2.19 - 1.71 (m, 6H). $^{13}\text{C-NMR}$ (CDCl_3 , 100 MHz): 176.4, 175.2, 158.1, 135.8, 133.6, 128.8, 128.1, 113.8, 113.4, 55.2, 55.2, 52.1, 51.6, 50.9, 49.8, 49.1, 48.5,

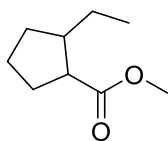
35.1, 31.5, 30.8, 28.5, 25.0, 24.8. HRSM (ESI+) m/z calculated for $C_{14}H_{18}O_3$ $[M+Na]^+$ 257.1148, found 257.1152.



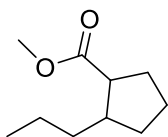
P22: Pure product was isolated as a colorless oil in a 86:14 mixture of diastereomers (39% yield). ¹H-NMR (CDCl₃, 400 MHz, 300K): δ 7.29 - 7.14 (m, 4H), 3.63 (s, 3H), 3.37 - 3.32 (m, 1H), 3.30 (s, 3H), 2.82 - 2.77 (m, 1H), 2.21 - 1.68 (m, 6H). ¹³C-NMR (CDCl₃, 100 MHz): 176.1, 174.9, 142.3, 140.2, 132.0, 129.2, 128.5, 128.1, 52.0, 51.7, 51.0, 49.7, 49.1, 48.5, 35.0, 31.3, 30.7, 28.6, 25.0, 24.7. HRSM (ESI+) m/z calculated for $C_{13}H_{15}O_2Cl$ $[M+Na]^+$ 261.0653, found 261.0655.



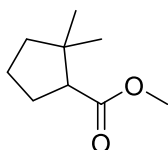
P23: Pure product was isolated as a colorless oil in a 99:1 mixture of diastereomers (30% yield). ¹H-NMR (CDCl₃, 400 MHz, 300K): δ 7.31 - 7.28 (m, 2H), 7.22 - 7.19 (m, 3H), 3.60 (s, 3H), 2.87 - 2.84 - 2.82 (m, 1H), 2.62 - 2.58 (m, 1H), 2.47 - 2.44 (m, 2H), 1.98 - 1.93 (m, 1H), 1.87 - 1.81 (m, 2H), 1.72 - 1.66 (m, 2H), 1.37 - 1.30 (m, 2H). ¹³C-NMR (CDCl₃, 100 MHz): 176.8, 140.7, 129.0, 128.2, 125.9, 51.5, 49.8, 45.9, 41.0, 32.2, 30.2, 24.3. HRSM (ESI+) m/z calculated for $C_{14}H_{18}O_2$ $[M+Na]^+$ 241.1199, found 241.1206.



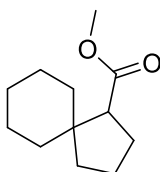
P24: Pure product was isolated as a colorless oil in a 94:6 mixture of diastereomers (64% yield). ¹H-NMR (CDCl₃, 400 MHz, 300K): δ 3.68 (s, 3H), 2.35 - 2.33 (m, 1H), 2.03 - 1.99 (m, 1H), 1.96 - 1.79 (m, 3H), 1.73 - 1.64 (m, 2H), 1.54 - 1.49 (m, 1H), 1.31 - 1.19 (m, 2H), 0.90 (t, J = 7.4Hz, 3H). ¹³C-NMR (CDCl₃, 100 MHz): 177.4, 51.5, 50.0, 46.2, 32.1, 30.4, 28.0, 24.7, 12.5. HRSM (ESI+) m/z calculated for $C_9H_{16}O_2$ $[M+Na]^+$ 179.1043, found 179.1038.



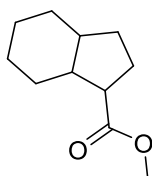
P25: Pure product was isolated as a colorless oil in a 96:4 mixture of diastereomers (60% yield). $^1\text{H-NMR}$ (CDCl_3 , 400 MHz, 300K): δ 3.68 (s, 3H), 2.34 - 2.30 (m, 1H), 2.14 - 2.08 (m, 1H), 1.97 - 1.78 (m, 3H), 1.73 - 1.66 (m, 2H), 1.50 - 1.44 (m, 1H), 1.37 - 1.20 (m, 4H), 0.90 (t, $J = 7\text{Hz}$, 3H). $^{13}\text{C-NMR}$ (CDCl_3 , 100 MHz): 177.4, 51.5, 50.4, 44.3, 37.6, 32.5, 30.4, 24.8, 21.4, 14.3. HRSM (ESI+) m/z calculated for $\text{C}_{10}\text{H}_{18}\text{O}_2$ $[\text{M}+\text{Na}]^+$ 193.1199, found 192.1205.



P26: Pure product was isolated as a colorless oil (56% yield). $^1\text{H-NMR}$ (CDCl_3 , 400 MHz, 300K): 3.68 (s, 3H), 2.44 (t, $J = 8.5\text{Hz}$, 1H), 2.12 - 2.02 (m, 1H), 1.93 - 1.45 (m, 5H), 1.16 (s, 3H), 0.90 (s, 3H). $^{13}\text{C-NMR}$ (CDCl_3 , 100 MHz): 175.4, 54.5, 51.1, 42.8, 41.7, 29.2, 27.6, 23.9, 22.4. HRSM (ESI+) m/z calculated for $\text{C}_9\text{H}_{16}\text{O}_2$ $[\text{M}+\text{Na}]^+$ 179.1043, found 179.1039.

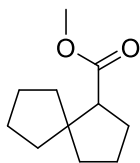


P27: Pure product was isolated as a colorless oil in a 99:1 mixture of diastereomers (70% yield). $^1\text{H-NMR}$ (CDCl_3 , 400 MHz, 300K): δ 3.66 (s, 3H), 2.42 (t, $J = 7.8\text{Hz}$, 1H), 1.96 - 1.12 (m, 16H). $^{13}\text{C-NMR}$ (CDCl_3 , 100 MHz): 175.6, 55.2, 51.1, 46.7, 37.9, 35.4, 33.2, 27.6, 26.1, 23.7, 23.0, 22.8. HRSM (ESI+) m/z calculated for $\text{C}_{12}\text{H}_{20}\text{O}_2$ $[\text{M}+\text{Na}]^+$ 219.1356, found 219.1359.

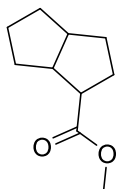


P28: Pure product was isolated as a colorless oil in a 68:29:3 mixture of diastereomers (47% yield). $^1\text{H-NMR}$ (CDCl_3 , 400 MHz, 300K): δ 3.68 (s, 3H), 3.67 (s, 3H), 2.73 - 2.67 (m, 1H), 2.37 - 2.32 (m, 1H), 2.20 - 2.15 (m, 1H), 2.03 - 1.01 (m, 14H). $^{13}\text{C-NMR}$ (CDCl_3 , 100 MHz): 177.6, 177.0, 51.5, 51.5, 50.4, 49.0, 46.7, 45.7, 43.8, 39.4, 31.7, 30.7, 30.6,

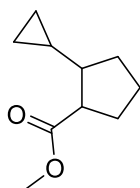
30.0, 27.8, 27.0, 26.8, 26.7, 26.1, 26.0, 24.1, 22.3. HRSM (ESI+) m/z calculated for $C_{11}H_{18}O_2$ $[M+Na]^+$ 205.1199, found 205.1208.



P29: Pure product was isolated as a colorless oil in a >99:1 mixture of diastereomers (63% yield). 1H -NMR ($CDCl_3$, 400 MHz, 300K): δ 3.63 (s, 3H), 2.57 (t, $J = 7.5$ Hz, 1H), 1.98 - 1.41 (m, 14H). ^{13}C -NMR ($CDCl_3$, 100 MHz): 176.0, 54.4, 52.7, 51.1, 39.2, 38.9, 34.2, 28.1, 24.5, 24.1, 22.9. HRSM (ESI+) m/z calculated for $C_{11}H_{18}O_2$ $[M+Na]^+$ 205.1199, found 205.1203.



P30: Pure product was isolated as a yellow oil in a 94:6 mixture of diastereomers (67% yield). 1H -NMR ($CDCl_3$, 400 MHz, 300K): δ 3.68 (s, 3H), 3.67 (s, 3H), 2.64 - 2.51 (m, 2H), 2.33 - 2.26 (m, 1H), 2.04 - 1.86 (m, 2H), 1.77 - 1.44 (m, 6H), 1.34 - 1.16 (m, 2H). ^{13}C -NMR ($CDCl_3$, 100 MHz): 176.8, 175.1, 51.7, 51.5, 51.2, 48.6, 47.8, 45.5, 43.3, 42.8, 35.0, 33.5, 33.4, 32.9, 31.8, 31.4, 29.9, 27.5, 26.4, 25.3. HRSM (ESI+) m/z calculated for $C_{10}H_{16}O_2$ $[M+Na]^+$ 191.1043, found 191.1049.



P32: Pure product was isolated as a colorless oil in a 86:14 mixture of diastereomers (72% yield). 1H -NMR ($CDCl_3$, 400 MHz, 300K): δ 3.69 (s, 3H), 3.69 (s, 3H), 2.86 - 2.82 (m, 1H), 2.57 - 2.50 (m, 1H), 1.87 - 1.78 (m, 3H), 1.70 - 1.67 (m, 2H), 1.59 - 1.50 (m, 1H), 1.44 - 1.37 (m, 1H), 0.71 - 0.62 (m, 1H), 0.42 - 0.40 (m, 2H), 0.13 - 0.08 (m, 2H). ^{13}C -NMR ($CDCl_3$, 100 MHz): 177.4, 175.7, 51.6, 51.1, 50.3, 49.6, 48.9, 47.8, 32.1, 31.8, 30.4, 27.8, 24.5, 23.9, 15.2, 12.5, 4.4, 3.4, 3.3, 3.1. HRSM (ESI+) m/z calculated for $C_{10}H_{16}O_2$ $[M+Na]^+$ 191.1043, found 191.1046.

VII.3.6 IR studies

22-Fe + S20

To a solution of diazo reagent **S20** (0.02 M) in DCM, **22-Fe** (0.02M) was added, immediately after, the DCM was evaporated under nitrogen flow, and infrared spectrum was registered. Comparison of infrared spectra reveals that only the band at 1690 cm⁻¹ assigned to the carbonyl group of the diazo reagent **1** is shifted.

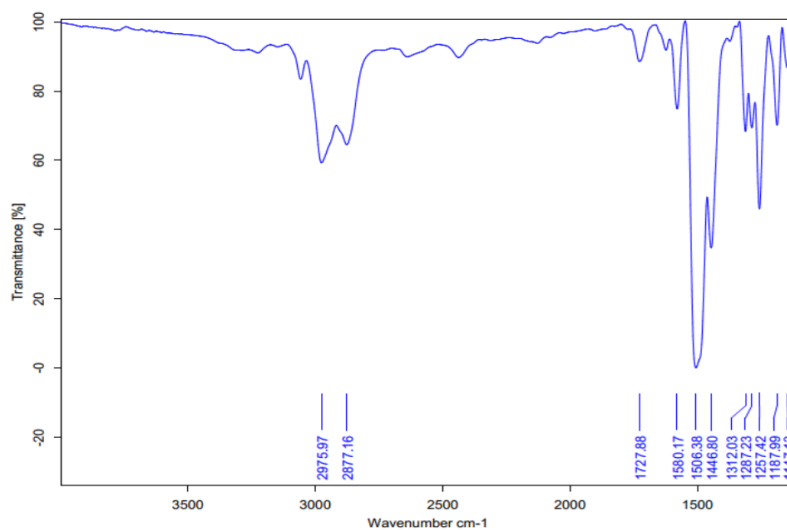


Figure VII.1. IR spectrum of **22-Fe**

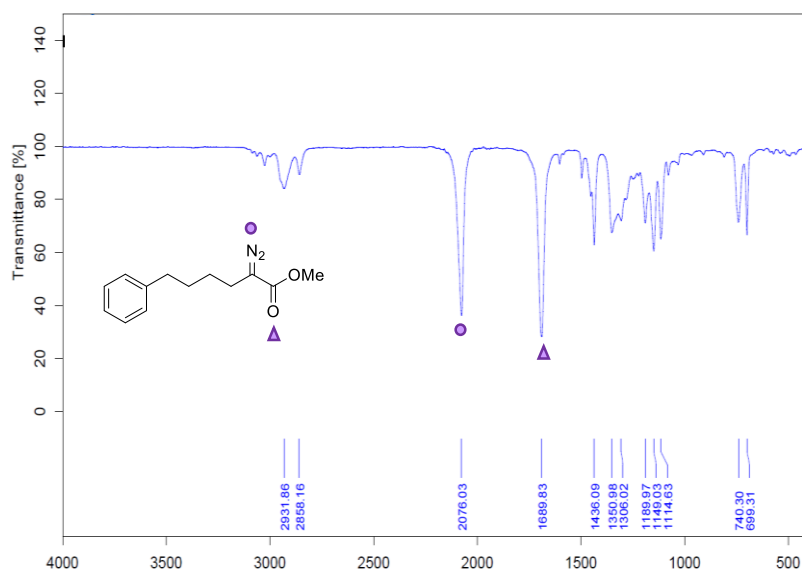


Figure VII.2. IR spectrum of **S20**.

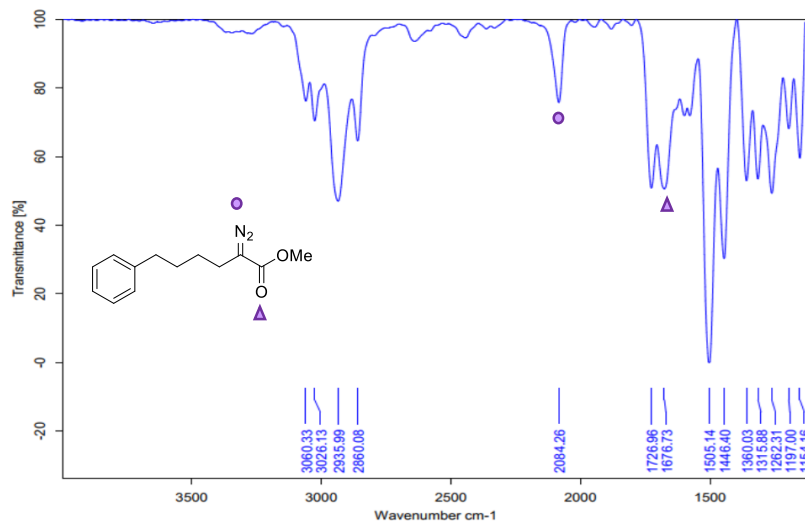


Figure VII.3. IR spectrum of **S20:22-Fe** (1:1).

[LiAl(OC(CF₃)₃)₄] + **S20**

To a solution of **S20** (0.09 M) in DCM, compound [LiAl(OC(CF₃)₃)₄] was added in a range of concentrations 0.0045 - 0.09 M, immediately after the DCM was evaporated under nitrogen flow, and infrared spectra of each sample was registered. Comparison of the registered infrared spectra reveals that the signals assigned to the diazo fragment (2076 cm⁻¹) and the carbonyl group (1690 cm⁻¹) are shifted, being the shift of the latter band the most significant.

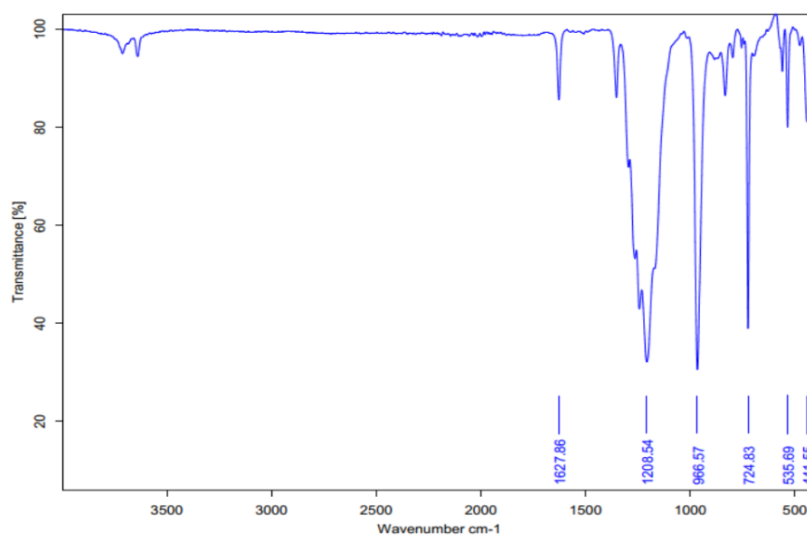


Figure VII.4. IR spectrum of [LiAl(OC(CF₃)₃)₄]

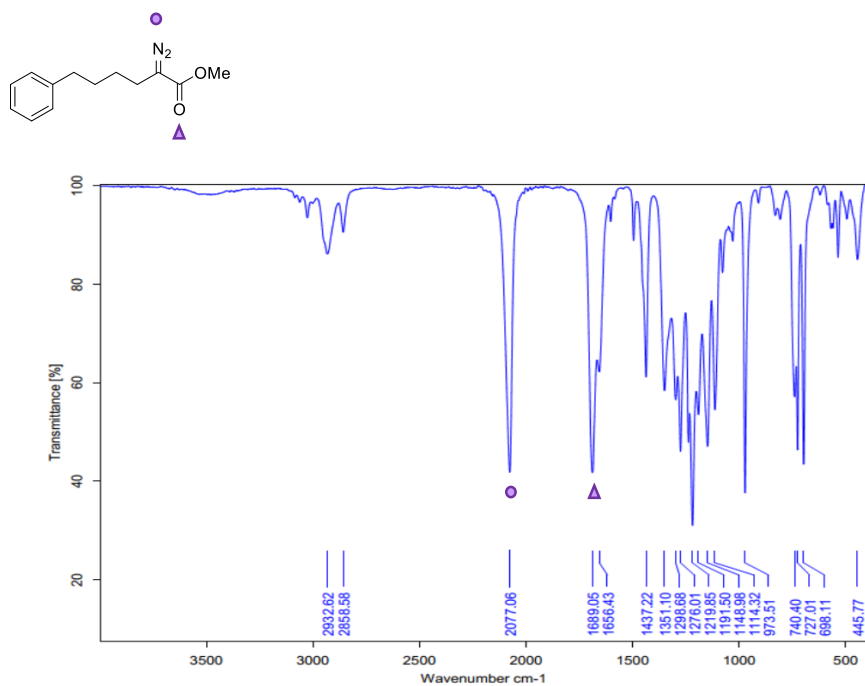


Figure VII.5. IR spectrum of **S20**: $[\text{LiAl}(\text{OC}(\text{CF}_3)_3)_4]$ (1:0.05).

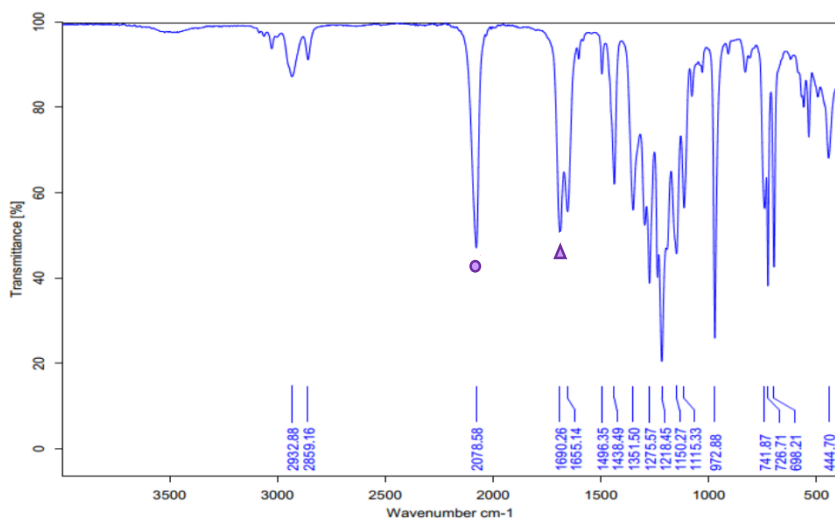


Figure VII.6. IR spectrum of **S20**: $[\text{LiAl}(\text{OC}(\text{CF}_3)_3)_4]$ (1:0.1).

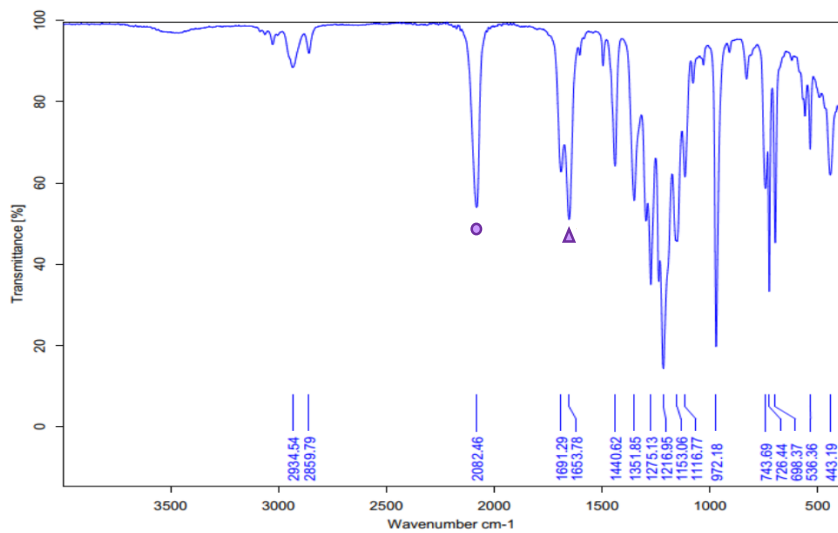


Figure VII.7. IR spectrum of $S_{20}:[LiAl(OC(CF_3)_3)_4]$ (1:0.15).

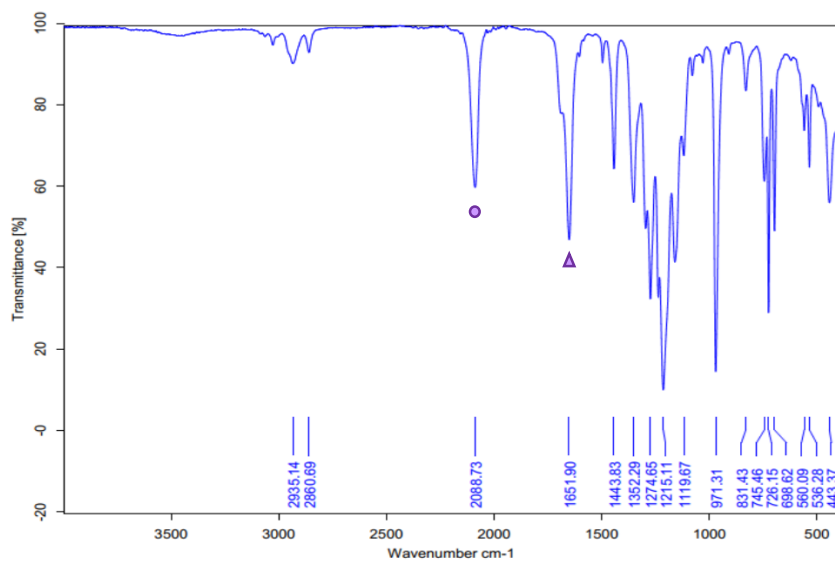


Figure VII.8. IR spectrum of $S_{20}:[LiAl(OC(CF_3)_3)_4]$ (1:0.2).

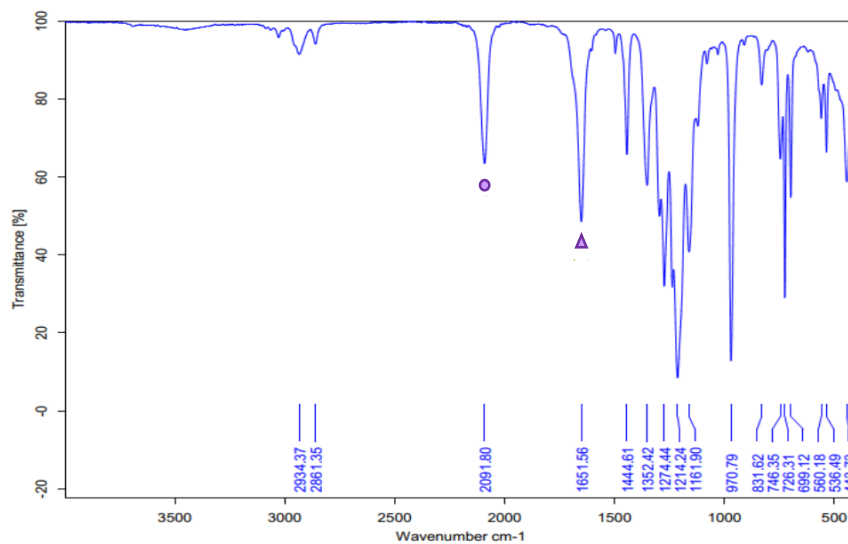


Figure VII.9. IR spectrum of **S20**: $[\text{LiAl}(\text{OC}(\text{CF}_3)_3)_4]$ (1:0.25).

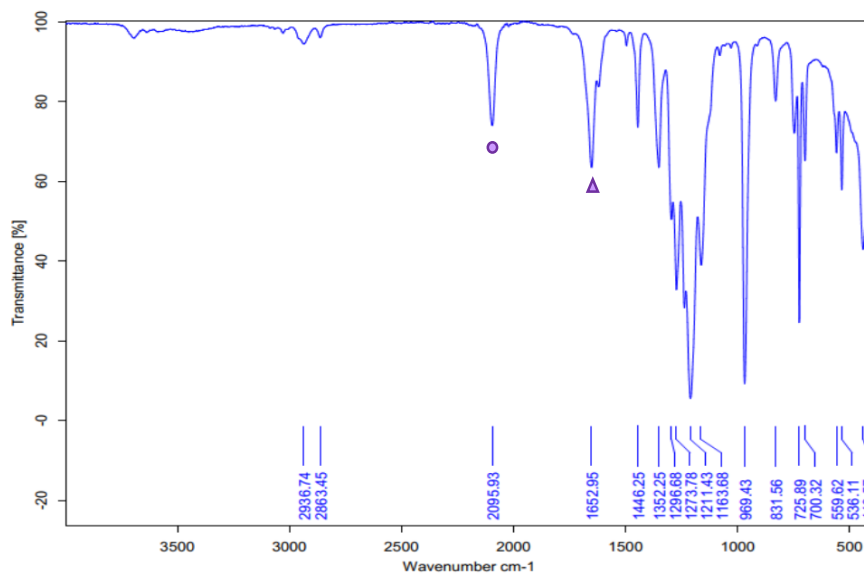


Figure VII.10. IR spectrum of **S20**: $[\text{LiAl}(\text{OC}(\text{CF}_3)_3)_4]$ (1:0.5).

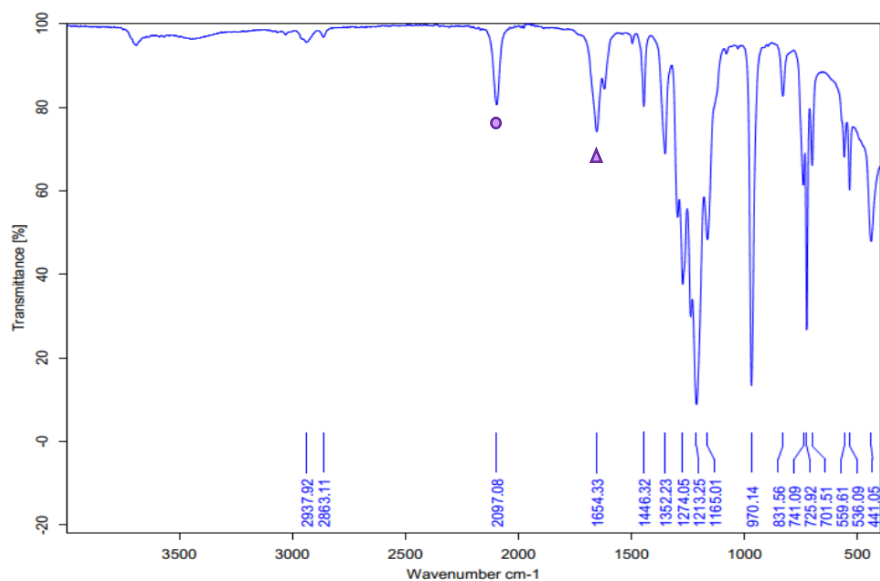


Figure VII.11. IR spectrum of **S20**: $[\text{LiAl}(\text{OC}(\text{CF}_3)_3)_4]$ (1:0.75).

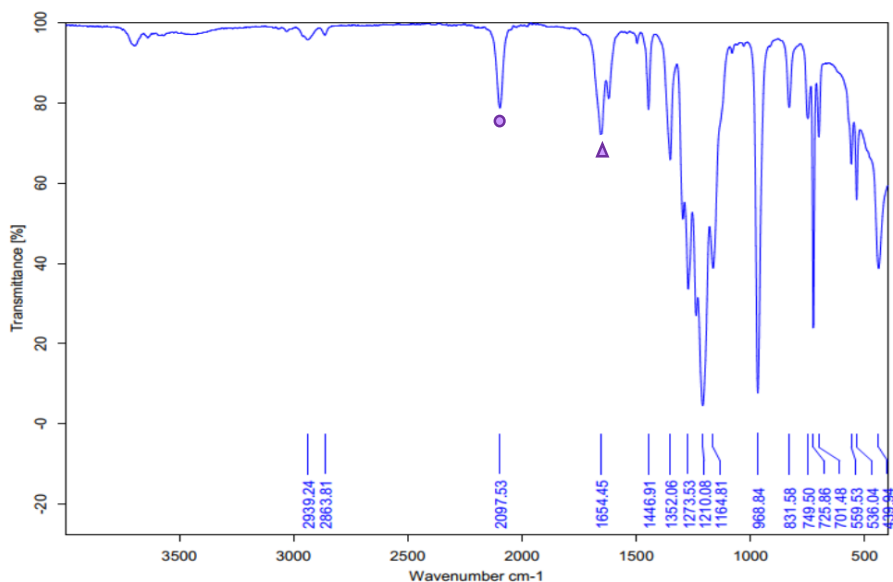


Figure VII.12. IR spectrum of **S20**: $[\text{LiAl}(\text{OC}(\text{CF}_3)_3)_4]$ (1:1).

VII.3.6 KIE studies

Diazo reagent was synthesized as described in the literature.²²⁰ Following the general methodology described for small scale (0.08 mM) catalysis, compound $[\text{D}_1]\text{-S20}$ was subjected to intramolecular C-H alkylation in DCM using **22-Fe** (2.5 mol%) as catalyst. The resulting reaction mixture was filtered through a silica plug to remove paramagnetic impurities, the solvent was evaporated under vacuum and the sample was analysed by ^1H NMR spectroscopy. The KIE value was calculated by integration of the new formed C-H fragment attached to the ester CO_2Me group upon alkylation reaction.

KIE **22-Fe** = 2.3 (E), 4.4 (Z)

KIE $[\text{Rh}_2(\text{OAc})_4]$ = 2.3 (E), 3.7 (Z)

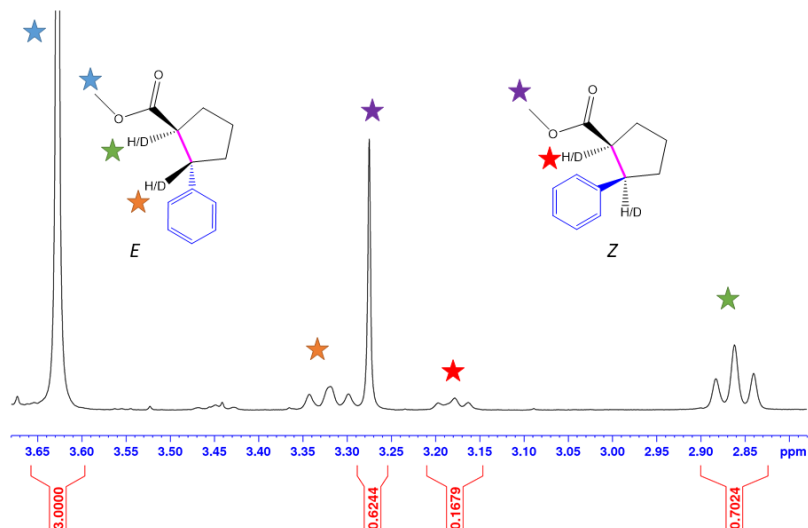


Figure VII.13. ¹H-NMR spectrum of C-H alkylation of [D₁]-S₂₀ catalyzed by **22-Fe** (2.5 mol%) and $[\text{LiAl}(\text{OC}(\text{CF}_3)_3)_4]$ (25 mol%)

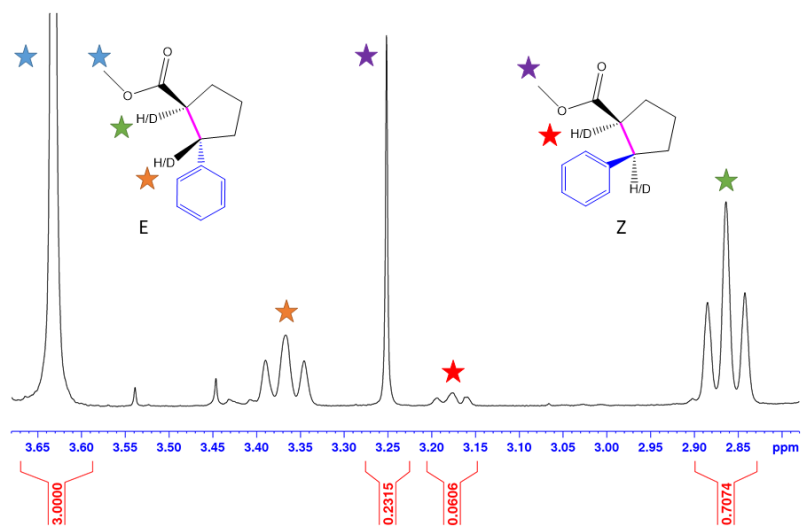


Figure VII.14. ¹H-NMR spectrum of C-H alkylation of [D₁]-S₂₀ catalyzed by $\text{Rh}_2(\text{OAc})_4$ (2.5 mol%)

References

1. Hermann, M. *Justus Liebigs Ann. Chem.* **1855**, 95, 211.
2. Demselben *Justus Liebigs Ann. Chem.* **1862**, 123, 121.
3. Nef, J. U. *Justus Liebigs Ann. Chem.* **1897**, 298, 202.
4. Buchner, E.; Geronimus, J. *Ber. Dtsch. Che. Ges.* **1903**, 36, 3782.
5. Buchner, E.; Feldmann, L. *Ber. Dtsch. Che. Ges.* **1903**, 36, 3509.
6. Doering, W. v. E.; Knox, L. H. *J. Am. Chem. Soc.* **1953**, 75, 297.
7. Doering, W. v. E.; Hoffmann, A. K. *J. Am. Chem. Soc.* **1954**, 76, 6162.
8. Tschugajeff, L.; Skanawy-Grigorjewa, M.; Posnjak, A.; Skanawy-Grigorjewa, M. *Z. Anorg. Allg. Chem.* **1925**, 148, 37.
9. Rouschias, G.; Shaw, B. L. *J. Chem. Soc. Chem. Commun.* **1970**, 183.
10. Burke, A.; Balch, A. L.; Enemark, J. H. *J. Am. Chem. Soc.* **1970**, 92, 2555.
11. Butler, W. M.; Enemark, J. H.; Parks, J.; Balch, A. L. *Inorg. Chem.* **1973**, 12, 451.
12. Fischer, E. O.; Maasböl, A. *Angew. Chem. Int. Ed.* **1964**, 3, 580.
13. Schrock, R. R. *J. Am. Chem. Soc.* **1974**, 96, 6796.
14. Öfele, K. *J. Organomet. Chem.* **1968**, 12, 42.
15. Wanzlick, H. W.; Schönherr, H. *J. Angew. Chem. Int. Ed.* **1968**, 7, 141.
16. Igau, A.; Grutzmacher, H.; Baceiredo, A.; Bertrand, G. *J. Am. Chem. Soc.* **1988**, 110, 6463.
17. Arduengo, A. J.; Harlow, R. L.; Kline, M. *J. Am. Chem. Soc.* **1991**, 113, 361.
18. Herrmann, W. A.; Köcher, C. *Angew. Chem. Int. Ed.* **1997**, 36, 2162.
19. Hopkinson, M. N.; Richter, C.; Schedler, M.; Glorius, F. *Nature* **2014**, 510, 485.
20. Johnson, N. A.; Southerland, M. R.; Youngs, W. J. *Molecules* **2017**, 22, 1263.
21. Visbal, R.; Gimeno, M. C. *Chem. Soc. Rev.* **2014**, 43, 3551.
22. de Frémont, P.; Marion, N.; Nolan, S. P. *Coord. Chem. Rev.* **2009**, 253, 862.
23. Vyboishchikov, S. F.; Frenking, G. *Chem. Eur. J.* **1998**, 4, 1428.
24. Santamaría, J.; Aguilar, E. *Org. Chem. Front.* **2016**, 3, 1561.
25. Arduengo, A. J.; Gamper, S. F.; Calabrese, J. C.; Davidson, F. *J. Am. Chem. Soc.* **1994**, 116, 4391.
26. Jazzar, R. F. R.; Macgregor, S. A.; Mahon, M. F.; Richards, S. P.; Whittlesey, M. K. *J. Am. Chem. Soc.* **2002**, 124, 4944.
27. T., T. A.; Marius, S.; W., E. A.; Martin, L.; L., S. A.; Koop, L. *Chem. Eur. J.* **2003**, 9, 3577.
28. Jacobsen, H.; Correa, A.; Poater, A.; Costabile, C.; Cavallo, L. *Coord. Chem. Rev.* **2009**, 253, 687.
29. Cazin, C. S. J. *N-Heterocyclic Carbenes in Transition Metal Catalysis and Organocatalysis*; Springer, 2011; Vol. 32.
30. Díez-González, S.; Marion, N.; Nolan, S. P. *Chem. Rev.* **2009**, 109, 3612.
31. Trnka, T. M.; Grubbs, R. H. *Acc. Chem. Res.* **2001**, 34, 18.
32. Kantchev, E. A. B.; O'Brien, C. J.; Organ, M. G. *Angew. Chem. Int. Ed.* **2007**, 46, 2768.
33. Dorta, R.; Stevens, E. D.; Scott, N. M.; Costabile, C.; Cavallo, L.; Hoff, C. D.; Nolan, S. P. *J. Am. Chem. Soc.* **2005**, 127, 2485.
34. Tolman, C. A. *Chem. Rev.* **1977**, 77, 313.
35. Clavier, H.; Nolan, S. P. *Chem. Commun.* **2010**, 46, 841.
36. Benhamou, L.; Chardon, E.; Lavigne, G.; Bellemin-Laponnaz, S.; César, V. *Chem. Rev.* **2011**, 111, 2705.
37. Gründemann, S.; Kovacevic, A.; Albrecht, M.; Faller Robert, J. W.; Crabtree, H. *Chem. Commun.* **2001**, 2274.
38. IUPAC definition of mesoionic compounds: Dipolar five- (possibly six-) membered heterocyclic compounds in which both the negative and the positive charge are delocalized, for which a totally covalent structure cannot be written, and which cannot be represented satisfactorily by any one polar structure.
39. Charra, V.; de Frémont, P.; Braunstein, P. *Coord. Chem. Rev.* **2017**, 341, 53.
40. Grohmann, C.; Hashimoto, T.; Fröhlich, R.; Ohki, Y.; Tatsumi, K.; Glorius, F. *Organometallics* **2012**, 31, 8047.
41. Käß, M.; Hohenberger, J.; Adelhardt, M.; Zolnhofer, E. M.; Mossin, S.; Heinemann, F. W.; Sutter, J.; Meyer, K. *Inorg. Chem.* **2014**, 53, 2460.
42. Chianese, A. R.; Kovacevic, A.; Zeglis, B. M.; Faller, J. W.; Crabtree, R. H. *Organometallics* **2004**, 23, 2461.
43. Iglesias, M.; Albrecht, M. *Dalton Trans.* **2010**, 39, 5213.
44. Gusev, D. G. *Organometallics* **2009**, 28, 6458.
45. Lebel, H.; Janes, M. K.; Charette, A. B.; Nolan, S. P. *J. Am. Chem. Soc.* **2004**, 126, 5046.

46. Yang, L.; Krüger, A.; Neels, A.; Albrecht, M. *Organometallics* **2008**, *27*, 3161.
47. Zhukhovitskiy, A. V.; Kobylanskiy, I. J.; Wu, C.-Y.; Toste, F. D. *J. Am. Chem. Soc.* **2018**, *140*, 466.
48. Aizpurua, J. M.; Fratila, R. M.; Monasterio, Z.; Pérez-Esnaola, N.; Andreieff, E.; Irastorza, A.; Sagartzazu-Aizpurua, M. *New J. Chem.* **2014**, *38*, 474.
49. Tornøe, C. W.; Christensen, C.; Meldal, M. *J. Org. Chem.* **2002**, *67*, 3057.
50. Rostovtsev, V. V.; Green, L. G.; Fokin, V. V.; Sharpless, K. B. *Angew. Chem. Int. Ed.* **2002**, *41*, 2596.
51. Zhang, L.; Chen, X.; Xue, P.; Sun, H. H. Y.; Williams, I. D.; Sharpless, K. B.; Fokin, V. V.; Jia, G. *J. Am. Chem. Soc.* **2005**, *127*, 15998.
52. Kwok, S. W.; Fotsing, J. R.; Fraser, R. J.; Rodionov, V. O.; Fokin, V. V. *Org. Lett.* **2010**, *12*, 4217.
53. Bouffard, J.; Keitz, B. K.; Tonner, R.; Guisado-Barrios, G.; Frenking, G.; Grubbs, R. H.; Bertrand, G. *Organometallics* **2011**, *30*, 2617.
54. Alder, R. W.; Blake, M. E.; Chaker, L.; Harvey, J. N.; Paolini, F.; Schütz, J. *Angew. Chem. Int. Ed.* **2004**, *43*, 5896.
55. Guisado-Barrios, G.; Bouffard, J.; Donnadiou, B.; Bertrand, G. *Angew. Chem. Int. Ed.* **2010**, *49*, 4759.
56. Guisado-Barrios, G.; Bouffard, J.; Donnadiou, B.; Bertrand, G. *Organometallics* **2011**, *30*, 6017.
57. Iwasaki, H.; Yamada, Y.; Ishikawa, R.; Koga, Y.; Matsubara, K. *Eur. J. Org. Chem.* **2016**, *2016*, 1651.
58. Aucamp, D.; Witteler, T.; Dielmann, F.; Siangwata, S.; Liles, D. C.; Smith, G. S.; Bezuidenhout, D. I. *Eur. J. Inorg. Chem.* **2017**, *2017*, 1227.
59. Vivancos, Á.; Segarra, C.; Albrecht, M. *Chem. Rev.* **2018**, *118*, 9493.
60. Cai, J.; Yang, X.; Arumugam, K.; Bielawski, C. W.; Sessler, J. L. *Organometallics* **2011**, *30*, 5033.
61. Keske, E. C.; Zenkina, O. V.; Wang, R.; Crudden, C. M. *Organometallics* **2012**, *31*, 456.
62. Poulain, A.; Canseco-Gonzalez, D.; Hynes-Roche, R.; Müller-Bunz, H.; Schuster, O.; Stoeckli-Evans, H.; Neels, A.; Albrecht, M. *Organometallics* **2011**, *30*, 1021.
63. Zamora, M. T.; Ferguson, M. J.; McDonald, R.; Cowie, M. *Organometallics* **2012**, *31*, 5463.
64. Kelly, R. A.; Clavier, H.; Giudice, S.; Scott, N. M.; Stevens, E. D.; Bordner, J.; Samardjiev, I.; Hoff, C. D.; Cavallo, L.; Nolan, S. P. *Organometallics* **2008**, *27*, 202.
65. Chianese, A. R.; Li, X.; Janzen, M. C.; Faller, J. W.; Crabtree, R. H. *Organometallics* **2003**, *22*, 1663.
66. Terashima, T.; Inomata, S.; Ogata, K.; Fukuzawa, S. *Eur. J. Inorg. Chem.* **2012**, *2012*, 1387.
67. Sluijter, S. N.; Jongkind, L. J.; Elsevier, C. J. *Eur. J. Inorg. Chem.* **2015**, *2015*, 2948.
68. Mendoza-Espinosa, D.; González-Olvera, R.; Osornio, C.; Negrón-Silva, G. E.; Santillan, R. *New J. Chem.* **2015**, *39*, 1587.
69. Strydom, I.; Guisado-Barrios, G.; Fernández, I.; Liles, D. C.; Peris, E.; Bezuidenhout, D. I. *Chem. Eur. J.* **2017**, *23*, 1393.
70. Wolf, S.; Plenio, H. *J. Organomet. Chem.* **2009**, *694*, 1487.
71. Bidal, Y. D.; Santoro, O.; Melaimi, M.; Cordes, D. B.; Slawin, A. M. Z.; Bertrand, G.; Cazin, C. S. J. *Chem. Eur. J.* **2016**, *22*, 9404.
72. Nakamura, T.; Terashima, T.; Ogata, K.; Fukuzawa, S. *Org. Lett.* **2011**, *13*, 620.
73. Hohloch, S.; Duecker, F.; van der Meer, M.; Sarkar, B. *Molecules* **2015**, *20*, 7379.
74. Petronilho, A.; Müller-Bunz, H.; Albrecht, M. *Chem. Commun.* **2012**, *48*, 6499.
75. Hohloch, S.; Sarkar, B.; Nauton, L.; Cisnetti, F.; Gautier, A. *Tetrahedron Letters* **2013**, *54*, 1808.
76. Hohloch, S.; Su, C.; Sarkar, B. *Eur. J. Inorg. Chem.* **2011**, *2011*, 3067.
77. Hohloch, S.; Scheiffele, D.; Sarkar, B. *Eur. J. Inorg. Chem.* **2013**, *2013*, 3956.
78. Bidal, Y. D.; Lesieur, M.; Melaimi, M.; Nagra, F.; Cordes, D. B.; Athukorala Arachchige, K. S.; Slawin, A. M. Z.; Bertrand, G.; Cazin, C. S. J. *Adv. Synth. Catal.* **2015**, *357*, 3155.
79. Inomata, H.; Ogata, K.; Fukuzawa, S.; Hou, Z. *Org. Lett.* **2012**, *14*, 3986.
80. Johnson, C.; Albrecht, M. *Organometallics* **2017**, *36*, 2902.
81. Wei, Y.; Liu, S.; Mueller-Bunz, H.; Albrecht, M. *ACS Catal.* **2016**, *6*, 8192.
82. Wei, Y.; Petronilho, A.; Mueller-Bunz, H.; Albrecht, M. *Organometallics* **2014**, *33*, 5834.
83. Mncube, S. G.; Bala, M. D. *Polyhedron* **2019**, *157*, 467.

84. Mendoza-Espinosa, D.; Alvarez-Hernández, A.; Angeles-Beltrán, D.; Negrón-Silva, G. E.; Suárez-Castillo, O. R.; Vásquez-Pérez, J. M. *Inorg. Chem.* **2017**, *56*, 2092.
85. Iwasaki, H.; Teshima, Y.; Yamada, Y.; Ishikawa, R.; Koga, Y.; Matsubara, K. *Dalton Trans.* **2016**, *45*, 5713.
86. Vanicek, S.; Podewitz, M.; Stubbe, J.; Schulze, D.; Kopacka, H.; Wurst, K.; Müller, T.; Lippmann, P.; Haslinger, S.; Schottenberger, H.; Liedl, K. R.; Ott, I.; Sarkar, B.; Bildstein, B. *Chem. Eur. J.* **2018**, *24*, 3742.
87. Mejuto, C.; Royo, B.; Guisado-Barrios, G.; Peris, E. *Beilstein J. Org. Chem.* **2015**, *11*, 2584.
88. Cao, L.; Huang, S.; Liu, W.; Yan, X. *Organometallics* **2018**, *37*, 2010.
89. Bezuidenhout, D. I.; Kleinhans, G.; Guisado-Barrios, G.; Liles, D. C.; Ung, G.; Bertrand, G. *Chem. Commun.* **2014**, *50*, 2431.
90. Chábera, P.; Kjaer, K. S.; Prakash, O.; Honarfar, A.; Liu, Y.; Fredin, L. A.; Harlang, T. C. B.; Lidin, S.; Uhlig, J.; Sundström, V.; Lomoth, R.; Persson, P.; Wärnmark, K. *J. Phys. Chem. Lett.* **2018**, *9*, 459.
91. Chábera, P.; Liu, Y.; Prakash, O.; Thyraug, E.; Nahhas, A. E.; Honarfar, A.; Essén, S.; Fredin, L. A.; Harlang, T. C. B.; Kjær, K. S.; Handrup, K.; Ericson, F.; Tatsuno, H.; Morgan, K.; Schnadt, J.; Häggström, L.; Ericsson, T.; Sobkowiak, A.; Lidin, S.; Huang, P.; Styring, S.; Uhlig, J.; Bendix, J.; Lomoth, R.; Sundström, V.; Persson, P.; Wärnmark, K. *Nature* **2017**, *543*, 695.
92. Liu, Y.; Kjær, K. S.; Fredin, L. A.; Chábera, P.; Harlang, T.; Canton, S. E.; Lidin, S.; Zhang, J.; Lomoth, R.; Bergquist, K.-E.; Persson, P.; Wärnmark, K.; Sundström, V. *Chem. Eur. J.* **2015**, *21*, 3628.
93. van der Meer, M.; Glais, E.; Siewert, I.; Sarkar, B. *Angew. Chem. Int. Ed.* **2015**, *54*, 13792.
94. Silberrad, O.; Roy, C. S. *J. Chem. Soc.* **1906**, *89*, 179.
95. Zhang, Z.; Wang, J. *Tetrahedron* **2008**, *64*, 6577.
96. Ford, A.; Miel, H.; Ring, A.; Slattery, C. N.; Maguire, A. R.; McKerverey, M. A. *Chem. Rev.* **2015**, *115*, 9981.
97. Xue, X.-S.; Ji, P.; Zhou, B.; Cheng, J.-P. *Chem. Rev.* **2017**, *117*, 8622.
98. Hartwig, J. F.; Larsen, M. A. *ACS Cent. Sci.* **2016**, *2*, 281.
99. Qin, Y.; Zhu, L.; Luo, S. *Chem. Rev.* **2017**, *117*, 9433.
100. Yates, P.; Danishefsky, S. *J. Am. Chem. Soc.* **1962**, *84*, 879.
101. Scott, L. T.; DeCicco, G. J. *J. Am. Chem. Soc.* **1974**, *96*, 322.
102. Demonceau, A.; Noels, A. F.; Hubert, A. J.; Teyssié, P. *J. Chem. Soc., Chem. Commun.* **1981**, 688.
103. Wenkert, E.; Davis, L. L.; Mylari, B. L.; Solomon, M. F.; Da Silva, R. R.; Shulman, S.; Warnet, R. J.; Ceccherelli, P.; Curini, M.; Pellicciari, R. *J. Org. Chem.* **1982**, *47*, 3242.
104. Taber, D. F.; Petty, E. H. *J. Org. Chem.* **1982**, *47*, 4808.
105. Davies, H. M. L.; Manning, J. R. *Nature* **2008**, *451*, 417.
106. Doyle, M. P.; Duffy, R.; Ratnikov, M.; Zhou, L. *Chem. Rev.* **2010**, *110*, 704.
107. Davies, H. M. L.; Beckwith, R. E. J. *Chem. Rev.* **2003**, *103*, 2861.
108. Flynn, C. J.; Elcoate, C. J.; Lawrence, S. E.; Maguire, A. R. *J. Am. Chem. Soc.* **2010**, *132*, 1184.
109. Shiely, A. E.; Slattery, C. N.; Ford, A.; Eccles, K. S.; Lawrence, S. E.; Maguire, A. R. *Org. Biomol. Chem.* **2017**, *15*, 2609.
110. Caballero, A.; Díaz-Requejo, M. M.; Belderrain, T. R.; Nicasio, M. C.; Trofimenko, S.; Pérez, P. J. *J. Am. Chem. Soc.* **2003**, *125*, 1446.
111. Morilla, M. E.; Díaz-Requejo, M. M.; Belderrain, T. R.; Nicasio, M. C.; Trofimenko, S.; Pérez, P. J. *Organometallics* **2004**, *23*, 293.
112. Gava, R.; Olmos, A.; Noverges, B.; Varea, T.; Álvarez, E.; Belderrain, T. R.; Caballero, A.; Asensio, G.; Pérez, P. J. *ACS Catal.* **2015**, *5*, 3726.
113. Díaz-Requejo, M. M.; Pérez, P. J. *Chem. Rev.* **2008**, *108*, 3379.
114. Crichton, R. *Iron Metabolism: From Molecular Mechanisms to Clinical Consequences*; John Wiley & Sons, Ltd 2009.
115. Mansuy, D.; Lange, M.; Chottard, J.-C.; Guerin, P.; Morliere, P.; Brault, D.; Rougee, M. *J. Chem. Soc., Chem. Commun.* **1977**, 648.
116. Mansuy, D.; Lange, M.; Chottard, J. C.; Bartoli, J. F.; Chevrier, B.; Weiss, R. *Angew. Chem. Int. Ed.* **1978**, *17*, 781.
117. Ziegler, C. J.; Suslick, K. S. *J. Am. Chem. Soc.* **1996**, *118*, 5306.
118. Ziegler, C. J.; Suslick, K. S. *J. Organomet. Chem.* **1997**, *528*, 83.

119. Knors, C.; Kuo, G. H.; Lauher, J. W.; Eigenbrot, C.; Helquist, P. *Organometallics* **1987**, *6*, 988.
120. Ishii, S.; Zhao, S.; Helquist, P. *J. Am. Chem. Soc.* **2000**, *122*, 5897.
121. Zhao, S. K.; Helquist, P. *J. Org. Chem.* **1990**, *55*, 5820.
122. Klose, A.; Solari, E.; Floriani, C.; Re, N.; Chiesi-Villa, A.; Rizzoli, C. *Chem. Commun.* **1997**, 2297.
123. Esposito, V.; Solari, E.; Floriani, C.; Re, N.; Rizzoli, C.; Chiesi-Villa, A. *Inorg. Chem.* **2000**, *39*, 2604.
124. Li, Y.; Huang, J.-S.; Zhou, Z.-Y.; Che, C.-M.; You, X.-Z. *J. Am. Chem. Soc.* **2002**, *124*, 13185.
125. Khade, R. L.; Fan, W.; Ling, Y.; Yang, L.; Oldfield, E.; Zhang, Y. *Angew. Chem. Int. Ed.* **2014**, *53*, 7574.
126. Sharon, D. A.; Mallick, D.; Wang, B.; Shaik, S. *J. Am. Chem. Soc.* **2016**, *138*, 9597.
127. Liu, Y.; Xu, W.; Zhang, J.; Fuller, W.; Schulz, C. E.; Li, J. *J. Am. Chem. Soc.* **2017**, *139*, 5023.
128. Russell, S. K.; Hoyt, J. M.; Bart, S. C.; Milsmann, C.; Stieber, S. C. E.; Semproni, S. P.; DeBeer, S.; Chirik, P. J. *Chem. Sci.* **2014**, *5*, 1168.
129. Reesbeck, M. E.; Grubel, K.; Kim, D.; Brennessel, W. W.; Mercado, B. Q.; Holland, P. L. *Inorg. Chem.* **2017**, *56*, 1019.
130. Mbuvi, H. M.; Woo, L. K. *Organometallics* **2008**, *27*, 637.
131. Mbuvi, H. M.; Woo, L. K. *J. Porphyrins Phthalocyanines* **2009**, *13*, 136.
132. Cai, Y.; Zhu, S.-F.; Wang, G.-P.; Zhou, Q.-L. *Adv. Synth. Catal.* **2011**, *353*, 2939.
133. Hock, K. J.; Knorrscheidt, A.; Hommelsheim, R.; Ho, J.; Weissenborn, M. J.; Koenigs, R. M. *Angew. Chem. Int. Ed.* **2019**, *58*, 3630.
134. Cheng, Q.-Q.; Yang, J.-M.; Xu, H.; Zhu, S.-F. *Synlett* **2017**, *28*, 1327.
135. Griffin, J. R.; Wendell, C. I.; Garwin, J. A.; White, M. C. *J. Am. Chem. Soc.* **2017**, *139*, 13624.
136. Coelho, P. S.; Brustad, E. M.; Kannan, A.; Arnold, F. H. *Science* **2013**, *339*, 307.
137. Zhang, R. K.; Chen, K.; Huang, X.; Wohlschlager, L.; Renata, H.; Arnold, F. H. *Nature* **2019**, *565*, 67.
138. Company, A.; Gómez, L.; Güell, M.; Ribas, X.; Luis, J. M.; Que, L.; Costas, M. *J. Am. Chem. Soc.* **2007**, *129*, 15766.
139. Sabenya, G.; Lázaro, L.; Gamba, I.; Martin-Diaconescu, V.; Andris, E.; Weyhermüller, T.; Neese, F.; Roithova, J.; Bill, E.; Lloret-Fillol, J.; Costas, M. *J. Am. Chem. Soc.* **2017**, *139*, 9168.
140. Conde, A.; Sabenya, G.; Rodríguez, M.; Postils, V.; Luis, J. M.; Díaz-Requejo, M. M.; Costas, M.; Pérez, P. J. *Angew. Chem. Int. Ed.* **2016**, *55*, 6530.
141. Zhang, H.; Liu, J.; Chen, J.; Zhao, J.; Zhao, Y.; Li, L. *Synthesis* **2003**, 2661.
142. Riener, K.; Haslinger, S.; Raba, A.; Högerl, M. P.; Cokoja, M.; Herrmann, W. A.; Kühn, F. E. *Chem. Rev.* **2014**, *114*, 5215.
143. Addison, A. W.; Rao, T. N.; Reedijk, J.; van Rijn, J.; Verschoor, G. C. *J. Chem. Soc., Dalton Trans.*, **1984**, 1349.
144. The synthesis of Zn(OTf)₂(Me₂Pytacn) is described in Chapter IV. Its crystal structure is attached in the supplementary material of this thesis.
145. Ronson, Tanya K.; Nelson, J.; Jameson, Geoffrey B.; Jeffery, John C.; Brooker, S. *Eur. J. Inorg. Chem.* **2004**, *2004*, 2570.
146. Goodwin, J. M.; Olmstead, M. M.; Patten, T. E. *J. Am. Chem. Soc.* **2004**, *126*, 14352.
147. Kazuya, K.; Hideki, F.; Shigenori, N.; Akifumi, H.; Hideki, H.; Shuhei, F.; Masatatsu, S.; Teizo, K. *Bull. Chem. Soc. Jpn.* **2004**, *77*, 59.
148. Halfen, J. A.; Young, V. G.; Tolman, W. B. *J. Am. Chem. Soc.* **1996**, *118*, 10920.
149. Wu, J.; Dai, W.; Farnaby, J. H.; Hazari, N.; Le Roy, J. J.; Mereacre, V.; Murugesu, M.; Powell, A. K.; Takase, M. K. *Dalton Trans.* **2013**, *42*, 7404.
150. Louie, J.; Grubbs, R. H. *Chem. Commun.* **2000**, 1479.
151. Zlatogorsky, S.; Muryn, C. A.; Tuna, F.; Evans, D. J.; Ingleson, M. J. *Organometallics* **2011**, *30*, 4974.
152. Suzuki, K.; Oldenburg, P. D.; Que Jr., L. *Angew. Chem. Int. Ed.* **2008**, *47*, 1887.
153. He, Y.; Gorden, J. D.; Goldsmith, C. R. *Inorg. Chem.* **2011**, *50*, 12651.
154. Gómez, L.; Canta, M.; Font, D.; Prat, I.; Ribas, X.; Costas, M. *J. Org. Chem.* **2013**, *78*, 1421.
155. Mikata, Y.; Kawata, K.; Iwatsuki, S.; Konno, H. *Inorg. Chem.* **2012**, *51*, 1859.

156. Anderson, S. N.; Noble, M.; Grubel, K.; Marshall, B.; Arif, A. M.; Berreau, L. M. *Journal of Coordination Chemistry* **2014**, *67*, 4061.
157. Okeke, U.; Gultneh, Y.; Butcher, R. J. *Acta Cryst. E* **2017**, *73*, 1568.
158. Naumann, S.; Schmidt, F. G.; Frey, W.; Buchmeiser, M. R. *Polym. Chem.* **2013**, *4*, 4172.
159. Jochmann, P.; Stephan, D. W. *Chem. Eur. J.* **2014**, *20*, 8370.
160. Bossek, U.; Nühlen, D.; Bill, E.; Glaser, T.; Krebs, C.; Weyhermüller, T.; Wieghardt, K.; Lengen, M.; Trautwein, A. X. *Inorg. Chem.* **1997**, *36*, 2834.
161. Garcia-Bosch, I.; Company, A.; Fontrodona, X.; Ribas, X.; Costas, M. *Org. Lett.* **2008**, *10*, 2095.
162. Park, D.-A.; Ryu, J. Y.; Lee, J.; Hong, S. *RSC Adv.* **2017**, *7*, 52496.
163. Kim, S.; Lee, J. Y.; Cowley, R. E.; Ginsbach, J. W.; Siegler, M. A.; Solomon, E. I.; Karlin, K. D. *J. Am. Chem. Soc.* **2015**, *137*, 2796.
164. Frutos, M.; Ortuño, M. A.; Lledos, A.; Viso, A.; Fernández de la Pradilla, R.; de la Torre, M. C.; Sierra, M. A.; Gornitzka, H.; Hemmert, C. *Org. Lett.* **2017**, *19*, 822.
165. de Frémont, P.; Scott, N. M.; Stevens, E. D.; Ramnial, T.; Lightbody, O. C.; Macdonald, C. L. B.; Clyburne, J. A. C.; Abernethy, C. D.; Nolan, S. P. *Organometallics* **2005**, *24*, 6301.
166. Domyati, D.; Hope, S. L.; Latifi, R.; Hearn, M. D.; Tahsini, L. *Inorg. Chem.* **2016**, *55*, 11685.
167. Liu, J. J.; Diaz, D. E.; Quist, D. A.; Karlin, K. D. *Isr. J. Chem.* **2016**, *56*, 738.
168. Pavlishchuk, V. V.; Addison, A. W. *Inorganica Chimica Acta* **2000**, *298*, 97.
169. Elwell, C. E.; Gagnon, N. L.; Neisen, B. D.; Dhar, D.; Spaeth, A. D.; Yee, G. M.; Tolman, W. B. *Chem. Rev.* **2017**, *117*, 2059.
170. Maiti, D.; Fry, H. C.; Woertink, J. S.; Vance, M. A.; Solomon, E. I.; Karlin, K. D. *J. Am. Chem. Soc.* **2007**, *129*, 264.
171. Kunishita, A.; Kubo, M.; Sugimoto, H.; Ogura, T.; Sato, K.; Takui, T.; Itoh, S. *J. Am. Chem. Soc.* **2009**, *131*, 2788.
172. Bhadra, M.; Lee, J. Y. C.; Cowley, R. E.; Kim, S.; Siegler, M. A.; Solomon, E. I.; Karlin, K. D. *J. Am. Chem. Soc.* **2018**, *140*, 9042.
173. Fujisawa, K.; Tanaka, M.; Moro-oka, Y.; Kitajima, N. *J. Am. Chem. Soc.* **1994**, *116*, 12079.
174. Warren, J. J.; Tronic, T. A.; Mayer, J. M. *Chem. Rev.* **2010**, *110*, 6961.
175. Lee, J. Y.; Peterson, R. L.; Ohkubo, K.; Garcia-Bosch, I.; Himes, R. A.; Woertink, J.; Moore, C. D.; Solomon, E. I.; Fukuzumi, S.; Karlin, K. D. *J. Am. Chem. Soc.* **2014**, *136*, 9925.
176. Yang, M.; Webb, T. R.; Livant, P. *J. Org. Chem.* **2001**, *66*, 4945.
177. Fructos, M. R.; Besora, M.; Braga, A. A. C.; Díaz-Requejo, M. M.; Maseras, F.; Pérez, P. *J. Organometallics* **2017**, *36*, 172.
178. Tortoreto, C.; Rackl, D.; Davies, H. M. L. *Org. Lett.* **2017**, *19*, 770.
179. Pérez, P. J.; Díaz-Requejo, M. M.; Rivilla, I. *Beilstein J. Org. Chem.* **2011**, *7*, 653.
180. Zhu, S.-F.; Zhou, Q.-L. *Acc. Chem. Res.* **2012**, *45*, 1365.
181. Kulkarni, N. V.; Dash, C.; Jayaratna, N. B.; Ridlen, S. G.; Karbalaei Khani, S.; Das, A.; Kou, X.; Yousufuddin, M.; Cundari, T. R.; Dias, H. V. R. *Inorg. Chem.* **2015**, *54*, 11043.
182. Davies, H. M. L.; Grazini, M. V. A.; Aouad, E. *Org. Lett.* **2001**, *3*, 1475.
183. Doyle, M. P.; Hu, W. *Chirality* **2002**, *14*, 169.
184. Yoon, C. H.; Nagle, A.; Chen, C.; Gandhi, D.; Jung, K. W. *Org. Lett.* **2003**, *5*, 2259.
185. Minami, K.; Saito, H.; Tsutsui, H.; Nambu, H.; Anada, M.; Hashimoto, S. *Adv. Synth. Catal.* **2005**, *347*, 1483.
186. Heasley, B. *Current Organic Chemistry* **2014**, *18*, 641.
187. Panda, A.; Stender, M.; Wright, R. J.; Olmstead, M. M.; Klavins, P.; Power, P. P. *Inorg. Chem.* **2002**, *41*, 3909.
188. Zhang, L.; Xiang, L.; Yu, Y.; Deng, L. *Inorg. Chem.* **2013**, *52*, 5906.
189. Milocco, F.; Demeshko, S.; Meyer, F.; Otten, E. *Dalton Trans.* **2018**, *47*, 8817.
190. DeAngelis, A.; Panish, R.; Fox, J. M. *Acc. Chem. Res.* **2016**, *49*, 115.
191. Postils, V.; Rodríguez, M.; Sabenya, G.; Conde, A.; Díaz-Requejo, M. M.; Pérez, P. J.; Costas, M.; Solà, M.; Luis, J. M. *ACS Catal.* **2018**, *8*, 4313.
192. Gómez-Gallego, M.; Sierra, M. A. *Chem. Rev.* **2011**, *111*, 4857.
193. Ali, G.; VanNatta, P. E.; Ramirez, D. A.; Light, K. M.; Kieber-Emmons, M. T. *J. Am. Chem. Soc.* **2017**, *139*, 18448.
194. Flassbeck, C.; Wieghardt, K. *Z. Anorg. Allg. Chem.* **1992**, *608*, 60.
195. Sun, L.; Gai, Y.; Anderson, C. J.; Zeng, D. *Chem. Commun.* **2015**, *51*, 17072.
196. Andersen, R. A.; Faegri, K.; Green, J. C.; Haaland, A.; Lappert, M. F.; Leung, W. P.; Rypdal, K. *Inorg. Chem.* **1988**, *27*, 1782.

197. James, A. M.; Laxman, R. K.; Fronczek, F. R.; Maverick, A. W. *Inorg. Chem.* **1998**, *37*, 3785.
198. In *Inorganic Syntheses*; Cowley, A. H., Ed. 1996; Vol. 31.
199. Haldón, E.; Delgado-Rebollo, M.; Prieto, A.; Álvarez, E.; Maya, C.; Nicasio, M. C.; Pérez, P. J. *Inorg. Chem.* **2014**, *53*, 4192.
200. Mairena, M. A.; Urbano, J.; Carbajo, J.; Maraver, J. J.; Alvarez, E.; Díaz-Requejo, M. M.; Pérez, P. J. *Inorg. Chem.* **2007**, *46*, 7428.
201. López-Rodríguez, R.; Ros, A.; Fernández, R.; Lassaletta, J. M. *J. Org. Chem.* **2012**, *77*, 9915.
202. Prat, I.; Font, D.; Company, A.; Junge, K.; Ribas, X.; Beller, M.; Costas, M. *Adv. Synth. Catal.* **2013**, *355*, 947.
203. Prat, I.; Company, A.; Corona, T.; Parella, T.; Ribas, X.; Costas, M. *Inorg. Chem.* **2013**, *52*, 9229.
204. Company, A.; Gómez, L.; Fontrodona, X.; Ribas, X.; Costas, M. *Chem. Eur.J.* **2008**, *14*, 5727.
205. Nakanishi, S.-i.; Kawamura, M.; Kai, H.; Jin, R.-H.; Sunada, Y.; Nagashima, H. *Chem. Eur.J.* **2014**, *20*, 5802.
206. Company, A.; Sabenya, G.; González-Béjar, M.; Gómez, L.; Clémancey, M.; Blondin, G.; Jasniewski, A. J.; Puri, M.; Browne, W. R.; Latour, J.-M.; Que, L.; Costas, M.; Pérez-Prieto, J.; Lloret-Fillol, J. *J. Am. Chem. Soc.* **2014**, *136*, 4624.
207. Costas, M.; Tipton, A. K.; Chen, K.; Jo, D.-H.; Que, L. *J. Am. Chem. Soc.* **2001**, *123*, 6722.
208. Font, D.; Canta, M.; Milan, M.; Cussó, O.; Ribas, X.; Klein Gebbink, R. J. M.; Costas, M. *Angew. Chem. Int. Ed.* **2016**, *55*, 5776.
209. Chen, M. S.; White, M. C. *Science* **2007**, *318*, 783.
210. Corona, T.; Padamati, S. K.; Acuña-Parés, F.; Duboc, C.; Browne, W. R.; Company, A. *Chem. Commun.* **2017**, *53*, 11782.
211. Draksharapu, A.; Codolà, Z.; Gómez, L.; Lloret-Fillol, J.; Browne, W. R.; Costas, M. *Inorg. Chem.* **2015**, *54*, 10656.
212. Hu, M.; Rong, J.; Miao, W.; Ni, C.; Han, Y.; Hu, J. *Org. Lett.* **2014**, *16*, 2030.
213. Davis, O. A.; Croft, R. A.; Bull, J. A. *Chem. Commun.* **2015**, *51*, 15446.
214. Peng, Z.-Y.; Wang, J.-P.; Cheng, J.; Xie, X.-m.; Zhang, Z. *Tetrahedron* **2010**, *66*, 8238.
215. Grünberg, M. F.; Gooßen, L. J. *Chem. Eur.J.* **2013**, *19*, 7334.
216. Zimmermann, B.; Dzik, W. I.; Himmler, T.; Goossen, L. J. *J. Org. Chem.* **2011**, *76*, 8107.
217. Lau, C. K.; Tardif, S.; Dufresne, C.; Scheigetz, J. *J. Org. Chem.* **1989**, *54*, 491.
218. Taber, D. F.; Herr, R. J.; Pack, S. K.; Geremia, J. M. *J. Org. Chem.* **1996**, *61*, 2908.
219. Luo, Z.-b.; Zhao, C.; Xie, J.; Lu, H.-f. *Synthesis* **2016**, *48*, 3696.
220. Yang, M.; Su, B.; Wang, Y.; Chen, K.; Jiang, X.; Zhang, Y.-F.; Zhang, X.-S.; Chen, G.; Cheng, Y.; Cao, Z.; Guo, Q.-Y.; Wang, L.; Shi, Z.-J. *Nat. Commun.* **2014**, *5*, 4707.

